Modeling and Numerical Investigation of Acoustic Cavitation with Applications in Sonochemistry

D o c t o r a l T h e s i s

(D i s s e r t a t i o n)

to be awarded the degree

Doctor of Engineering (Dr.-Ing.)

submitted by

Rashid Jamshidi

from Rasht, Iran

approved by

the Faculty of Mathematics/ Computer Science and Mechanical Engineering,

Clausthal University of Technology

Date of oral examination

20.12.2013

Dean

Prof. Dr.-Ing. Alfons Esderts

Supervising tutor

Prof. Dr. -Ing. Gunther Brenner

Reviewer

Prof. Dr. Werner Lauterborn

To my parents,

my sister Leyli
and my brother Farshid

Acknowledgments

First and foremost, I would like to express my sincerest thanks to my supervisor, Prof. Dr.-Ing. habil. Gunther Brenner for his guidance, insight and patience throughout these past three and a half years. He has provided a fantastic working environment and research facilities, the freedom to follow my own initiative and continual support and guidance. I do appreciate his generosity that allowed me to pursue my own ideas. I shall also state my deepest appreciation and admiration about his exceptional enthusiasm and interest in my work. Our fruitful discussions on the subject made enormous contributions to this thesis. I am also grateful for the opportunity of acting as a teaching assistant at his lecture “Fluid Mechanics for Petroleum Engineers”.

Deepest gratitude are also due to the members of the examination committee, for their suggestions on improving my Thesis. Prof. Dr.-Ing. habil. Alfons Esderts has willingly accepted the position of chairperson of the examining committee and Prof. Dr. Werner Lauterborn has acted as my co-examiner with a great interest in the subject. Many thanks for his valuable comments and detailed review of the manuscript.

I was very fortunate to collaborate with many researchers. Discussions with Dr. Robert Mettin from the Drittes Physikalisches Institut Göttingen really helped me understand the fundamental physics of acoustically excited bubbles. I gratefully acknowledge his suggestions and comments on my thesis which are invaluable to the quality of this dissertation.

Finally, I would like to thank my family, for their invaluable patience, trust and encouragement during this thesis. Words can not express how grateful I am to my hard-working mother and father for all of the sacrifices that they have made on my behalf. You never stop believing in me even the times I have lost my confidence and hope. I would certainly not be where I stand today without the unconditional and everlasting support and love from you. You have been there for me consistently, through good and bad times. Your prayer for me was what sustained me thus far. You raised me with a love of science and supported me in all my pursuits. Thank you. I would also like to thank to my beloved sister, Leyli. Thank you for supporting me for everything and especially I can’t thank you enough for encouraging me throughout my stay in Germany. For the presence of my lovely brother Farshid in Clausthal for about two of my years here. Thank you. I know I always have my family to count on when times are rough.

Abstract

The focus of the present thesis is to provide more detailed and reliable descriptions and models to quantify the mutual relation between flow and sound field, cavitation bubbles and energy dissipation in sonochemical reactors. The major problem regarding the simulation of such a phenomenon is that different time and spatial scales have to be considered simultaneously. The starting point of the research is the numerical investigation of the cavitational activity using linearized assumptions in a conical shape reactor. Different working assumptions for modeling of the wave propagation, attenuation of pressure due to cavitation bubbles and the influence of wave frequency, input power and reactor geometry are examined. Based on the linearized wave equation in the frequency domain, a fast and robust numerical method is developed and applied in the COMSOL Multiphysics software. Results illustrate that both, the frequency and power of the ultrasound source may be optimized with respect to the location and strength of cavitation. In addition, different boundary conditions to model the absorbing properties of wall boundaries, lead to significantly different wave patterns.

Based on the quasi-linear analysis performed in the first part, the approach is enhanced to account for the attenuating effect of gas bubbles in cavitating flows considering more rigorous physical models. Firstly, using an energy conservation approach, a new model is developed for nonlinear damping of acoustic waves considering the compressibility of the liquid around bubbles. Different types of damping are introduced into the nonlinear damping models and their sources are illustrated. Secondly, a unified computational method is developed to couple the dynamics of cavitating bubbles and wave propagation in a turbulent flow. The approach is based on the OpenFOAM software library, which allows implementing different models and numerical schemes in an efficient way. To investigate the structure of bubbles, an Eulerian-Lagrangian approach for bubbles with varying radii is developed. Furthermore, the interaction among bubbles (collision and the effect of secondary Bjerknes force) and also between the bubbles swarm and acoustic waves (nonlinear damping and primary Bjerknes force) are considered. To verify and validate the present approach, several generic test cases as well as experimental configurations are selected for comparison. Results show that the solver predicts the structure of bubbles, their interaction with acoustic waves and the flow field due to acoustic streaming in a precise way. Therefore, the approach is beneficial for numerical simulation of three-dimensional sonochemical reactors with complex geometry, including the essential physics.

Zusammenfassung

Das Ziel der vorliegenden Dissertation ist es, genauere und zuverlässigere Modelle zur Quantifizierung der Wechselwirkungen zwischen Strömungs- und Schallfeld, Kavitationsblasen und Energiedissipation in sonochemischen Reaktoren zu erhalten. Das hauptsächliche Problem bezüglich der Simulation eines solchen Phänomens ist, dass verschiedene Zeit- und Raumskalen gleichzeitig betrachtet werden müssen. Die Dissertation beginnt mit der numerischen Untersuchung der Kavitationsaktivität in einem konischen Reaktor unter Verwendung linearisierter Annahmen. Es werden sowohl unterschiedliche Annahmen für die Modellierung der Wellenausbreitung, das Abschwächen des Drucks infolge der Kavitationsblasen, als auch der Einfluss der Wellenfrequenz, der Aufnahmeleistung der Sonotrode und der Reaktorgeometrie überprüft. Basierend auf der linearisierten Wellengleichung im Frequenzbereich wird eine schnelle und robuste numerische Methode entwickelt und in der COMSOL Multiphysics Software implementiert. Die Ergebnisse zeigen, dass die Frequenz und die Leistung des Ultraschallkopfes bezüglich des Ortes und der Stärke der Kavitation optimiert werden können. Außerdem führen verschiedene Randbedingungen für die Modellierung der absorbierenden Eigenschaften der Wände zu erheblich unterschiedlichen Wellenformen. Bezogen auf die quasilineare Analyse, die im ersten Teil durchgeführt wurde, wird die Vorgehensweise weiterentwickelt, wobei der abschwächende Einfluss der Gasblasen durch rigorosere physikalische Modelle beschrieben wird. Zum Ersten wird ein neues Modell für die nichtlineare Dämpfung der akustischen Wellen angesichts der Kompressibilität der umgebenden Flüssigkeit durch einen Energieerhaltungssatz entwickelt. Verschiedene Dämpfungsarten werden in den nichtlinearen Dämpfungsmodellen eingeführt und ihre Quellen werden aufgezeigt. Zum Zweiten wird eine numerische Methode entwickelt, um die Kavitationsblasendynamik und Wellenausbreitung in einer turbulenten Strömung zu koppeln. Die Basis für das Programm ist OpenFOAM, so dass die Implementierung der verschiedenen Modelle und numerischen Schemen leistungsfähig möglich ist. Die Untersuchung der Blasenstruktur ist durch eine Euler-Lagrange Methode für die Blasen mit veränderlichen Radien entwickelt. Darüber hinaus sind die Wechselwirkungen zwischen den Blasen (Kollision und der Einfluss der sekundären Bjerknes Kraft) und auch zwischen dem Blasenschwarm und den akustischen Wellen (nichtlineare Dämpfung und die primäre Bjerknes Kraft) berücksichtigt. Um die vorliegende Methode zu verifizieren und validieren, werden einige generische Testfälle sowie experimentelle Konfigurationen ausgewählt. Die Ergebnisse illustrieren, dass der Solver die Blasenstruktur, die Wechselwirkung von Blasen mit akustischen Wellen und das Strömungsfeld auf-

grund von akustischen Felden präzise voraussagt. Deshalb ist die Methode vorteilhaft für die numerische Simulation von drei-dimensionalen sonochemischen Reaktoren mit der komplexen Geometrie inklusive der essenziellen Physik. Die grundsätzliche Eignung des Verfahrens zur Berechnung von Strömungen und Kavitation in drei-dimensionalen Reaktoren wird gezeigt, so dass zukünftig bessere Modelle zur Auslegung und Optimierung zur Verfügung stehen.

Contents

1. Introduction **1**

1.1. Background 1

1.2. Motivation and objectives 4

1.3. Outline of the thesis 7

2. Physical model **9**

2.1. Bubble radial dynamics 9

2.2. Wave propagation in bubbly liquids 18

2.2.1. Derivation of the effective equations of the Caflisch model 22

2.2.2. Linear wave equation without bubbles 24

2.2.3. Linearized wave equation in bubbly liquids- Linear attenuation 25

2.2.4. Nonlinear attenuation of wave propagation 26

2.3. Lagrangian tracing of bubbles with varying radii 39

2.3.1. Flow field equations 40

2.3.2. Acoustic streaming source term $\mathbf{F}_{\mathbf{A.S.}}$ 42

2.3.3. Lagrangian frame formulation 43

2.4. Population of bubbles 49

3. Numerical method **53**

3.1. Numerical set-up for linear analysis 54

3.1.1. Geometries, boundary conditions and physical properties 54

3.1.2. Procedure of the linear analysis 57

3.1.3. Grid generation and grid study 58

3.2. Numerical set-up for nonlinear analysis 61

3.2.1. Geometries, boundary conditions and physical properties 65

3.2.2. Procedure of the nonlinear analysis 68

4. Results: Linearized approximations **69**

4.1. Simple geometries as benchmarks 69

4.1.1. Simulation of wave propagation 69

4.1.2. Simulation of acoustic streaming 74

4.2. Pressure distribution in conical reactor 75

4.2.1. Pressure distribution without attenuation due to bubbles 75

4.2.2. Pressure distribution for homogeneous distribution of bubbles 82

4.2.3. Pressure distribution for inhomogeneous distribution of bubbles 87

4.3. Flow field simulation in the conical reactor 93

5. Results: Nonlinear approximations **97**

5.1. Benchmarks for numerical implementations 98

5.1.1. Backward Facing Step (BSF) 98

5.1.2. Sudden expansion: convection of a single bubble with varying radius in a sound field 99

5.2. Orders of magnitude of the forces on bubbles 100

5.3. One-dimensional simulation 103

5.3.1. Single bubble motion- Linear oscillations 103

5.3.2. Single bubble motion- Nonlinear oscillations and convection 106

5.4. Two-dimensional simulation 109

5.4.1. Single bubble motion- Linear oscillations 109

5.4.2. Multiple bubbles motion- Nonlinear oscillations 110

5.4.3. Multiple bubbles motion- Nonlinear damping 112

5.5. Three-dimensional simulation 117

6. Summary and recommendation for future work **119**

A. Appendix **I**

A.1. List of Tables I

A.2. List of Figures I

A.3. Nomenclature VI

B. Bibliography **XI**

C. Declaration **XXIII**

D. Curriculum Vitae **XXV**

1. Introduction

To myself I am only a child playing on the beach, while vast oceans of truth lie undiscovered before me.

"Isaac Newton"

1.1. Background

The background of the present research is the application of high intensity ultrasound to liquids, often referred to as ultrasonication. This technique is widespread in process engineering for homogenizing, disintegration, sonochemistry, degassing or cleaning processes, chemical synthesis, atomization, extraction and crystallization [1], shock wave lithotripsy, to improve the micro mixing [2], convective transport due to acoustic streaming [3] or the catalytic activity [4]. In ultrasonic dispersing and deagglomeration, cavitation is used to generate high shear forces in the liquid causing particle agglomerates to break into single dispersed particles. In ultrasonic emulsifying imploding cavitation bubbles cause intensive shock waves in the surrounding liquid and result in the formation of liquid jets of high velocity. In sonochemistry, the hot interior of collapsing cavitation bubbles is used to increase reaction rates, e.g., by increasing the reactivity of reagents or catalysts or by switching reaction pathways [5].

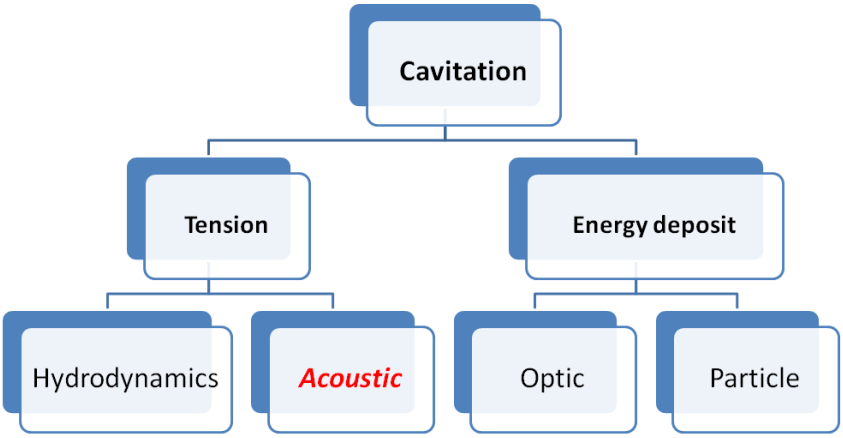

Figure 1.1.: Different types of cavitation [6].

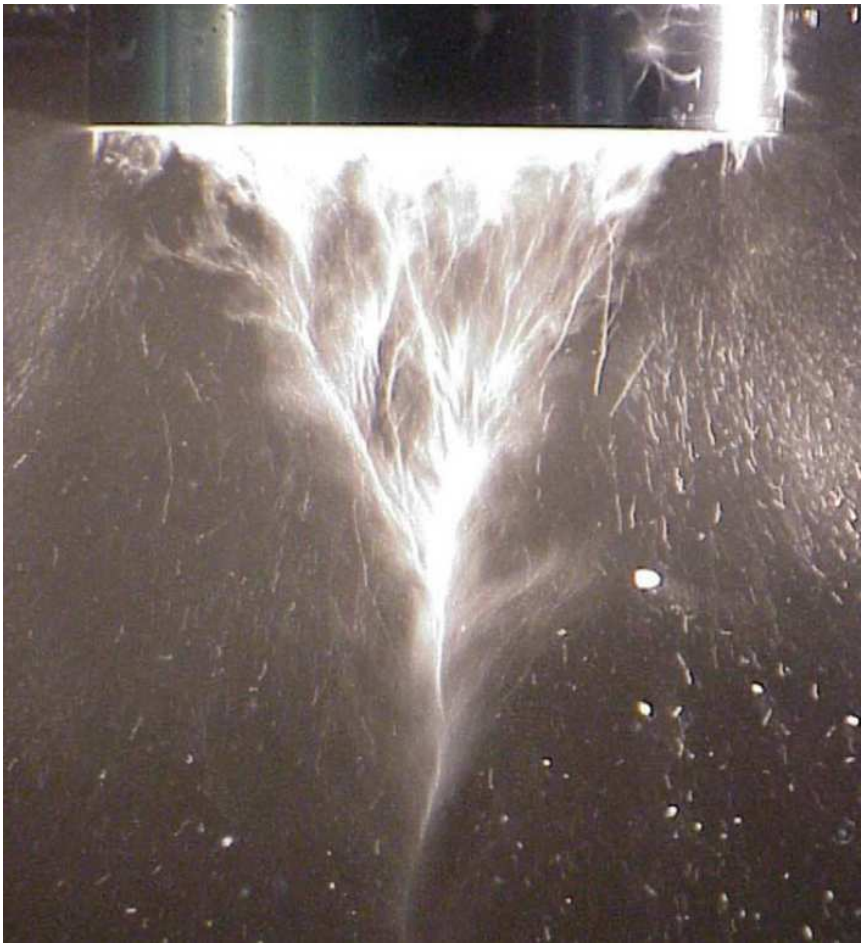

Figure 1.2.: Conical Bubble Structure (CBS) below a sonotrode [7].

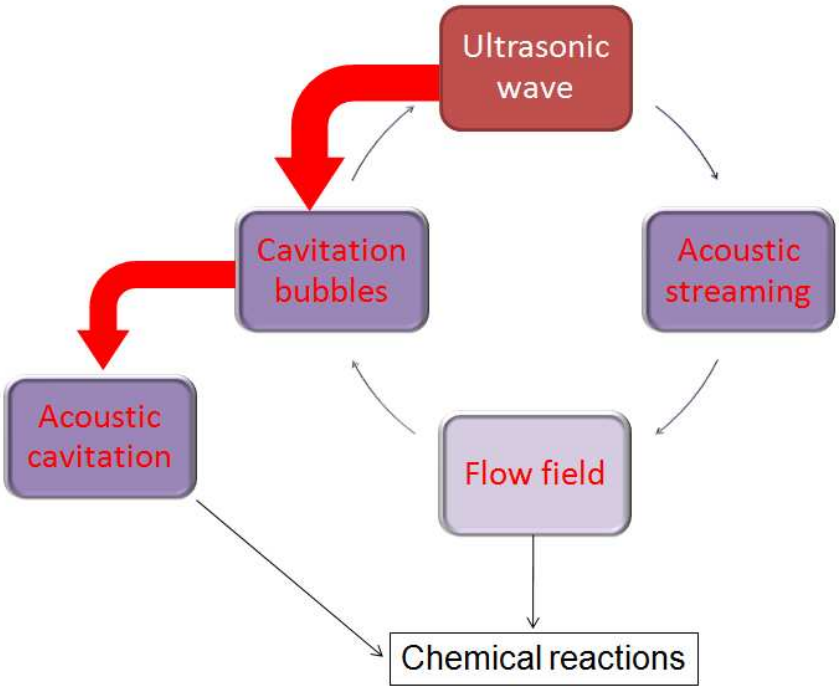

Figure 1.3.: Interaction among physical phenomena inside a sonochemical reactor.

Although cavitation may have different origins, such as in hydrodynamics or in ultrasonics, the results and eventually the main target of producing cavitating liquids is almost the same for all types of cavitation. It may occur by applying tensile stress to liquid elements using pressure change. This pressure change may be a result of an external oscillatory pressure source as in ultrasonication or due to high velocity of a flow in hydrodynamic cavitation. Furthermore, by accumulating energy, for instance using laser beams, cavitation is also accessible. Different types of cavitation are summarized in Fig. 1.1. For all types of cavitation, the effects of cavitation is basically the result of formation, growth and implosive collapse of gas and vapor bubbles in a liquid [6]. In case the source of excitation of these bubbles is a strong ultrasonic field, we are dealing with “acoustic cavitation”. Rapid variation of normal stresses in the liquid causes the bubbles to show spatially and temporarily undetermined, time dependent and stochastic behavior [8]. A typical structure of such bubbles near an ultrasound source is shown in Fig. 1.2. The acoustic energy increases the quality and the rate of chemical activities due to the presence of these bubbles [9]. Since the initial distributions of the size and the positions of the nuclei in a liquid are random, the bubble clouds formed under the influence of an acoustic field are usually deterministic and show distinct structures.

The design of sonochemical reactors requires a reliable modeling and prediction of the absorbed sound energy in the liquid, which is intimately coupled to the distribution of cavitation bubbles. The cavitation bubble dynamics, in turn, is directly or indirectly linked to the desired reactive effects. One reason why the task of modeling of acoustic cavitation is very demanding - and still not sufficiently solved - is the complicated mutual coupling of flow field, sound field, bubble dynamics, and reactive effects. This coupling is shown schematically in Fig. 1.3. A crucial point is the typically *inhomogeneous* and *dynamic* distribution of bubbles location and bubbles size.

Various geometrical reactor designs have been used or proposed in the past, as batch or through-flow systems. In any case, a central issue in their design is the choice of acoustic frequency. Most of the systems work in the lower ultrasonic range, that is, between 20 kHz and 200 kHz. However, frequencies up to the MHz range are common in the meantime. The sources of ultrasound might range from localized emitters (such as sonotrode systems with a vibrating horn or rod) to focused ones (e.g. curved or tube wall transducers) and distributed sources (e.g. bath systems). Typical design problems include:

- The variability of physical, geometrical and operation parameters such as frequency and type of the transducer and geometry of the reactor complicates a systematic design.
- The cavitation activity does not necessarily occur where wanted or expected.
- The cavitation activity is rather sensitive to various liquid parameters (e.g., temperature or dissolved gas content).
- Too high cavitation activity close to the transducer leads to shielding and strong attenuation of the wave in the volume further away.
- Inhomogeneous bubble distributions in the bulk or at objects due to shielding and/or standing acoustic waves.
- High cavitation activity may cause damage of transducer surfaces, container walls or submerged objects.

Usually the solution strategies for these issues rely on heuristic arguments, experience or trial-and-error. Reliable numerical simulation tools are still not available. Apart from these design issues, it is a matter of experience that even the same reactor or bath under virtually similar conditions can vary drastically in efficacy due to a rather sensitive dependence of the cavitation bubble population on various parameters (such as liquid temperature or dissolved gas content of the liquid). Therefore, a comprehensive model as well as a rigorous computational approach is required to tackle the problem.

1.2. Motivation and objectives

Many experimental investigations have been performed with the use of laboratory scale reactors to achieve uniformity of cavitational activity. This parameter is defined as the dissipated energy in the medium per unit volume of the reactor which is radiated from the ultrasonic source. The ideas were, for instance, investigating the extent of uniformity of the cavitational activity through the whole volume of the reactor in order to determine the degree of uniformity [10] or by taking photographs of visible bubble structures [11]. However, measuring the cavitational activity is basically impossible without disturbing the flow by intrusive measuring instruments such as hydrophones [5]. Moreover, analytical techniques for quantifying the cavitational activity, such

as the Weissler reaction, provide only integral information. Furthermore, the results of measurements are subject to uncertainties due to insufficient knowledge of process parameters such as the degree of purity of the medium [12]. Besides this group, there are other experimental investigations which concentrate on the dynamics of a single bubble and provide data to understand the single bubble behavior, such as the works of Lauterborn et al. [13] and Dangla and Poulain [14]. Since these experiments focus on a single bubble during a short period of time, they are of limited value to understand the dynamics in a bubble swarm. They suffer from providing integral and technological information required for a suitable design of the reactors.

Computational models on the other hand, are capable of predicting the cavitational activity, if suitable and validated physical models are available. Such methods may help in optimizing the geometry and operating parameters of a reactor. However, formulating a comprehensive physical model is still a challenge since not all of the phenomena are completely understood [15]. Furthermore, the disparity of the length and time scales causes severe mathematical problems. The time scale ranges from 10^{-9} sec for sonoluminecense (light emission due to the violent collapse of the bubbles) to 10^{-2} sec for the motion of the bulk liquid. The length scale varies from 10^{-6} m for the initial radius of the bubbles to 10^{-1} m for the dimensions of the reactor. In this context, the models may be divided into two major categories. The first group deals with individual bubbles in an acoustic field. For a single bubble, a Rayleigh type equation is proposed to define the radius [16] or the volume of the bubble [7] during one or several acoustic periods. As a result the pressure and temperature at the bubble position during the oscillation and after its collapse are available. Predicting the heat and mass transfer as well as the chemical consequences at a microscopic scale in these models is still challenging. Furthermore, the swarm behavior of bubbles can not be figured out from the single bubble dynamics. The second group of models concerns the modeling of the cavitational activity by finding the acoustic pressure amplitude as a field quantity. In this category, the acoustic pressure is predicted without considering the effect of bubbles [17] or by estimating their effect using simplifications [18, 19]. These approaches allow to determine the effect of parameters such as frequency and intensity of the ultrasound source or the boundaries, with respect to sound propagation and damping [20].

The governing equations of a system with flow field as well as acoustic cavitation are highly nonlinear and should cover the physics of several strong varying field magnitudes, such as for

bubbles density and their radii. This causes significant computational effort due to the need for refining computational time steps in a numerical scheme. One possibility to assassinate excessive computational tasks is to extract reasonable information from more economic and reliable numerical methods. These methods, are usually based on decoupling the problem of a single bubble (small time scale) and the whole geometry (large time scale). The first objective of the present research is to realize a coupling between the previous models for the multi-scale problem using a novel computational approach. Subsequently, the results are validated with experimental measurments and verified with analytical solutions for simplified cases. In addition, the second motivation of the present work is to extend the available models to cover more physical aspects of the phenomena. In that context, whenever possible and necessary, the essential phenomena have been modeled more rigorously.

In order to reach these goals, it is necessary to provide more detailed and reliable descriptions and models to quantify the mutual relation between flow and sound field, cavitation bubble population and energy dissipation respecting sonochemical effects. The idea here is to find a robust numerical scheme to cover different time and spatial scales as much as possible. Thus, the previous models which are developed to investigate the wave propagation phenomenon in bubbly liquids are considered for numerical simulation. However, some modifications are frequently made on these models throughout the thesis.

In the first part, the available models are extended for more realistic conditions based on physical hypotheses. Considering the compressibility of the liquid or the mutual influence of radial and translational motion of the bubbles, for instance, are two examples of these extensions. In this part, the focus of the present work is a further development of existing models documented in the literatures that are able to discover the wave propagation phenomena in bubbly liquids with severe simplifications. In the simulation part, available numerical schemes to combine the micro- and macroscopic scales are used and the novelty of this part is transferring information between these two scales. In particular, the focus is on the formulation of robust numerical schemes that are able to cover different time and length scales. One example is to generalize the information obtained from the single bubble dynamics to the swarm behavior of bubbles in the whole geometry of a reactor. To numerically investigate the problem, different computational tools are used. For instance, to investigate the linear wave equation in the frequency domain which reduces to a

Helmholtz equation, the Finite Element Method (FEM) is preferred. This method is robust and quick enough to find the acoustic pressure amplitude. However, it is not well developed to investigate the flow field of a mixture of bubbles and liquid in an Euler-Lagrange approach. Thus, the Finite Volume Method (FVM) is selected to consider the latter. A combination of different approaches is seen throughout the thesis which shows the main objective of the research.

1.3. Outline of the thesis

In chapter 2, the theory of modeling wave phenomena, which forms the basis for the present calculations, is described. Firstly, the bubble radial dynamics is explained and by combining the method proposed by Keller and Kolonder and Doinikov [21], a new formulation is derived. This equation takes the compressibility of the liquid to the first order of acoustical Mach number and also the effect of translational motion of the bubble on its radial motion into account. The nonlinear attenuation of the wave due to the bubbles is also presented in this section. Thereafter, wave propagation in bubbly liquid is explained and the basic equations, which were initially developed by Foldy [22] and then generalized by van Wijngaardan [23, 24] and Caflisch et al. [25], are presented. Here, a new method for finding the attenuation of the wave in presence of bubbles is derived which is based on the energy conservation approach. In the Lagrangian formulation for the bubble translational motion, the effect of radial motion is also considered by adding the volume change force to the summation of the forces on the bubbles. It is shown that the equation has a similar form as the ones obtained by Doinikov [26, 21], Mettin and Doinikov [27], Hay et al. [28] and Harkin et al. [29]. However, the new method is simply based on Newton's second law rather than considering a Lagrangian for the motion of a particle in an incompressible liquid. Finally, the population of bubbles and the respecting conservation equation for this population is explained.

Chapter 3 deals with details of the numerical methods used in the present work. Due to the disparity of the length and time scales, a reasonable combination between micro- and macroscopic scales should be made in the numerical approach. The generalization of the data from a single bubble motion to integral information for the whole reactor is done based on physical hypotheses. In addition, the numerical setups required for different test cases are also summarized. This section includes the definitions of the geometries, boundary conditions, grid independency stud-

ies and physical properties of the test cases.

The results of the work are presented in chapters 4 and 5 for linear and nonlinear approximations, respectively. In chapter 4, computational results for the wave propagation based on linear theory in geometrically complex sonoreactors are presented in order to shed some light on the mutual interaction of boundary conditions, wave frequency and size of the reactors and to verify results against data from literature. The goal is to analyze acoustic pressure distribution in absence and presence of cavitational bubbles. Since the linear theory is computationally less troublesome, it is used for such a parameter analyses. To take the nonlinear effect of bubbles on wave propagation, several generic test cases are constructed as well as some geometries similar to experiments in chapter 5. To verify the implemented numerical algorithms, results for simplified test cases are compared with analytical solutions. Moreover, comparisons with experimental observations are conducted. They are mainly based on pattern formation of bubbles in a sound field and their motion, especially in the vicinity of ultrasound source.

Finally, the summary of the work and some unknown aspects which are left to subsequent studies are mentioned in chapter 6.

2. Physical model

One must divide one's time between politics and equations. But our equations are much more important to me, because politics is for the present, while our equations are for eternity.

"Albert Einstein"

2.1. Bubble radial dynamics

The history of investigation of bubble radial motion goes back to Besant [30] and thereafter Rayleigh [31]. Rayleigh considered the radial motion of a spherical empty cavity by applying conservation laws of mechanical energy for the surrounding liquid and setting its time derivative to zero at the bubble surface. Although the background of Rayleigh's work was to investigate the influence of cavitation bubbles on erosion of ship propellers, the differential equation derived by him laid down the basic theory of cavitation bubbles. Later, the equation was modified by several researchers. The modification developed by Plesset [32] is the most popular one. The so-called Rayleigh-Plesset equation (RPE) for bubble dynamics is based on several assumptions from which the most important ones are the uniformity of the gas pressure inside the bubble, the incompressibility of the liquid around the bubble and the absence of translational motion of the bubble and the surrounding liquid.

Uniformity of the gas pressure inside the bubble

This assumption is verified by several models and also Direct Numerical Simulation (DNS) of the gas inside and the liquid outside of the bubble by Lin et al. [33]. It has been shown that for a wide range of parameters, this assumption is valid. Due to the rapid oscillation of the bubble and its small size, the pressure of the gas cannot vary locally. Therefore, one can assume that the parameter p_g is a uniform value inside the bubble. It may be obtained by comparing the equilibrium pressure and the instantaneous pressure during the oscillation. The method of calculation of this pressure in the frame of the present computational models will be explained later in this chapter.

Compressibility of the liquid around the bubble

The effect of compressibility of the liquid on the radial motion of a bubble has been studied by Gilmore [34], Keller and Kolodner [35], Keller and Miksis [36], Prosperetti [37], Prosperetti and Lezzi [38] and Lezzi and Prosperetti [39] and others. It has been shown that the compressibility of the liquid has significant effect on the oscillation of the bubble at the final stages of its collapse, the dissipation of energy during the radial motion and the local pressure and temperature of the liquid after bubble collapse. In the last two references, it is revealed that expanding the enthalpy of the liquid as a series of pressure leads to errors in the final solution of the equation. It is proposed that the enthalpy should be considered directly in the equation. In this way, the Gilmore equation describes the bubble radial dynamics more precisely. However, this equation also considers the change of the speed of sound in the liquid as a function of enthalpy (it is not related to the change of sound velocity due to damping of the waves in bubbly liquids). It is also shown by Parlitz et al. [40] and Lauterborn and Kurz [41] that the results of Gilmore equation are similar to the ones obtained by considering the speed of sound as a constant, which is a Keller-type equation [36]. Consequently, in the present work the enthalpy is not expanded as a series of pressure.

The influence of liquid compressibility appears in the differential equation for bubble oscillation as a dimensionless number which is called acoustical Mach number. This number is the ratio between the radial velocity of the bubble wall $\dot{R}$ to the celerity of pressure waves c. It is clear that when this ratio is in the order of one, which is typical at the collapse time, one should consider its effects. Neppiras [42] found that the incompressible form of the Rayleigh-Plesset equation is accurate enough, if this ratio does not exceed 0.2. This is valid for bubbles in “stable cavitation”. This type of oscillation usually occurs in the case of low pressure amplitude which causes the bubbles to oscillate from one to even hundreds of acoustic cycles. However, for moderate and high pressure amplitudes which leads to violent collapse of bubbles, the compressibility effect should be taken into account.

It is widely discussed in the literatures that the considered order of acoustical Mach number affects the role of compressibility in the radial dynamics equation. Leppington and Levine [43], for instance, proposed a velocity potential around a pulsating and translating bubble to the third order of the speed of sound. The final form of the differential equation is complicated and

not explained here. However, it is commonly accepted that the equations which are accurate to the second order of $\dot{R}/c$, give reasonable predictions for the bubble radius. Thus, the terms containing $(\dot{R}/c)^2$ may be ignored.

Considering the above discussions, one may restrict the problem to the first order of the acoustical Mach number. However, according to Parlitz et al. [40] and Lauterborn and Kurz [41], the speed of sound is assumed as a constant in deriving the radial dynamics equation. It is worth mentioning that this assumption is to avoid additional complexity in the radial dynamics part of the model. Obviously, the change of speed of sound due to the presence of bubbles in propagation of the wave is considered and the corresponding method is described later.

Translational motion of the bubble

Under the action of an ultrasound source the habitat of bubbles is of great importance. This is due to their effect on the damping of the wave. In addition, it has been shown that translation has influence on their radial oscillation. This effect, which is based on the conservation of energy in the liquid around the bubble is studied by several authors. The main idea is deduced by writing a Lagrangian or Hamiltonian of the total energy of the liquid and finding the coupled pulsation and translational motion of the bubble, such as the works of Doinikov [21, 26], Harkin et al. [29] and Hay et al. [28]. However, in the case of a compressible liquid, the Lagrangian formulation is not valid anymore because the informations are moving with a finite speed of sound. Thus, other approaches, such as the Oguz-Prosperetti theorem [44] or starting from the initial wave equation for the potential flow of the liquid around the bubble should be used. Here, the second one which is also used by Keller and Kolodner [35] and also recently by Fuster and Colonius [45] is used.

Derivation of bubble radial dynamics equation

Usually, the effects of heat transfer, mass transfer, phase change and chemical reactions are neglected. These effects influence the radius of the bubble through the pressure of the gas in it [9]. Besides that, complex shape oscillations are another family of phenomena that cause instability in the bubble surface and change the shape of the initially spherical bubble. For the sake of simplicity, in the present work it is assumed that the bubble always remains spherical. Moreover, the bubble moves with the translational velocity u in x direction. The geometry of the

model is shown in Fig. 2.1.

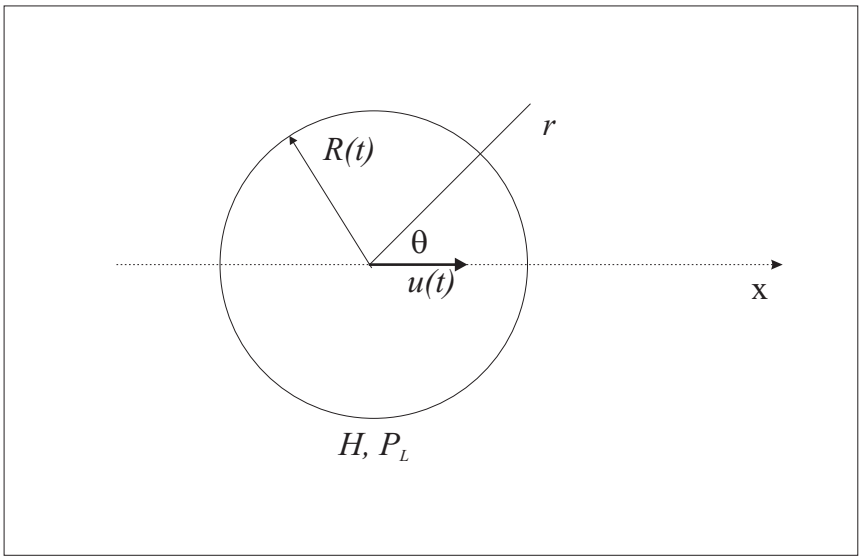

Figure 2.1.: Geometry of a bubble with coupled pulsation and translation.

The potential function of liquid motion in a compressible liquid should satisfy the wave equation

$$\nabla^2\phi - \frac{1}{c^2}\phi_{tt} = 0\,. \tag{2.1}$$

The general solution of this equation in spherical coordinates has the form [21]

$$\phi(r,t) = \frac{f(\eta(r,t))}{r} + \left(\frac{g(\eta(r,t))}{r^2} + \frac{g'(\eta(r,t))}{cr}\right) P_1(cos\theta)\,, \eta(r,t) = t - \frac{r}{c}. \tag{2.2}$$

in which $P_1(x) = x$ is the second Legendre polynomial. The following kinematic and dynamic boundary conditions at $r = R(t)$ are applicable to Eq. (2.2):

$$\phi_r = \dot{R} + ucos\theta, \tag{2.3}$$

$$h(r) = H = -(\phi_t + \frac{1}{2}v^2)\,, \tag{2.4}$$

where $h(r)$ is the enthalpy as a function of radial coordinate and v is the radial velocity of the liquid. From Eq. (2.2), it is concluded that

$$\phi_t = \frac{f'}{r} + (\frac{g'}{r^2} + \frac{g''}{cr})cos\theta\,, \tag{2.5}$$

$$\phi_r = -(\frac{f}{r^2} + \frac{f'}{cr}) - (\frac{2g}{r^3} + \frac{2g'}{cr^2} + O(c^{-2}))cos\theta\,. \tag{2.6}$$

In what follows, the terms including $O(c^{-2})$ are ignored. Comparing Eq. (2.3) and Eq. (2.6) reveals that

$$\frac{f}{R^2} + \frac{f'}{cR} = -\dot{R}\,, \tag{2.7}$$

and

$$\frac{g}{R^3} + \frac{g'}{cR^2} = -\frac{1}{2}u\,. \tag{2.8}$$

In addition, by substituting Eq. (2.5) and Eq. (2.6) in Eq. (2.4) and integrating over θ for the whole sphere, one obtains

$$\frac{f'}{R} + \frac{1}{2}\left(\frac{f}{R^2} + \frac{f'}{cR}\right)^2 + \frac{1}{4}\left(\frac{2g}{R^3} + \frac{2g'}{cR^2}\right)^2 = -H\,. \tag{2.9}$$

The reason of integration is that the enthalpy (or pressure) of the liquid around the small bubble is assumed constant. Otherwise, one should expect that the translational motion leads to a non-spherical shape for the bubble. In this case, the basic assumption of sphericity is no more valid. Besides that, assuming constant enthalpy (or pressure) is reasonable because the size of the bubbles is much smaller than the wave length of the external wave. This assumption is also made elsewhere to derive the radial dynamics equation for pulsating bubbles [46, 47].

Now, by replacing the second and third terms on the left hand side of Eq. (2.9) from Eq. (2.7) and Eq. (2.8) respectively, one obtains

$$f' = -R\left(H + \frac{1}{2}\dot{R}^2 + \frac{1}{4}u^2\right)\,, \tag{2.10}$$

and substituting in Eq. (2.7) reads

$$f = -\dot{R}R^2 + \frac{R^2}{c}\left(H + \frac{1}{2}\dot{R}^2 + \frac{1}{4}u^2\right)\,. \tag{2.11}$$

Derivating Eq. (2.11) with respect to time by knowing that at $r = R(t)$, $\dot{f} = (1 - \dot{R}/c)f'$ leads to

$$f'\big(1 - \frac{\dot{R}}{c}\big) = -\ddot{R}R^2 - 2\dot{R}^2R + \frac{2R\dot{R}}{c}\left(H + \frac{1}{2}\dot{R}^2 + \frac{1}{4}u^2\right) + \frac{R^2}{c}\left(\dot{H} + \dot{R}\ddot{R} + \frac{1}{2}u\dot{u}\right)\,. \tag{2.12}$$

Finally, substituting f' form Eq. (2.10) in Eq. (2.12) and rearranging, gives

$$R\ddot{R}\left(1-\frac{\dot{R}}{c}\right)+\frac{3}{2}\dot{R}^2\left(1-\frac{\dot{R}}{3c}\right)=\left(1+\frac{\dot{R}}{c}+\frac{R}{c}\frac{d}{dt}\right)\left(H+\frac{1}{4}u^2\right)\,, \tag{2.13}$$

in which overdots denote differentiation with respect to time. This equation is precise to the order of $O(c^{-2})$. In addition, it can be compared to the one obtained by Doinikov [21] and Fuster and Colonius [45]. However, in the former, the enthalpy of the liquid is approximated by the pressure difference divided by the density, while in the latter the effect of translation is ignored. Here, H is calculated from the equation of state for liquids which relates the pressure and the density to each other and is valid over a wide range of these parameters, i.e.

$$p=A(\frac{\rho}{\rho_0})^n-B\,, \tag{2.14}$$

where A and B are two constants differing by the ambient pressure and n is an integer. For water, for instance, they are equal to $A=(3000+p_0)$ bar, $B=3000$ bar and $n=7$ [42]. By applying Eq. (2.14) to the definition of enthalpy which is

$$h(r)=\int_{p_\infty}^{p}\frac{dp}{\rho} \tag{2.15}$$

the value of H in Eq. (2.13) is obtained as

$$H=\frac{nA^{1/n}}{(n-1)\rho}\big((p_l+B)^{(n-1)/n}-(p_\infty+B)^{(n-1)/n}\big)\,. \tag{2.16}$$

In this equation, p_l is the pressure in the liquid just outside of the bubble. This pressure differs from the pressure inside the bubble due to the effects of viscosity and surface tension. In the present work, the vapor pressure inside the bubble is neglected and it is assumed that the bubble is totally filled with gas. Thus, balance of forces at the surface of the bubble gives

$$p_l(r=R)=p_g(r=R)-\frac{2\sigma}{R}-\frac{4\mu\dot{R}}{R}\,. \tag{2.17}$$

Besides that, the value of p_∞ in case of an external acoustic excitation is written as

$$p_\infty(t)=p_0-P_a sin(\omega t)\,, \tag{2.18}$$

which means there is no difference between the bubble center and its surface regarding the value of the external pressure source. As it is described before, this is valid when the radius of a bubble

is much smaller than the wavelength of the ultrasonic wave.

The gas inside the bubble can be treated isothermally or adiabatically depending on the time scales of heat transfer and radial motion [48]. Thus, the following relation is proposed to find the pressure of the gas inside the bubble, p_g, during an oscillation

$$p_g = (p_0 + 2\frac{\sigma}{R_0})(\frac{R}{R_0})^{3\eta}\,, \tag{2.19}$$

in which $\eta = 1$ stands for isothermal situations and $\eta = \gamma$ is related to adiabatic changes. It is proposed by Storey and Szeri [9] that by comparing the two dynamic and heat transfer time scales, one of the two possible values for η can be used to calculate the gas pressure. The dynamic and heat transfer time scales are defined as

$$\tau_{dyn} = \frac{R}{\dot{R}}\,, \tag{2.20}$$

and

$$\tau_{diff} = (\frac{RR_0}{\alpha})^2\omega\,, \tag{2.21}$$

where α is the thermal diffusivity of the gas inside the bubble. If the bubble undergoes violent collapse, τ_{dyn} decreases and the gas behaves adiabatically. Before that time, the gas has sufficient time to exchange heat with the liquid and behaves isothermally. The set of Eq. (2.13) and Eqs. (2.16) to (2.21) is sufficient to investigate the radial dynamics of the bubbles.

If the linear theory of bubbles oscillation is considered, some approximate solutions for estimating a single bubble behavior such as the magnitude and direction of the primary Bjerknes force on the bubble are accessible. These approximate solutions, however, are helpful in verifying the results of the numerical algorithms which are applied in Computational Fluid Dynamics (CFD) methods. The main concept is deduced by applying a small amplitude perturbation in pressure that results in small amplitudes in bubble radius. Thus, one can write

$$p = p_0(1 - \epsilon_1 sin(\omega t))\,, \tag{2.22}$$

and

$$R = R_0(1 + \epsilon_2 sin(\omega t)) \,. \tag{2.23}$$

Upon this linearization, the ordinary differential equation (ODE) for the bubble dynamics, leads to an inhomogeneous second order ODE. Therefore, if the two conditions as $4\mu/\rho c \ll R_0 \ll c/\omega$ and $P_a \ll p_0$ are fulfilled simultaneously, by expanding the enthalpy as

$$H = \frac{p - p_\infty}{\rho} \,, \tag{2.24}$$

and assuming $R(t) = R_0 + R'(t)$, one obtains

$$\ddot{R}' + b\dot{R}' + \omega_0^2 R' = -\frac{P_a}{\rho R_0} sin(\omega t) \,, \tag{2.25}$$

where ω_0 is the resonant frequency of the bubbles and b is the damping factor. Equation (2.25) clearly states that a single bubble in a sound field oscillates as a damped spring-mass system. The dissipation of acoustic energy is a result of viscous, thermal and radiation damping which is discussed later in this chapter. The solution of this equation has the form of $R'(t) = R'_a sin(\omega t + \phi)$ in which the phase shift ϕ depends on the initial radius of the bubble and the frequency of the wave and R'_a is the amplitude of oscillations. The main question here is that up to which amplitude of acoustic pressure, the assumption of linearization is valid. The variation of bubble radius obtained from Eq. (2.13) and Eq. (2.25) is shown in Fig. 2.2. The results are compared for a pressure amplitude of P_a= 10 kPa, ultrasound frequency of f= 20 kHz and initial radius of R_0= 5 μm in Fig. 2.2-b. To solve the radial dynamics equation an adaptive 4^{th} order Runge-Kutta method is used. It is clear that for this range of pressure amplitudes, the linear theory predicts the bubble behavior quite well. However, the solution of Eq. (2.13) in the case of P_a= 120 kPa in Fig. 2.2-c, which is in the non-linear region, shows that the linear approximation is pointless. Therefore, the average values required for calculating the forces on the bubble in the Lagrangian frame (such as primary Bjerknes and volume variation forces) must be obtained from the solution of Eq. (2.13) instead of linear theory. However, to verify the applied method in numerical simulations, for some simple test cases the results of linear theory are mentioned and compared. In addition, the idea of linearizing the bubble radial dynamics equation as well as the pressure propagation equation leads to the linear theory which is used in chapter 4.

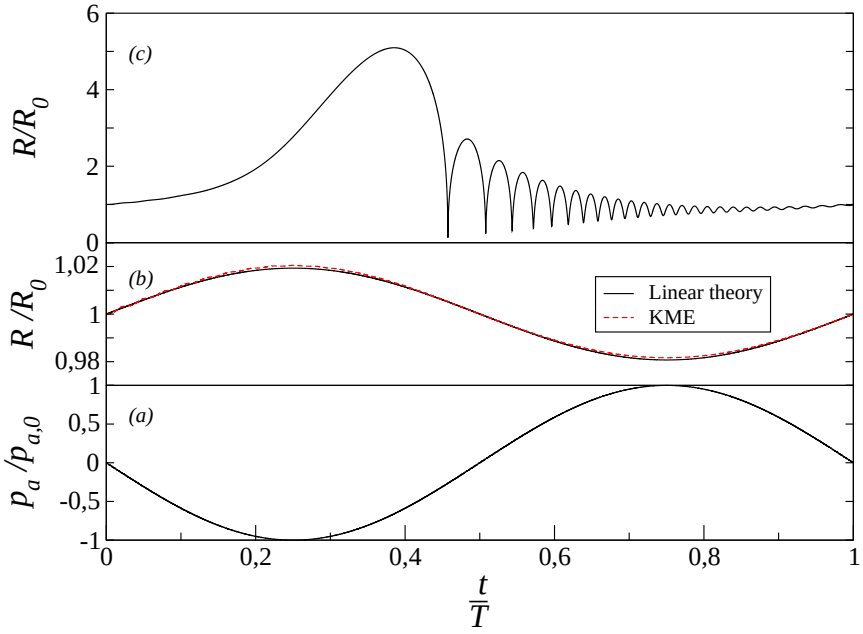

Figure 2.2.: Variation of radius of a 5 μm bubble excited by a 20 kHz wave. (a): normalized acoustic pressure, (b): comparison between linear theory (Eq. (2.25)) and Eq. (2.13) for P_a= 10 kPa and (c) Variation of bubble radius for P_a= 120 kPa.

2.2. Wave propagation in bubbly liquids

Remarkable progress in investigating wave propagation in bubbly liquids is due to underwater explosion research started during and after the second world war [49]. Since the 1940s, it is well-known that waves are dissipated in water due to the presence of gas bubbles. The physical background of this dissipation can be explained as propagation of a wave through bubbles which are considered as mechanical oscillators. These oscillatory objects cause loss of energy which is called "wave attenuation". The wave propagation equation including the effect of damping due to the presence of bubbles is often termed "dispersion relation". The pioneering work of Foldy [22] was one of the first attempts which assumed statistically random distributed bubbles as linear scattering objects. The result was a linear dispersion relation which suffered from many simplifying assumptions.

Van Wijngaardan [23, 24] made a comprehensive study on the phenomenon and proposed a closed set of equations. This set of equations, known as "effective equations", usually contains the conservation of mass and momentum for the mixture, the equation of state for the gas phase and the radial dynamics of bubbles. His model was based on small amplitude disturbances propagating in a bubbly liquid which in turn was modeled based on volume-averaged properties for a multiphase medium. Although his method was heuristic, it was generally accepted and is the basis of several studies after him. Caflisch et al. [25] derived a similar set of effective equations in a more rigorous, rather than heuristic approach. The main idea of the model is to formulate the problem in terms of field variables, such as bubbles radii $R(t, \vec{x})$. However, there is only one ODE available for this parameter which is the bubble radial dynamics equation. This is one of the limitations of the model from a computational point of view since relating a time varying field quantity at small time scale to other field quantities such as pressure at much larger time scales is problematic. The reason is that the effect of bubbles radii with much smaller time scale appears in the equation of pressure wave propagation as a source term. The method was later modified by the same authors [50] for higher concentrations of bubbles and also by Miksis and Ting [51] for finite amplitudes of bubble oscillations. The simple form of their equations is still in use elsewhere. The main assumptions of the Caflisch "continuum approach" [52] which is the

A part of this section has been published as: R. Jamshidi; G. Brenner, Dissipation of ultrasonic wave propagation in bubbly liquids considering the effect of compressibility to the first order of acoustical Mach number. *Ultrasonics*, 53(4):842-848, 2013.

basis of the present approach, can be summarized as follows:

- The pressure and velocity fields felt by each bubble are local fields, i.e., each bubble is not influenced by local fields of the other bubbles.
- The typical interbubble distance is large compared with typical bubble radii which corresponds to a small bubble volume fraction.
- The bubble centers do not move, since the wave propagation is of interest rather than the bulk liquid motion.
- The bubbles are assumed spherical with a uniform internal pressure.
- The liquid is nearly incompressible with constant density and sound speed which leads to an irrotational radial potential flow around any individual bubble.

The first assumption states that there is one pressure field, p, which is felt by bubbles in a mixture. This assumption could be justified by considering a large distance between two bubbles. In other words, it states that the bubbles and the liquid have the same velocities and pressure which in case of a dilute bubbly system is reasonable.
The second assumption is often justified by experimental observations. For instance, the observed microbubbles radii are in the range of 5 μm to 100 μm. For a typical value of 20 kHz of the frequency of an acoustic wave, the wavelength λ is equal to 75 mm which is much larger than the radii of the bubbles.
The third assumption can be justified since that the time scale of the motion of bubbles in a liquid is some orders of magnitude larger than their radial oscillation. In other words, in the time scale of a typical acoustic wave propagation (around μs), it is reasonable to assume bubbles as fixed objects in space. However, for larger time scales, different phenomena such as external convective source, acoustic streaming and primary and secondary Bjerknes forces result in bubbles motion. This motion changes the wave pattern in a bubbly liquid and is considered in the present approach using a Lagrangian tracing of bubbles.
The forth assumption is sensible until the violent collapse of inertial bubbles. Surface fluctuations, such as Kelvin-Helmholtz instabilities, are of importance in case of augmented surface tension effects. This usually happens for small bubble radii at the collapse time. Otherwise, the

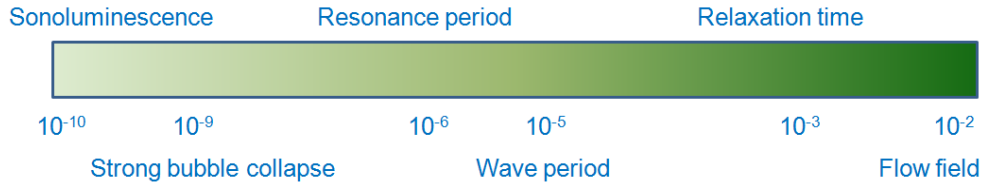

Figure 2.3.: Temporal scales of relevant physical phenomena inside a sonochemical reactor.

assumption of sphericity for the bubbles is valid especially when their population and migration is of interest. In addition, considering a uniform pressure inside the bubble is shown to be precise enough by DNS simulation [33].

Assuming an incompressible liquid around the bubble is widely studied in the literatures. It is well known that validity of this assumption depends on different length scales of the problem, that are bubble radius, distance among bubbles and wavelength of the acoustic wave. Near the bubble surface, where the lengths are in the order of bubble radius, it can be assumed that information are propagated with infinite speed. Therefore, the Laplace equation is valid to find the velocity potential around the bubble [37, 38, 39]. However, for length scales of the order of the acoustic wave length, the compressibility of the medium should be taken into account and the wave equation with a finite speed of sound should be considered [46, 47]. It is well accepted that, even if the compressibility is only considered in the radial dynamics of the bubbles rather than the bulk liquid motion, the model is still valid. Therefore, for modeling the wave propagation in the whole geometry of a reactor with approximately the same dimensions as the wavelength and considering bubble dynamics simultaneously, one should assume the flow to be incompressible in the bulk liquid and compressible around the bubble to cover the collapse phenomenon, see Sec. 2.1.

The problem regarding the Caflisch model is the high degree of nonlinearity as well as relating the microscale phenomena of bubble oscillations to macroscale events which occur in a bubbly liquid. For instance, in the case of sonochemical applications, the time scale for sonoluminecense is 10^{-9} sec [53]. The resonance period of the observed nuclei in experiments is in the order of 10^{-6} sec. The period of the common ultrasound waves in sonochemical reactors has the order of 10^{-5} sec. The time scale of the flow in the bulk liquid which transforms the bubbles from one point to another is 10^{-1} sec. On the other hand, the length scale changes from 10^{-6} m for the radius of bubbles to 10^{-1} m for the reactor geometry. This wide range of temporal scales is shown in Fig 2.3.

Several authors have tried to solve the effective equations of the Caflisch model mainly by linearization of the equations. The most popular method was firstly presented by Prosperetti [54] which was later accomplished by the work of Commander and Prosperetti [55]. All these attempts were based on the linearization of the bubble radial motion in a mass-spring-like model. The effect of acoustic power appears as an external force and the dissipation as the damping term in the differential equation, see for example Devin [56], Medwin [57] and Prosperetti [58]. However, it is shown that such expansions as $R = R_0(1 + x)$ for bubble radius will not capture all the energy which is lost during a bubble oscillation accurately [59]. For sonochemistry, the linearized formulation is applied by Dähnke and Keil [17]. In a first step, they solved the linear wave equation in the frequency domain, that is, the Helmholtz equation, in absence and in presence of cavitation bubbles. The volume fraction of bubbles was considered at different constant values that are common for sonochemical reactors (between 10^{-5} and 10^{-1}) [18]. The volume fraction of cavitation bubbles was later approximated as a linear function of the ultrasound pressure amplitude after the so-called “Blake threshold” [19]. On the basis of that model, they investigated different geometries and arrangements of ultrasound sources to determine the pressure amplitude and the extent of uniformity in the reactor. Their results show that a larger fraction of the reactor volume is excited by ultrasound at higher frequencies. In addition, if the volume fraction of bubbles is increased, the waves are completely damped in the vicinity of the irradiation source, regardless of the frequency of the wave [60]. Although the approach is satisfactory for qualitative design of sonochemical reactors, it suffers from deficiencies regarding the dissipation of wave in the bubbly liquid. The assumption of ”Bubble density is high where acoustic pressure is high”, should be addressed more precisely, which is one of the main goals of the present work. Therefore, in this section the method of Commander and Prosperetti [55] to derive the effective equations of the Caflisch model is presented. Then, several damping factors which lead to dissipation of the wave due to the presence of bubbles are discussed and it is shown that the nonlinear models are more robust with respect to the previous linear ones.

2.2.1. Derivation of the effective equations of the Caflisch model

Assume a bubbly liquid in which all N bubbles per unit volume have the same radius R. Then, the parameter β, the volume fraction of bubbles, is defined as

$$\beta = \frac{4\pi}{3} N R^3 \,. \tag{2.26}$$

It should be noted that both N and R are functions of time. However, one can consider N as a constant at the time scale of bubbles oscillation. The density of a mixture of liquid and gas is written as

$$\rho_{mix} = \beta \rho_g + (1-\beta)\rho_l \,, \tag{2.27}$$

in which ρ_g and ρ_l denote the densities of the gas and the liquid, respectively. The first term is negligible due to small value of the gas density as well as low volume fraction of bubbles. The volume-averaged models which work with the properties of a mixture in a multiphase flow is of interest in this approach. Thus, the equation of conservation of mass for the mixture is written as

$$\frac{\partial \rho_{mix}}{\partial t} + \nabla \cdot (\rho_{mix} \vec{u}) = 0 \,, \tag{2.28}$$

where $\vec{u}$ is the average velocity for both phases. By substituting Eq. (2.27) in Eq. (2.28), one obtains

$$\frac{1}{\rho_l} \frac{D\rho_l}{Dt} + \nabla \cdot \vec{u} = \frac{1}{1-\beta} \frac{D\beta}{Dt} \,, \tag{2.29}$$

in which $\frac{D}{Dt}$ denotes the material derivative of a variable. For small values of bubble volume fraction, i.e., $\beta \ll 1$, the coefficient of the derivative on the Right Hand Side (RHS) of this equation is approximately equals to 1. Moreover, comparing the two counterparts of the material derivative of β reveals that its time derivative is much larger than its spatial one. The reason is that the radii of the bubbles change much fast in time and cause high values for $\partial\beta/\partial t$. Meanwhile, the spatial change in β, i.e., $\vec{u} \cdot \nabla\beta$ occurs much slower due to lower values for the mixture velocity. The same analysis is applicable to ρ_l. Thus, Eq. (2.29) is simplified to

$$\frac{1}{\rho_l} \frac{\partial \rho_l}{\partial t} + \nabla \cdot \vec{u} = \frac{\partial \beta}{\partial t} \,. \tag{2.30}$$

Furthermore, the equation of state for an incompressible liquid reads

$$\frac{\partial p}{\partial \rho} = c^2 \,. \tag{2.31}$$

Finally, substituting Eq. (2.31) in Eq. (2.30) gives the continuity equation of the Caflisch model

$$\frac{1}{\rho_l c^2}\frac{\partial p}{\partial t} + \nabla \cdot \vec{u} = \frac{\partial \beta}{\partial t} \,. \tag{2.32}$$

The conservation of momentum is obtained in an easier way since all of the convective terms are eliminated. The terms which contain spatial derivatives of $\vec{u}$ are ignored as discussed before. Thus, only the time derivative of the velocity field as well as the pressure gradient remains in the equation. The momentum conservation equation reads

$$\rho_{mix}\frac{\partial \vec{u}}{\partial t} = -\nabla p \,, \tag{2.33}$$

and using Eq. (2.27), one obtains the momentum equation of the Caflisch model for a bubbly liquid

$$\rho_l \frac{\partial \vec{u}}{\partial t} + \nabla p = 0 \,. \tag{2.34}$$

The set of Eqs. (2.32), (2.34) and (2.13) comprises a closed system of equations for solving the propagation of pressure fluctuation in a mixture of gas bubbles and a liquid. To derive the "wave equation" form of this set of equations, one can apply a partial time derivative to Eq. (2.32) and taking the divergence of Eq.(2.34) to eliminate $\vec{u}$. The result is

$$\frac{1}{c^2}\frac{\partial^2 p}{\partial t^2} - \nabla^2 p = \rho_l \frac{\partial^2 \beta}{\partial t^2} \,. \tag{2.35}$$

By neglecting the RHS and assuming a harmonic wave, it is easy to show that the integral of the RHS over one acoustic cycle is zero. Thus, this form of the equation is an energy balance equation for pressure fluctuations in a liquid. In other words, the RHS which is nonzero for a bubbly liquid is the factor that leads to dissipation of acoustic energy.

From this point forward, Eq. (2.35) as well as the radial dynamics of bubbles are considered for numerical simulation. The simplifying assumptions required for simulations should be consistent and meanwhile should let us to tackle the problem in an economic way. To avoid expensive computational efforts, one requires to assassinate the time derivative in the model. Otherwise, the

time steps have to be discretized to smaller intervals than μs. Therefore, transforming the time-dependent equations to time-independent ones is a solution. This is usually done by assuming mono-harmonic wave propagation and finding the spatially varying component of the wave. The main novel assumption of the present work which is applicable in sonochemical reactors, is that in Eq. (2.35), the Left Hand Side (LHS) has a time scale in the order of μs while the RHS could be considered to change with larger time scales, namely milliseconds. This assumption is discussed later in this chapter after investigating simplified forms of the problem.

2.2.2. Linear wave equation without bubbles

Neglecting the RHS of Eq. (2.35), i.e., neglecting damping of the wave due to bubbles, the equation is reduced to the linear wave equation

$$\frac{\partial^2 p}{\partial t^2} - c^2 \nabla^2 p = 0\,. \tag{2.36}$$

For a given frequency ω, the pressure may be decomposed into a spatially varying amplitude and a harmonic contribution as

$$p(\vec{r},t) = \frac{1}{2}\big(P(\vec{r})e^{i\omega t} + \overline{P}(\vec{r})e^{-i\omega t}\big)\,, \tag{2.37}$$

where the overline denotes the complex conjugate. By substituting Eq. (2.37) in Eq. (2.36), the time independent wave equation in the frequency domain is obtained as

$$\nabla^2 P + k^2 P = 0\,. \tag{2.38}$$

In this equation, $k = \omega/c$ denotes the wave number. Equation (2.38) is usually denoted as Helmholtz equation.

This simple form of the wave propagation is useful, fast to analyze and robust enough in investigating different geometries and the boundary conditions of a reactor. Using a numerical approach, such as the Finite Difference Method (FDM), FVM or FEM the equation may be solved in an arbitrary geometry with high degree of precision. Thus, the Helmholtz equation may be used to estimate the influence of frequency, wall boundary conditions or power input on the principle form of wave patterns in an ultrasound reactor.

2.2.3. Linearized wave equation in bubbly liquids- Linear attenuation

Using linearized form of the wave propagation equation in bubbly liquids, different damping mechanisms due to bubbles may be understood in a straightforward way. Recent review of Ainslie and Leighton [59] describes the damping factors in details. The linearization procedure which is made by Prosperetti [54] and later Commander and Prosperetti [55] are explained briefly and the theory is called the "linear theory" hereafter. The theory is validated by comparison with experimental results [55] for different test cases. Moreover, plenty of investigations are conducted to improve the theory from which the one proposed by Ando et al. is the most recent and rigorous one [61]. It has been shown that by considering a reasonable log-normal size distribution function for the bubbles, the theory is precise enough in computing the phase velocity and "attenuation" of the wave. The goal of the theory is to show how a time-independent wave equation including the effect of bubbles assists in realizing the scattering of acoustic waves. The final form of the wave equation may be written as

$$\nabla^2 P + k_m^2 P = 0\,, \tag{2.39}$$

where k_m is the complex wave number defined as

$$k_m^2 = \frac{\omega^2}{c^2} + 4\pi\omega^2 \int_O^\infty \frac{R_0 f(R_0, \mathbf{r})}{\omega_0^2 - \omega^2 + 2ib\omega} dR_0\,. \tag{2.40}$$

The resonant frequency of the bubbles, ω_0 is defined as

$$\omega_0^2 = \frac{p_0}{\rho {R_0}^2} \left(Re\Phi - \frac{2\sigma}{R_0 p_0} \right)\,. \tag{2.41}$$

Here, p_0 is the undisturbed pressure in the bubble position that is higher than the equilibrium pressure p_∞ in the liquid by the amount of $2\sigma/R_0$ due to the surface tension σ. The complex dimensionless parameter Φ is defined as

$$\Phi = \frac{3\gamma}{1 - 3(\gamma - 1)i\chi \left[(i/\chi)^{1/2} \coth(i/\chi)^{1/2} - 1 \right]}\,. \tag{2.42}$$

In this expression, γ is the specific heat ratio of the gas inside the bubble and the dimensionless parameter χ is defined as

$$\chi = \frac{D}{\omega {R_0}^2}\,. \tag{2.43}$$

Here, D is the thermal diffusivity of the gas. The damping factor b in Eq. (2.40) is defined as

$$b = \frac{2\mu}{\rho {R_0}^2} + \frac{p_0}{2\rho\omega {R_0}^2} Im\Phi + \frac{\omega^2 R_0}{2c}\,, \tag{2.44}$$

where μ denotes the viscosity of the medium. For a monodisperse bubble distribution with equal equilibrium radius R_0, the complex wave number can be simplified to

$$k_m^2 = \frac{\omega^2}{c^2}\left(1 + \frac{4\pi c^2 N R_0}{\omega_0^2 - \omega^2 + 2ib\omega}\right)\,. \tag{2.45}$$

The final expression for the complex wave number has an imaginary part denoted as the "attenuation coefficient". This coefficient indicates the amount of acoustic energy which is dissipated in the medium. Once k_m has been obtained, Eq. (2.39) can be solved by numerical methods. To solve this equation, one should consider reasonable magnitudes for β. This is done in this work by taking β as zero, a constant value or a function of pressure amplitude.

2.2.4. Nonlinear attenuation of wave propagation

In this section, a new method for calculating the damping of the wave based on an energy conservation approach is proposed. The method was developed first by Louisnard [62] using the RPE. Since the linear theory predicts much lower values for the dissipation of the wave, higher local amplitudes for the acoustic pressure compared to measured values in experiments are calculated [7]. The new method depicts that the nonlinear damping is several orders of magnitude higher than the linear one and leads to reasonable results in modeling the wave propagation. However, in his preliminary work and thereafter [63, 64], Louisnard considered only the viscous and thermal damping. Since the RPE is developed for the radial dynamics of bubbles in an incompressible liquid, the radiation damping can not be extracted from investigating this equation. The applied method is straightforward because the term related to viscosity appears in the bubble dynamics equation explicitly. Previously, the same idea was applied by Joseph and Wang [65] and the same expression for the dissipation of energy due to viscosity was obtained. As it is discussed before (Sec. 2.1), it is essential to take the compressibility of the liquid at the time of the bubble collapse. Thus, the approach is modified by considering the KME which is precise enough to the first order of the acoustical Mach number. The reason for selecting KME is that for the range of parameters in this study, this equation gives the same results as Gilmore equation [34] for bubble

radial dynamics [40]. In addition, the mathematical work is more straightforward compared to considering the Gilmore equation and the sources of dissipated power are distinguishable and justifiable. The effect of compressibility on the viscosity of the bulk liquid is not considered as in the work of Chapman and Plesset [66]. However, it is concluded that the radiation damping plays its role via the kinetic energy of the slightly compressible liquid as denoted by Doinikov and Dayton [67]. The pursued target is to investigate the significance of the radiation damping as a result of the compressibility of the liquid around the bubble. It is well known that the Caflisch model is developed for incompressible fluids and the compressibility of the liquid is considered only to the first order of acoustical Mach number in the KME, as stated in [63]. However, even in its simplified form in the KME, it is shown that the the acoustic radiation is of importance.
The approach starts from the basic mass and momentum equations of the Caflisch model which are Eqs. (2.32), (2.34) and repeating here the dynamics of the bubbles including compressibility effects to the first order of acoustic Mach number [36] for convenience

$$\rho\left((1-\frac{\dot{R}}{c})R\ddot{R}+\frac{3}{2}\dot{R}^2(1-\frac{\dot{R}}{3c})\right)=\left(1+\frac{\dot{R}}{c}+\frac{R}{c}\frac{d}{dt}\right)\left(p_g-\frac{2\sigma}{R}-\frac{4\mu\dot{R}}{R}-p\right). \quad (2.46)$$

Multiplying Eq. (2.46) by the time derivative of the bubble volume $\partial V/\partial t$ and N(number of bubbles per unit volume), Eq. (2.32) by p and Eq. (2.34) by v and summing them up together leads to

$$\begin{aligned}\rho N(R\ddot{R}+\frac{3}{2}\dot{R}^2)\frac{\partial V}{\partial t}-\rho N\frac{\dot{R}}{c}(R\ddot{R}+\frac{1}{2}\dot{R}^2)\frac{\partial V}{\partial t}+\frac{\partial}{\partial t}(\frac{1}{2}\frac{p^2}{\rho c^2}+\frac{1}{2}\rho v^2)+\nabla.(pv)=\\ N(p_g+\frac{\dot{R}}{c}p_g+\frac{R}{c}\frac{dp_g}{dt})\frac{\partial V}{\partial t}-N(\frac{2\sigma}{R}+\frac{\dot{R}}{c}\frac{2\sigma}{R}+\frac{R}{c}\frac{d(\frac{2\sigma}{R})}{dt})\frac{\partial V}{\partial t}-\\ N(\frac{4\mu\dot{R}}{R}+\frac{\dot{R}}{c}\frac{4\mu\dot{R}}{R}+\frac{R}{c}\frac{d(\frac{4\mu\dot{R}}{R})}{dt})\frac{\partial V}{\partial t}-N(\frac{\dot{R}}{c}p+\frac{R}{c}\frac{dp}{dt})\frac{\partial V}{\partial t}. \quad (2.47)\end{aligned}$$

The LHS of Eq. (2.47) can be simplified using the radial kinetic energy of the liquid around the bubble as

$$K_l=\frac{1}{2}\int_R^\infty\rho(\frac{\partial\phi}{\partial r})^2 4\pi r^2 dr=2\pi\rho R^3\dot{R}^2\,, \quad (2.48)$$

in which ϕ is the velocity potential of the radial motion of the liquid. Thus, the LHS can be written as

$$LHS = \frac{\partial}{\partial t}(\frac{1}{2}\frac{p^2}{\rho c^2} + \frac{1}{2}\rho v^2) + N((1-\frac{\dot{R}}{c})\frac{\partial K_l}{\partial t} + \frac{\rho \dot{R}^3}{c}\frac{\partial V}{\partial t}) + \nabla.(pv). \tag{2.49}$$

There are two terms in the LHS related to the compressibility of the liquid. These terms contribute to the acoustic damping factor and are brought to the RHS [67]. The first term related to surface tension in the RHS is the time derivative of the interfacial potential energy per unit volume and goes to the LHS. Thus, the final form of the mechanical energy balance is written as

$$\begin{aligned}\frac{\partial}{\partial t}(\frac{1}{2}\frac{p^2}{\rho c^2} + \frac{1}{2}\rho v^2 + NK_l + N4\pi R^2\sigma) + \nabla.(pv) = N(p_g + \frac{\dot{R}}{c}p_g + \frac{R}{c}\frac{dp_g}{dt})\frac{\partial V}{\partial t} - \\ N(\frac{\dot{R}}{c}\frac{2\sigma}{R} + \frac{R}{c}\frac{d(\frac{2\sigma}{R})}{dt})\frac{\partial V}{\partial t} - N(\frac{4\mu\dot{R}}{R} + \frac{\dot{R}}{c}\frac{4\mu\dot{R}}{R} + \frac{R}{c}\frac{d(\frac{4\mu\dot{R}}{R})}{dt})\frac{\partial V}{\partial t} - \\ N((\frac{\dot{R}}{c}p + \frac{R}{c}\frac{dp}{dt} + \frac{\rho\dot{R}^3}{c})\frac{\partial V}{\partial t} - \frac{\dot{R}}{c}\frac{\partial K_l}{\partial t}).\end{aligned} \tag{2.50}$$

The RHS has twelve terms. Three terms related to gas pressure (thermal effects), two terms related to surface tension (interfacial effects), three terms related to viscosity (viscous effects) and four terms related to compressibility of the liquid (acoustic effects). Except the terms which do not contain the speed of sound (the first ones for gas pressure and viscosity), all of the others are related to the effect of compressibility of the liquid. These terms are comparing the rate of change of different energies per unit area (which are multiplied here by $\partial V/\partial t$ to change to power) to the speed of sound. If this rate of change is negligible to the speed of sound, the equation is simplified to the one which is presented by Louisnard [62]. However, these secondary effects may cause differences with respect to the case of the incompressibility assumption, as is shown later. This deviation increases by increasing the acoustic pressure amplitude which is the main reason of violent bubble collapse. The RHS can also be written as below

$$RHS = N\frac{\partial V}{\partial t}\big((p_g - \frac{4\mu\dot{R}}{R} + \frac{1}{c}(\frac{d}{dt}((p_g - p)R) - \frac{d(2\sigma)}{dt} - \frac{d(4\mu\dot{R})}{dt} + \frac{d}{dt}(\frac{1}{2}\rho\dot{R}^2R))\big). \tag{2.51}$$

Here, the terms containing the factor $1/c$, are the rate of change of energies that are stated above. These terms can be summarized as follows:

1. The rate of change of the work done by pressure difference at bubble surface per unit area,

2. the rate of change of surface tension which is the required work to stabilize the bubble

sphericity per unit area,

3. the rate of change of the work done by viscosity and

4. the rate of change of the work done by dynamic pressure of the liquid radial motion per unit area.

The last item in the above list is another representation of the last two terms in Eq. (2.50). If the disturbances in the liquid propagate at the speed of sound, this term is negligible. However, this "acoustic approximation" is valid up to the point in which the acoustical Mach number is much less than unity, $\dot{R}/c \ll 1$. Although in the present study, the effect of compressibility is of interest, to avoid facing severe mathematical ambiguities, the speed of sound is considered as a constant. Otherwise, the following analysis should be modified with the use of Kirkwood-Bether hypothesis [68] and thereafter the KME should be replaced with the Gilmore equation [34]. By assuming a constant sound speed, according to the acoustic equation for diverging spherical waves, one can write the following equation for the velocity potential [42]

$$(\frac{\partial}{\partial t} + c\frac{\partial}{\partial r})r\phi = 0\,. \tag{2.52}$$

Therefore, the quantity $r\phi$ and also $r\partial\phi/\partial t$ propagate with the speed of sound, as stated in [42]. The partial derivative of ϕ to time can be calculated from the integration of momentum equation of the liquid motion in the radial direction from infinity to the bubble surface. The result is

$$\frac{\partial\phi}{\partial t} = \frac{v^2}{2} + \int_{p_\infty}^{p} \frac{dp}{\rho}\,. \tag{2.53}$$

This derivative is the kinetic enthalpy of the liquid per unit mass. As it can be seen, the last two terms in Eq. (2.50) are the time derivative of the term $v^2/2$ in this energy definition multiplied by ρr at the bubble surface (BC: $r = R$). In the following, the first three terms in Eq. (2.50) are left temporarily and simplifying the other terms to reach the final form of the dissipated power is presented as the following.

Surface tension

The two terms related to surface tension resulting from considering the compressibility cancel each other. In other words, the work required to make the bubble surface spherical is not affected

by the compressibility of the liquid around the bubble if the change of surface tension with respect to the temperature is not considered, see Eq. (2.51). It is concluded that for a spherical bubble by neglecting the effect of strong instabilities at the final stages of collapse, the surface tension can not contribute as a damping phenomenon.

Viscosity

Assuming spherical bubbles, the terms related to the viscosity are simplified as follows

$$\frac{4\mu\dot{R}}{R}\frac{\partial V}{\partial t} = 16\pi\mu R\dot{R}^2\,, \tag{2.54}$$

$$\frac{\dot{R}}{c}\frac{4\mu\dot{R}}{R}\frac{\partial V}{\partial t} = \frac{16\pi\mu R\dot{R}^3}{c}\,, \tag{2.55}$$

$$\frac{R}{c}\frac{d(\frac{4\mu\dot{R}}{R})}{dt}\frac{\partial V}{\partial t} = \frac{16\pi\mu(-R\dot{R}^3 + R^2\dot{R}\ddot{R})}{c}\,. \tag{2.56}$$

The first term, which is not related to the compressibility, is also reported by [62] and [65]. It represents the dissipation of acoustic energy due to the viscosity in the incompressible potential flow field inside the liquid from bubble surface to infinity. Again two terms in the Eqs. (2.55) and (2.56) cancel each other but an extra term is obtained from Eq. (2.56). This term should be added as the effect of compressibility on the viscous damping factor introduced by [62] and here by Eq. (2.54).

Acoustic radiation

All of the four terms arising from the compressibility can be simplified by substituting $\partial V/\partial t$ and Eq. (2.48) in Eq. (2.50). This leads to

$$Acoustic\ damping : 4\pi R^2\frac{\dot{R}}{c}(\dot{R}p + \dot{p}R - \frac{1}{2}\rho\dot{R}^3 - \rho R\dot{R}\ddot{R})\,. \tag{2.57}$$

According to Neppiras [42], all of these terms related to the temporal change of the liquid pressure refer to the energy radiated as sound and include acoustic radiation damping.

Mechanical energy balance

Averaging Eq. (2.50) with the use of Eqs. (2.54) to (2.57) over one acoustic cycle results in

$$\frac{1}{T}\int_O^T \frac{\partial}{\partial t}(\frac{1}{2}\frac{p^2}{\rho c^2}+\frac{1}{2}\rho v^2+NK_l+N4\pi R^2\sigma)dt+\nabla.\langle pv\rangle=-N(\Pi_{th}+\Pi_v+\Pi_r)\,. \quad (2.58)$$

The RHS terms are defined as

$$\Pi_{th}=\frac{1}{T}\int_O^T -(p_g(1+\frac{\dot{R}}{c})+\frac{R}{c}\frac{dp_g}{dt})\frac{\partial V}{\partial t}dt\,, \quad (2.59)$$

$$\Pi_v=\frac{1}{T}\int_O^T 16\pi\mu(R\dot{R}^2+\frac{R^2\dot{R}\ddot{R}}{c})dt\,, \quad (2.60)$$

$$\Pi_r=\frac{4\pi}{Tc}\int_O^T R^2\dot{R}(\dot{R}p+\dot{p}R-\frac{1}{2}\rho\dot{R}^3-\rho R\dot{R}\ddot{R})dt\,. \quad (2.61)$$

The first two terms in the integral of the LHS of Eq. (2.58) cancel over a period of motion of the liquid around the bubble. However, the second two terms, depending on the bubble dynamics, can exhibit different behaviors. These terms can be simplified as

$$\frac{1}{T}\int_O^T \frac{\partial}{\partial t}NK_l dt=\frac{2\pi N}{T}\rho R^3\dot{R}^2\Big|_0^T\,. \quad (2.62)$$

$$\frac{1}{T}\int_O^T \frac{\partial}{\partial t}N4\pi R^2\sigma dt=\frac{4\pi N}{T}\sigma R^2\Big|_0^T\,. \quad (2.63)$$

As it can be seen, they are not periodic functions and can not be easily ignored. However, the reasons of vanishing these terms are explained as follow.

In the case of stable cavitation, the bubble starts to oscillate in a nonlinear way but around its equilibrium radius. At the end of a cycle, the radius is approximately equal to the initial radius and the next cycle starts similar to the previous one. Thus, it can be assumed that $R|_0 \approx R|_T$, $\dot{R}|_0=0$ and $\dot{R}|_T\approx 0$. These conditions happen usually for the amplitudes lower than the Blake threshold. This threshold is defined as [69]

$$p_B=p_0+\frac{8\sigma}{9}\sqrt{\frac{3\sigma}{2{R_0}^3(p_0+\frac{2\sigma}{R_0})}}\,. \quad (2.64)$$

In the case of transient collapse, the bubble collapses before reaching the end of a cycle. After a

violent collapse it starts to afterbounce to the end of the cycle. The frequency of these oscillations is about the natural frequency of the bubble. If the bubble collapses, then $R|_T = 0$ and $\dot{R}|_0 = 0$. If the bubble starts to oscillate after collapse, it can be assumed that $R|_0 \approx R|_T$, $\dot{R}|_0 = 0$ and $\dot{R}|_T \approx 0$. By applying these criteria to Eqs. (2.62) and (2.63), it is observed that these averages can be neglected over one cycle. In the case of a collapse before reaching to the end of the cycle (above the Blake threshold), an energy of about $4\pi R^2\sigma$ is dissipated to the liquid. For a bubble with the initial radius in the order of micrometers, this energy is approximately ten orders of magnitude less than the other dissipated energies as will be shown in the results and is also neglected.

By performing this analysis, it is concluded that all of the terms inside the integral of the LHS of Eq. (2.58) vanish and the equation reduces to

$$\nabla \cdot \langle pv \rangle = -N(\Pi_{th} + \Pi_v + \Pi_r)\,. \tag{2.65}$$

This is similar to the form presented by [62]. This equation shows the sources of damping which dissipate the acoustic energy (term inside the divergence operator) through the liquid. By solving the bubble dynamics equation and knowing the gas pressure inside the bubble, all of the terms in the RHS of Eq. (2.65) can be calculated numerically.

Modeling

- Gas pressure

  In the present work, the bubbles are assumed to contain gas and without vapor inside them during the oscillations. The pressure of the gas inside the bubble changes due to heat transfer, change of bubble volume, mass transfer, phase change and chemical reactions. Neglecting the last three, the gas inside the bubble can be treated isothermally or adiabatically, depending on the time scales of the heat transfer and radial motion [48]. Thus, Eq. (2.19) is proposed to find p_g during bubble oscillation. However, for isothermal conditions, there is a temperature gradient at the boundary layer over the bubble surface that may cause an increase in the pressure of the gas inside the bubble. Therefore, by considering the effect of this heat transfer, a more precise relation is developed for the pressure inside

the bubble. This model is an ODE as below [9, 48, 70]

$$\dot{p_g} = p_g\gamma(\frac{-3\dot{R}}{R}) + (\gamma - 1)(k\frac{3}{R}\frac{dT}{dr}) \,, \tag{2.66}$$

in which k is the conductivity of the gas and dT/dr is the temperature gradient at the bubble surface. This gradient can be approximated linearly as [70]

$$\frac{dT}{dr} = \frac{T - T_\infty}{\delta} \,, \tag{2.67}$$

where δ is the thermal boundary layer thickness and is calculated as $\delta = \sqrt{t_T\alpha}$. Here, α is the thermal diffusivity of the gas and the time scale of temperature changes can be calculated as $t_T = R/(3(\gamma - 1)\dot{R})$. Eq. (2.66) could be simplified to adiabatic conditions ($\eta = \gamma$) of Eq. (2.19) in the case of no temperature gradient. To find the variation of the bubble radius using KME, each of the Eqs. (2.19) or (2.66) can be used to calculate p_g. For the first one, there is no need to find the temperature, but this equation is not satisfactory at the time of violent collapse. To use Eq. (2.66), the temperature should be known and for this goal, the method of Toegel et al. [71] is applied here.

The heat flux from the liquid to the bubble contents can be predicted by

$$\dot{Q} = 4\pi R^2 k\frac{T_\infty - T}{l_{th}} \,, \tag{2.68}$$

in which l_{th} is the thermal diffusion length obtained by

$$l_{th} = min(\frac{R}{\pi}, \sqrt{\frac{R\alpha}{\dot{R}}}) \,. \tag{2.69}$$

Finally, the temperature of the gas inside the bubble can be calculated by solving the following ODE that is a result of the first law of thermodynamics

$$C_v\dot{T} = \dot{Q} - p\dot{V} \,. \tag{2.70}$$

- Modeling procedure

  According to the procedure described in the previous sections, the modeling is performed as follows for each time step

  1. Solving the bubble dynamics ODE (KME), Eq. (2.46),

Table 2.1.: Physical properties set for the test case.

$R_0(\mu$ m)	f(kHz)	k_{Ar}(W/(m.K))	α_{Ar}(m^2/s)	D_{Ar}(m^2/s)	γ
3.0	20.0	1.6e-2	3.83e-5	2.2e-5	1.667
μ(Pa.s)	C_v(j/(mol.K))	σ(N/m)	ρ(kg/m^3)	c($\frac{m}{s}$)	
1.0e-3	12.0	7.25e-2	1.0e3	1.5e3	

2. solving the ODE for the gas pressure inside bubble, Eq. (2.66),

3. solving the ODE for temperature, Eq. (2.70) and

4. finding the value of the integrals of Eqs. (2.59) to (2.61).

For the first two steps, a 4^{th} order Runge-Kutta method is used but for the third one the Euler method is applied. At the end of step 1, two damping factors due to viscous and acoustic radiation can be calculated. However, to precisely determine the thermal damping, the next two steps are necessary. There should be a criteria to stop the solution of the bubble radial dynamics equation. As it is necessary to define a collapse condition, here it is assumed that if the radial velocity of the bubble exceeds the speed of sound or the bubble radius reaches to two percent of its initial radius, the program stops [72]. To compare the results with the one proposed by Louisnard [62], the method is applied to a bubble containing Argon in water as the medium. The properties are listed in table 2.1 and the pressure and temperature of the surrounding liquid are set as 101325 Pa and 293 K, respectively.

It should be noted that the method can be compared to the one which is proposed by Harris et al. [73]. However, the advantage of the present approach is that there is no need to guess a value for the convection heat transfer coefficient of the liquid near the surface of the bubble to estimate the heat flux.

The result of applying the described method on a single bubble is shown in Fig. 2.4. The graph shows the dissipated power calculated by Eq. (2.65) for $N = 1$ versus the normalized acoustic pressure amplitude. The normalization is done by dividing the pressure amplitude to the ambient pressure. For comparison, the viscous and thermal damping terms obtained using this method are also calculated by RPE. The dissipated power due to acoustic radiation is calculated only by KME. The vertical dashed line shows the Blake threshold which is defined by Eq. (2.64). As the number of bubbles is not specified and should be considered as an arbitrary value, the comparison between the viscous, thermal and radiation losses is performed by applying Eq. (2.65) on a single bubble. The results are comparable with the ones proposed by [62]. However, there are some

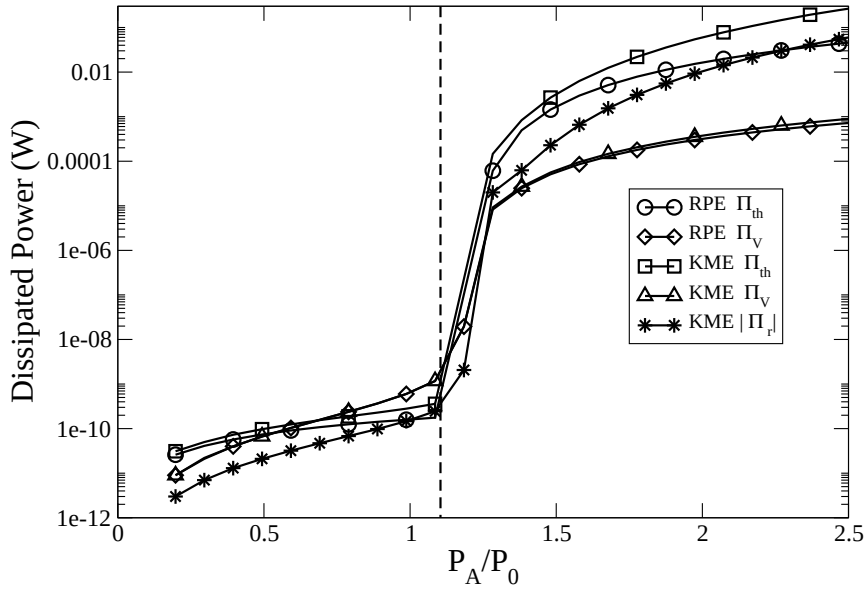

Figure 2.4.: Nonlinear damping of the wave versus normalized acoustic pressure amplitude for $N = 1$. The vertical dashed line shows the Blake threshold.

notes concerning the dissipated power above the Blake threshold to be mentioned:

1. The thermal damping calculated by this method using RPE is about four orders of magnitude higher than the value predicted by [62].

2. The compressibility does not affect the viscous damping considerably, but its effect increases by increasing the pressure amplitude slowly (second term in the RHS of Eq. (2.60)).

3. Considering the compressibility of the liquid increases the thermal damping by a factor of less than one order of magnitude and by increasing the pressure amplitudes, its effect becomes stronger.

4. The power dissipated by acoustic radiation is of the same order as the thermal damping and should be considered. Compressibility shows its strong damping effect above the Blake threshold and is more important than viscous damping.

Here, some observations in the present method are explained using linear theory. For this goal, it is assumed that small perturbations in the pressure amplitude, cause small perturbations in the bubble radius. Therefore it reads

$$p = p_0(1 - \epsilon_1 sin(\omega t)) \,, \tag{2.71}$$

and

$$R = R_0(1 + \epsilon_2 sin(\omega t)) \,. \tag{2.72}$$

The ratio between the second and the first terms in the RHS of Eq. (2.60) can be estimated by considering Eqs. (2.71) and (2.72). After rearrangement, one obtains

$$\frac{R^2 \dot{R} \ddot{R}}{cR\dot{R}^2} \approx \frac{R_0 \omega}{c} = 2\pi R_0 \lambda \,. \tag{2.73}$$

For the range of observed radii of bubbles and also applied frequencies in sonochemical reactors, this ratio is much smaller than one. This is the reason why the dissipated power due to viscous effects is not changed by compressibility. For violent collapse above the Blake threshold, this approximation is not valid and there is a small increase in viscous dissipated power. However, as this damping is negligible with respect to the other two, the effect of compressibility on viscous effects can be ignored as well as the one for surface tension.

Furthermore, the closed-form solution for the integral of Eq. (2.60) by applying Eq. (2.72) can be obtained as

$$\Pi_v = 8\pi\mu {R_0}^3 \omega^2 {\epsilon_2}^2 \,. \tag{2.74}$$

The result of viscous damping presented by Eq. (2.74) is only related to the first term inside the integral of Eq. (2.60) because the average of the second term is zero over one acoustic cycle. As the second term does not contribute to the damping in the case of linear theory assumptions and is also negligible as shown by Eq. (2.73), it is concluded that linear theory can predict the viscous damping in a reasonable way below the Blake threshold. This is also shown as the comparison between the results of the present method and linear theory in Fig. 2.5. To find the relation between the viscous damping and the pressure amplitude, ϵ_2 should be represented as a term of ϵ_1. The ratio between ϵ_1 and ϵ_2 can be obtained by the assumptions made by Commander and Prosperetti [55]. The magnitude of Φ which is a dimensionless complex parameter is a reasonable scale for this ratio which is defined by Eq. (2.42). The magnitude of Φ is calculated approximately as 3 for the parameters in the present study ($\epsilon_2 \approx \epsilon_1/3$). Therefore, the magnitude of viscous damping obtained from Eq. (2.74) can be plotted versus the pressure variation in Fig 2.5.

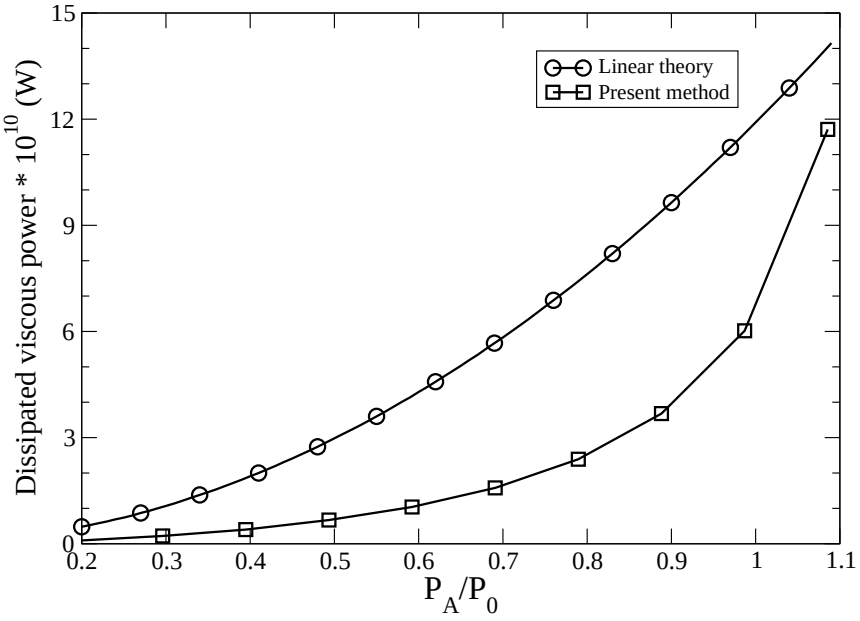

Figure 2.5.: Variation of Π_v for amplitudes lower than the Blake threshold.

The same analysis can be conducted by substituting Eqs. (2.71) and (2.72) into the radiation damping of Eq. (2.61) to find the following analytical solution:

$$\Pi_r = \frac{\pi}{8c} {R_0}^4 \omega^2 [4p_0({\epsilon_2}^4 - 5{\epsilon_2}^3\epsilon_1 + 4{\epsilon_2}^2 - 4\epsilon_1\epsilon_2) + \rho {R_0}^2\omega^2{\epsilon_2}^3({\epsilon_2}^3 - 6\epsilon_2 + 12)] \,. \qquad (2.75)$$

By knowing that $\epsilon_1, \epsilon_2 < 1$, it is easy to show that Π_r is alway negative below the Blake threshold. However, for amplitudes higher than the Blake threshold in which the bubble experiences violent collapse, compressibility dissipates a significant part of the acoustic energy to the liquid. Thus, considering the compressibility for amplitudes lower than the Blake threshold, not only damps the wave propagation but also reduces the damping of viscous and thermal effects. This is the reason why in Fig. 2.4 the absolute value of this dissipated power is shown. Variation of Π_r for amplitudes lower than the Blake threshold obtained from the present method and the linear theory is shown in Fig. 2.6. It is clear that the approximation of linear theory that is presented by Eq. (2.75) is acceptable for this range of pressure amplitudes. The final note about this comparison is that, the majority of the damping in this region results from the first term in the bracket in Eq. (2.75). This term is derived from the first two terms of Eq. (2.61) in which the variation of acoustic pressure appears. It can be concluded that the second two terms in which the acoustical Mach number appears, have insignificant effect on the damping below the Blake threshold. However, above the Blake threshold, this part may contribute to the damping due to considerable values of $\dot{R}$ at final stages of collapse.

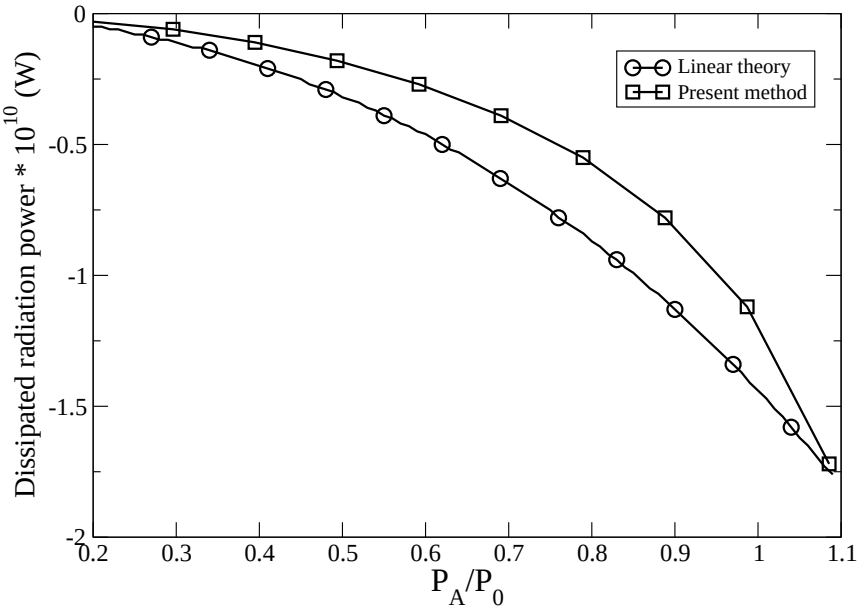

Figure 2.6.: Variation of Π_r for amplitudes lower than the Blake threshold.

2.3. Lagrangian tracing of bubbles with varying radii

Euler-Lagrange modeling of a dispersed phase in a multiphase system is a well known concept and is used widely in different applications. The most important advantage of this method is that the velocity and position of any individual particle or object may be obtained explicitly which in turn is useful for modeling collision and coalescence among bubbles [74]. Depending on the volume occupied by the dispersed phase in the continuous phase, the coupling between the two phases may change. In the simplest case of a dilute system only the effect of the bulk liquid on the dispersed phase is considered. This type of coupling is termed as “one-way coupling”. In the so-called “two-way coupling” model, the momentum transfer from the dispersed phase to the continuous phase should also be considered. This happens in cases with higher volume fraction of the dispersed phase or much higher velocities of the dispersed phase objects in a dilute system. In sonochemical reactors, this momentum source of the motion of bubbles in the bulk liquid momentum equation is of importance. Moreover, the collision of bubbles in zones with high concentration should be taken into account. Consequently, by adding the effect of collision on each bubble’s motion to the two-way coupling model, the so-called “Four-way coupling” Euler-Lagrange approach is considered in this section.

The approach is widely used to model many different multiphase systems. However, it is not yet applied to model the formation, destruction and motion of bubbles due to an ultrasound field. The most important challenge is the modeling of the state of bubbles in an acoustic field where the inception of bubbles and the forces exerting on them is still under question. The structure of bubbles, which is not stationary and uniform, is the main target of Lagrangian tracing of cavitation bubbles. Since the radius of an individual bubble is changing rapidly, the classical formulations for forces on a solid particle are not precise enough. However, some reasonable results are obtained from previous studies which are in qualitative agreement with experimental observations. Nonetheless, no combined simulation of bubbles pattern and flow field besides an acoustic field is observed.

The flow field inside a sonochemical reactor is a result of external momentum sources, such as for the inlet/outlet of a continuous feed reactor. Additionally, convection may be the result of a strong acoustic source (acoustic streaming). Previous studies on the fluid motion in presence of a sound field are limited to investigate the acoustic streaming and are not for a combination

with other momentum sources (see Refs. [3], [75], [76], [77] and references therein). Furthermore, the experimental works in this field are usually conducted by considering some chemical characteristics such as mixing time of the reactants in a sonochemical reactor [78]. Since recent sonochemical reactors may be designed for reacting flows [2], the influence of external convective sources should also be considered. Besides that, it is important to understand the mixing and hydrodynamic characteristics due to the presence of solid/gas phases in a continuous feed reactor [79]. The goal of modeling such a flow field is that it can help in placement of the reactants in zones of maximum cavitational intensity, flow distributors and near transducers for eliminating zones with weak cavitational activity [80].

The work of Parlitz et al. [40] is one of the first attempts in this context. By applying a particle model to the motion of bubbles, they found that the primary Bjerknes force creates filaments of bubbles (streamers) due to the motion of bubbles towards the nodes or antinodes of the acoustic field. However, in their model convection due to the bulk motion of the fluid is not considered. Koch [81] and Mettin et al [82] have developed a particle model and compared the structure of bubbles with experiment. According to Louisnard [52], this model is the most sophisticated one which involves all of the relevant phenomena.

Recently, hydrodynamic cavitation phenomena including the radial dynamics of externally driven bubbles are investigated by Abdel-Maksoud et al. [83]. However, due to the large difference between time scales of the oscillations of the bubbles and the bulk liquid flow, there are no attempts toward simultaneous modeling of these events using an Euler-Lagrange method in sonochemical reactors. Therefore, in this part the target is to find a new numerical method to investigate the motion of bubbles with varying radii and the formation of their quasi-steady structure under the action of a strong acoustic field.

2.3.1. Flow field equations

The turbulent motion of a Newtonian, incompressible fluid is governed by the Reynolds averaged Navier-Stokes equations and two transport equations for turbulent kinetic energy and dissipation rate. The standard $k-\epsilon$ model is selected here for turbulence modeling. Thus, the considered equations are

mass conservation

$$\frac{\partial \bar{u}_j}{\partial x_j} = 0\,, \tag{2.76}$$

momentum conservation

$$\frac{\partial \bar{u}_i}{\partial t} + \bar{u}_j \frac{\partial \bar{u}_i}{\partial x_j} = -\frac{1}{\rho_l}\frac{\partial p_h}{\partial x_i} + (\nu + \nu_T)\frac{\partial^2 \bar{u}_i}{\partial x_j \partial x_j} + F_b + F_{A.S.}\,, \tag{2.77}$$

turbulent kinetic energy

$$\frac{\partial k}{\partial t} + \bar{u}_j \frac{\partial k}{\partial x_j} - \frac{\partial}{\partial x_j}\left((\nu + \nu_T)\frac{\partial k}{\partial x_j}\right) = \nu_T \frac{\partial \bar{u}_i}{\partial x_j}\left(\frac{\partial \bar{u}_i}{\partial x_j} + \frac{\partial \bar{u}_j}{\partial x_i}\right) - \epsilon \tag{2.78}$$

and turbulent dissipation rate

$$\frac{\partial \epsilon}{\partial t} + \bar{u}_j \frac{\partial \epsilon}{\partial x_j} - \frac{\partial}{\partial x_j}\left((\nu + \frac{\nu_T}{\sigma_\epsilon})\frac{\partial \epsilon}{\partial x_j}\right) = C_1 \frac{\epsilon}{k}\nu_T \frac{\partial \bar{u}_i}{\partial x_j}\left(\frac{\partial \bar{u}_i}{\partial x_j} + \frac{\partial \bar{u}_j}{\partial x_i}\right) - C_2 \frac{\epsilon^2}{k}\,. \tag{2.79}$$

In these equations, x_i (i=1,2,3) are the Cartesian coordinates, u_i are the Cartesian components of the liquid velocity, $\bar{u}_i$ are their mean values in turbulent flow, p_h is the static pressure of the flow, ν is the kinematic viscosity, k is the turbulent kinetic energy, ν_T is the turbulent kinematic viscosity, ϵ is the turbulent dissipation rate and σ_ϵ, C_1 and C_2 are constant values.

The source term F_b models the momentum transfer between the dispersed phase and the main liquid and creates a two-way coupling between the two phases. In case of a dilute or moderate dilute suspension, it should be taken into account. It reads

$$F_b = \frac{-1}{V_{cell}\Delta t}\sum_{bubbles} m_b(\mathbf{U_{b,out}} - \mathbf{U_{b,in}})\,, \tag{2.80}$$

where V_{cell} denotes the volume of the computational cell where the bubbles are located at the present time and $\mathbf{U_b}$ is the bubble velocity. The summation is performed for the bubbles at each individual cell and the indices “out” and “in” stand for the exiting and incoming velocities of the bubbles. In case of a dense population of bubbles in sonochemistry, especially in the vicinity of the sonotrode, other phenomena such as collision of the bubbles is also of great importance. In that case, the four-way coupling which considers the momentum transfer between two individual bubble in the same phase should be applied. The classical formulation of the collision of two rigid particles which is recently applied by Vallier [84] in OpenFOAM is used here.

2.3.2. Acoustic streaming source term $\mathbf{F_{A.S.}}$

Acoustic streaming may be defined as the mean flow in a liquid by absorbing the sound energy. The physical reason is the dissipation of sound energy by viscosity of the liquid. Since the average shear velocities during one acoustic cycle is not zero in case of a viscous liquid, a net flow is developed. The phenomenon was firstly studied by Rayleigh [85] and thereafter explained more theoretically by several researchers, such as Schlichting [86], Eckert [87] and Nyborg [88]. Moreover, Lighthill [89] related the phenomenon to Reynolds shear stresses and explained the phenomenon more mathematically for different types of acoustic streaming. The review of Boluriaan and Morris [77] has described the history as well as physical background of acoustic streaming.

The effect of acoustic streaming appears in the momentum equation of the liquid as a source term. Here, the formulation of Nyborg [88] is used which leads to the strength of force in the direction of a confined beam as [90]

$$F_{A.S.} = -\frac{1}{{\rho_l}^3 c^5}\big(\zeta + \frac{4}{3}\mu\big)\langle p\frac{\partial^2 p}{\partial t^2}\rangle_t \,, \tag{2.81}$$

where μ and ζ show the shear and bulk viscosities, respectively. The $\langle . \rangle_t$ denotes averaging in time. Assuming the pressure as a mono-harmonic wave with the frequency f and expanding it into a Fourier series as

$$p = \sum_{n=0}^{\infty} p_n sin(2\pi f t + \phi_n) \,, \tag{2.82}$$

results in the magnitude of the acoustic streaming source as

$$F_{A.S.} = \frac{\alpha}{\rho_l c^2}\sum_{n=1}^{\infty} n^2 {p_n}^2 \,. \tag{2.83}$$

With high degree of accuracy, the contribution of the higher order harmonics of the wave may be ignored and the first harmonic is considered here which may be obtained from Helmholtz equation [90]. In this equation, α is the absorption coefficient of the wave. The Stokes law of sound attenuation is applied which proposes the following relation for α

$$\alpha = \frac{2(\mu + 3\zeta/4)\omega^2}{3\rho_l c^3} \,. \tag{2.84}$$

Here, ω is the frequency of the wave. Thus, the set of Eqs. (2.83) and (2.84) is required for

modeling the acoustic streaming.

2.3.3. Lagrangian frame formulation

The motion of each individual bubble in a Lagrangian approach is governed by Newton's second law

$$m_b \frac{d\mathbf{U_b}}{dt} = \Sigma \mathbf{F}\,, \tag{2.85}$$

in which m_b is the mass of the bubble and $\Sigma\mathbf{F}$ is the total force on the bubble exerting due to the surrounding fluid. The Magnus force due to bubble rotation is neglected because of the small size of the bubbles as well as negligible shear force. In addition, the Basset force, which represents the temporal variation of the bubble relative velocity, is ignored. Moreover, due to small radius of the bubbles and the low density of gas inside, the mass of the containing gas is negligible with respect to the added mass of the liquid. Thus, Eq. (2.85) reads

$$\mathbf{F_G} + \mathbf{F_{AM}} + \mathbf{F_{vol}} + \mathbf{F_D} + \mathbf{F_{Bj_1}} + \mathbf{F_{Bj_2}} = 0 \tag{2.86}$$

In this equation, $\mathbf{F_G} = (1 - \frac{\rho_l}{\rho_b}) m_b \mathbf{g}$ is the gravitational force, $\mathbf{F_{AM}} = \frac{m_b \rho_l}{2\rho_b}(\frac{D\mathbf{U_f}}{Dt} - \frac{d\mathbf{U_b}}{dt})$ is the added mass force and $\mathbf{F_{vol}} = \frac{\rho_l}{2\rho_b}\frac{dm_b}{dt}(\mathbf{U_f} - \mathbf{U_b})$ is the volume variation force which represents momentum transfer due to the changes in the bubble volume [91]. The last three forces are explained in the following:

- Drag force $\mathbf{F_D}$:

  The drag force is a result of the relative motion between the bubble and the surrounding fluid. Since the fluid flow around an oscillatory bubble is affected by rapid bubble pulsation, the equation of the drag force is more complicated than simple forms such as Stokes or Schiller- Naumann equations. However, the equation proposed by Magnaudet and Legendre [92] is accepted in literatures [41, 52] and is in quantitative agreement with experimental results by Krefting [93]. This equation states

$$\mathbf{F_D} = -12\pi\mu R \mathbf{U_b}\,. \tag{2.87}$$

As it can be seen, this equations predicts the drag force as two times of the Stokes formulation. This equation is used throughout this thesis for calculating the drag force on a bubble.

- Primary Bjerknes force $\mathbf{F_{Bj_1}}$:

  Any bubble in a pressure field experiences a force resulting from the pressure gradient. If the source of this gradient is the external acoustic pressure, the force is called primary Bjerknes force. Since the acoustic pressure is oscillatory in time, the average of the primary Bjerknes force on the bubble in one acoustic cycle is calculated as follows

$$\mathbf{F_{Bj1}} = -\langle V(t)\nabla p(t)\rangle_t \,, \tag{2.88}$$

  where $V(t)$ is the volume of the bubble and $\nabla p(t)$ is the pressure gradient at the bubble position. The $\langle\rangle_t$ denotes averaging in time [40]. This formulation leads to an analytical expression for the primary Bjerknes force in case of linearized oscillations. However, for nonlinear pulsation, the averaging over one acoustic cycle should be done after solving the radial dynamics equation for each bubble. In case of an acoustic standing wave, the gradient of pressure is only a function of spatial coordinates. The pressure is written as $p = P_a sin(\omega t - \phi)$ and by substituting this pressure in Eq. (2.88) the primary Bjerknes force reads

$$\mathbf{F_{Bj1}} = -\nabla P_a \langle V(t) sin(\omega t)\rangle \,. \tag{2.89}$$

  Therefore, the average value of $V sin(\omega t)$ is required which is shown hereafter as $\langle V_{Bj}\rangle$.

- Secondary Bjerknes force $\mathbf{F_{Bj_2}}$:

  If the pressure gradient on bubble's surface is a result of other bubbles, the force on the bubble is called secondary Bjerknes force. This secondary force can be calculated as below

$$\mathbf{F_{B_2}} = -\frac{\rho_l}{4\pi}\langle \dot{V}_1 \dot{V}_2\rangle \frac{\mathbf{x_2} - \mathbf{x_1}}{|\mathbf{x_2} - \mathbf{x_1}|^3} \,, \tag{2.90}$$

  in which $\mathbf{x_i}(i = 1, 2)$ is the spatial position of bubble number i. In calculating the secondary Bjerknes force on a bubble the effect of liquid compressibility is ignored. Thus, it

is assumed that the force is exerted to any bubble instantaneously from other bubbles. It can be seen from Eq. (2.90) that the average of the rate of change of the bubble volume over one acoustic cycle is required which reads

$$\langle \dot{V} \rangle = \frac{4\pi}{T} \int_0^T R^2 \dot{R} dt \,. \tag{2.91}$$

This magnitude is obtained for each single bubble at each computational time step after solving its radial dynamics equation. This parameter is shown as $\langle \dot{V} \rangle$ later in this thesis.

A simplified formulation for translational motion of bubbles in 1D could be obtained by considering the above forces. This has been done, for instance, by Doinikov [21, 26], Mettin and Doinikov [27], Hay et al. [28] and Harkin et al. [29]. The method is basically based on considering two independent coordinates (x for translational motion and R for radial motion), writing the summation of kinetic and potential energy, substituting these energies in a Lagrangian formulation and finding two coupled equations for translational and radial motion of a bubble. The idea was to investigate the coupling between these two motions in a sound field and the interaction between two different bubbles (or a bubble and a rigid particle) in 1D. In Sec.2.1, the effect of translational velocity is introduced in the radial dynamics of a single bubble. Here, the radial velocity appears in the translational ODE by considering the volume change force as the following.

Assuming a stagnant fluid ($\mathbf{U_f} = 0$) and neglecting gravity, Eq. (2.86) in 1D reads

$$-\frac{m_b \rho_l}{2\rho_b} \ddot{x} - \frac{\rho_l}{2\rho_b} \frac{dm_b}{dt} \dot{x} - \langle V \nabla p \rangle_t - 12\pi\mu R \dot{x} = 0 \,. \tag{2.92}$$

Multiplying by $-2\rho_b/(\rho_l m_b)$ leads to

$$\ddot{x} + \big(\frac{1}{m_b}\frac{dm_b}{dt} + \frac{18\mu}{\rho_l R^2}\big)\dot{x} + \frac{2\langle V \nabla p \rangle_t}{\rho_l V} = 0 \,, \tag{2.93}$$

where the first term inside the parentheses on the LHS is due to the volume change force and can be simplified as $3\dot{R}/R$. Thus, the final form of the translational motion coupled with radial dynamics is written as

$$\ddot{x} + \big(\frac{3\dot{R}}{R} + \frac{18\mu}{\rho_l R^2}\big)\dot{x} + \frac{2\langle V \nabla p \rangle_t}{\rho_l V} = 0 \,, \tag{2.94}$$

which is equal to the form presented by Doinikov [21, 26]. The result of coupling between

translational and radial motion and also between two different bubbles in 1D is widely discussed in literatures and is not repeated here. In case of 3D problems, the formulation of the coulping is not straightforward and nonetheless, should be taken into account. Therefore, in numerical simulation, the averaged values of the radius and volume and their time derivatives at each time step is used to investigate a swarm of bubbles.

Collision between two bubbles

The classical formulation of collision between two rigid particles are applied here to simulate the collision between two bubbles. Thus, coalescence is not considered, which is a reasonable assumption for the present problem due to low volume fraction of bubbles. Figure 2.7 illustrates the general case of collision including normal and tangential component of velocities for two bubbles. Firstly, it is checked that whether collision between two bubbles happens. Here, it is assumed that if the relative distance traveled by a bubble at one time step is larger than the actual distance, two bubbles will collide [84]. The relative distance is obtained by finding the relative velocity of two bubbles. Thereafter, the velocities of two bubbles after collision is calculated by

1. the equation of conservation of momentum in normal direction before and after collision,
2. definition of restitution coefficient and
3. assuming frictionless collision.

Conservation of momentum in normal direction reads

$$m_i \mathbf{U}_i^n + m_j \mathbf{U}_j^n = m_i \mathbf{U}_i'^n + m_j \mathbf{U}_j'^n \,, \tag{2.95}$$

where the primes stand for after collision situation. In addition, the restitution coefficient is defined as

$$e = \frac{\mathbf{U}_j'^n - \mathbf{U}_i'^n}{\mathbf{U}_i^n - \mathbf{U}_j^n} \,. \tag{2.96}$$

Since there is no accurate estimate available for this coefficient for oscillating bubbles, it is assumed as constant (e= 0.8) in this thesis. From Eqs. (2.95- 2.96), the normal components of velocities after collision is obtained as

$$\mathbf{U}_i'^n = \frac{m_i \mathbf{U}_i^n + m_j \mathbf{U}_j^n - m_j e(\mathbf{U}_i^n - \mathbf{U}_j^n)}{m_i + m_j} \,, \tag{2.97}$$

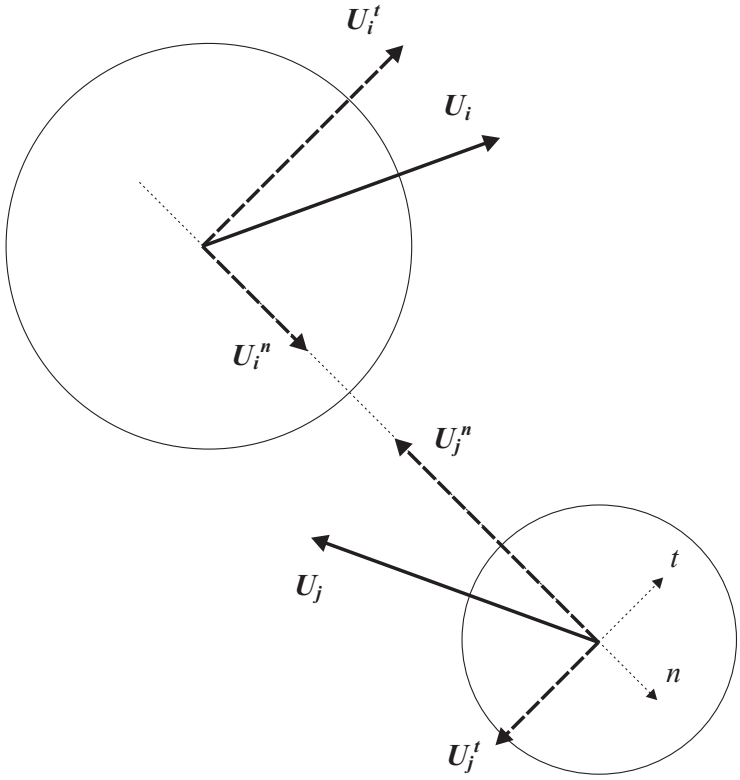

Figure 2.7.: Collision between two bubbles in a 2D configuration.

and

$$\mathbf{U}'^{n}_{j} = \frac{m_i \mathbf{U}^n_i + m_j \mathbf{U}^n_j - m_i e(\mathbf{U}^n_j - \mathbf{U}^n_i)}{m_i + m_j}\,. \tag{2.98}$$

The assumption of frictionless collision results in unchanged tangential components of velocities, i.e., $\mathbf{U}'^{t}_{i,j} = \mathbf{U}^t_{i,j}$. Hence, both components of velocities are obtained and will be updated at each time step. This update is conducted after modifying the velocities due to motion of bubbles under the action of external forces as below.

Updating the bubble position

To find the new position of a bubble as $\mathbf{x}_b^{n+1} = \mathbf{x}_b^n + \mathbf{U}_b^{n+1} dt$, the updated bubble velocity $\mathbf{U}_b^{n+1}$ is obtained by substituting Eqs. (2.87) and (2.88) and the gravitational, added mass and volume variation forces into Eq. (2.86). To calculate drag, added mass and volume variation forces, the current value for the bubble velocity is applied, that means a forward (explicit) Euler method is used. After some algebric operations, the updated bubble velocity is obtained as below

$$\mathbf{U}_b^{n+1} = \mathbf{U}_b^n + dt\frac{\big(-18\nu\langle R\rangle\mathbf{U}_b^n - 2\langle V_{Bj}\rangle\nabla P_a/\rho_l + \frac{1}{2\pi}\langle\dot{V}_1\dot{V}_2\rangle\frac{\mathbf{x_2}-\mathbf{x_1}}{|\mathbf{x_2}-\mathbf{x_1}|^3} + \langle\dot{V}\rangle\mathbf{U}_b^n\big)}{\langle V\rangle}, \quad (2.99)$$

where superscripts n and $n+1$ stands for current and next time steps, respectively. The numerical method of implementation of these equations is explained in details in chapter 3.

2.4. Population of bubbles

As soon as turning the ultrasound source on, plenty of microbubbles start to oscillate and move in a chaotic way. These cavities are created because of rupture of liquid elements due to high negative pressure (tensile stress). Theoretical calculations show that for pure water, a tensile stress of approximately -100 MPa is required to create such cavities. In reality, however, these mircobubbles are visible under the action of typical sonotrodes which are capable of creating a negative pressure amplitude around few bars. Therefore, the question arises which states "where the bubbles come from?".

Apfel [94] proposed the idea of trapped nuclei of bubbles in the crevices of the boundary walls or any other solid impurities in the liquid. He made theoretical investigations as well as experimental observations to show that these nuclei may be activated by high pressure amplitudes. This "high" amplitude is proposed to be the Blake threshold which is also applied as a criterion in this work. The review made by Crum [95] is also another reference, which besides the idea proposed by Apfel, states that free invisible gas nuclei exist in the liquid. These nuclei are avoided to be dissolved in liquid because of surface active species or hydrophobic ions [52]. For modeling and simulating such a stochastic swarm, the problem is more significant, since there are no information about where and how the sources of bubbles at the start of the process [96] should be selected.

The most simplifying assumption is considering a constant number of bubbles nuclei N with an arbitrary initial radius R_0. This is performed widely, for instance by Vanhille and Campos-Pozuelo [15] who considered N= 100 mm^{-3} and R_0= 4.5 μm or by Louisnard [64] by assuming N= 90 or 360 mm^{-3} and R_0= 2 μm. Meanwhile, Abdel-Maksoud et al. [83] proposed an amount of 100-1000 cm^{-3} which is much higher than the aforementioned examples beside the wide range of 5-200 μm for bubbles radii. Since these parameters have strong effect on the damping of the wave, assuming a constant value for them may cause significant error in numerical results.

It is a well known concept that the bubble number density must satisfy a conservation equation. The equation is used, for example by Commander and Prosperetti [55] to derive the linearized form of the wave propagation. In its easiest form, it reads

$$\frac{\partial(N)}{\partial\tau} + \nabla \cdot (N\mathbf{U_b}) = 0 \,, \tag{2.100}$$

in which τ is the time scale of change of the structure of bubbles. It is observed in experiments that this time is much larger than the acoustic period which is a helpful tool for numerical modeling of this equation. Using this assumption, linearization of the primary Bjerknes force to estimate the velocity of bubbles and assuming an exponential reduction of the volume of bubbles, Akhatov et al. [97] proposed a PDE for number density of bubbles. Their results depicted that this value could be estimated by log-normal functions in space for a certain range of parameters. The idea is named by Parlitz et al. [40] as the "continuum description" of the sound field and is helpful in presenting the distribution of bubbles as a field quantity. However, the basic assumptions of Eq. (2.100), does not allow to apply the dynamics of each individual bubble on their population. Therefore, a combination of the microscale problem of a single bubble dynamics and the macroscale problem of the bubbles population is essential. This is done by Mettin et al. [82]. They derived the structure of bubbles by applying a particle model to bubbles as individual objects and then transformed the results to a suitable form for the wave equation. This hybrid sequential model is shown to give reasonable results for bubbles structure in sound fields. However, the effect of bubbles on viscous, thermal and radiation damping of the wave is ignored because of several simplifications which were made in the computations.

In general, the conservation equation should consider the source terms which are of great importance for bubbles under the action of ultrasound. The equation which is usually called "population balance equation" can be written as

$$\frac{\partial(N)}{\partial\tau} + \nabla\cdot(N\mathbf{U_b}) + \frac{\partial}{\partial R_0}(Nw) = B - D. \tag{2.101}$$

In this equation, w is the growth or dissolution rate and B and D stand for the birth and death rates, respectively. The birth rate is a result of bubble nucleation, coalescence and fragmentation. The death rate comes from the bubble collapse, coalescence, break up and fragmentation. This equation is usually solved for agglomeration and break up problems using the Multiple Size Group (MUSIG) model or the Method of Moments (MoMs). However, for bubbly flows, the application of these methods is not extended for acoustic cavitation. The work of Selma et al. [98] is one of the recent works which apply MoMs to cavitational flows. However, the radial dynamics of the bubbles are not considered in that work. In addition, the cavitation is restricted to hydrodynamic type which is different from the acoustic cavitation in several aspects.

In analyzing Eq. (2.101), by coupling it with the Eulerian-Lagrangian approach for bubbles with varying radii (Sec. 2.3), some improvements are achievable. Firstly, w can be estimated from rectified diffusion theory. This theory is related to mass transfer from the surface of a bubble depending on the nature of boundary layers on the bubble surface and its radial dynamics. Secondly, $\mathbf{U}_\mathfrak{b}$ can be obtained form the balance of forces in the particle model at each time step. Finally, the source terms on the RHS can be approximated by investigating the collision probability of individual bubbles [81] as well as their collapse behavior. Furthermore, according to experimental observations and numerical simulations, some data fitting would also be available. The justification of these fittings will be explained later in this thesis. Once Eq. 2.101 is solved with the use of appropriate assumptions, the population distribution of bubbles can be applied to Eqs. (2.38) and (2.40) to find the acoustic pressure amplitude.

In the present research, since bubbles are assumed as individual particles in the Eulerian-Lagrangian method, it is assumed that the number density of bubbles is constant. Increasing the number of bubbles in the Eulerian-Lagrangian method leads to more reliable results for the effect of bubbles on wave propagation. Therefore, the program is examined in the nonlinear analysis for more than 10000 bubbles which are distributed in the vicinity of the sonotrode. The results, which are explained in chapter 5, indicate that this assumption is precise enough as a first attempt. However, it is worth mentioning that increasing the number of bubbles lead to more reliable results which should be done using parallel computations. Therefore, a value for N is not considered in the calculations and only initial values for radii of the nuclei at the beginning of the computations are assumed. These two parameters at $t = 0$ should be estimated according to experiments. They are stated throughout the thesis whenever it is necessary.

3. Numerical method

The fundamental laws necessary for the mathematical treatment of a large part of physics and the whole of chemistry are thus completely known, and the difficulty lies only in the fact that application of these laws leads to equations that are too complex to be solved.

"Paul Dirac"

From a technological point of view, the correct prediction of cavitational intensity is the main objective in modeling sonochemical reactors. A major problem regarding the application of sonochemical reactors at industrial scale is the non-uniform distribution of cavitational intensity. This parameter shows the amount of dissipated power inside the liquid due to the presence of bubbles. Thus, the population of bubbles as well as the pressure amplitude is of great importance in designing the geometry and setting the operating parameters of the reactor. Therefore, in the modeling process, the two main unknowns are the acoustic pressure amplitude $p_a(\vec{x}, t)$ and the spatial bubble distribution (bubble structure). In this thesis, the main target is the step by step modeling of these quantities.

In this chapter, the numerical approaches used for linear and nonlinear simulations are described. For the linear part, the focus is on the FEM analysis of wave propagation in simple and complicated geometries. The goal is to investigate the bubble volume fraction as a field variable and its influence on the wave propagation based on linearized formulations. Moreover, effects of different boundary conditions, frequencies and amplitudes are also of interest, since the linear analysis is computationally economic. Thus, in this part, a linear analysis using the COMSOL Multiphysics FEM package (COMSOL Multiphysics GmbH, Göttingen, Germany) is conducted. On the other hand, for a nonlinear analysis the FVM modeling of flow field as well as bubble migration as a dispersed phase in liquid is used. In this part, the effect of individual bubbles on wave propagation, the structure made by bubbles and radial dynamics of bubbles are of importance. Hence, implementing numerical methods in OpenFOAM (Open Field Operation and Manipulation) is of interest. This package is based on FVM and is capable of combining sev-

eral physical phenomena in a single numerical solver. Therefore, one can combine, for instance, flow field due to external convective sources, wave equation, single bubble radial dynamics and a Lagrangian solver for tracing bubbles in the same software framework.

3.1. Numerical set-up for linear analysis

In recent years, FEM has received significant interest in modeling of wave propagation phenomena, since it can provide more accurate results on coarse computational grids, in comparison with classical finite difference schemes. For instance, Raman et al. [99] applied FEM to determine the acoustic pressure distribution in a two-dimensional reactor by solving the Helmholtz equation with the use of the FEMLAB package. Mettin et al. [82] applied FEM for the temporal analysis of bubble dynamics by a hierarchical simulation of the acoustic field and bubble cloud distribution during a small interval of time. Klima et al. [100] presented an FEM approach to optimize the geometry of a cylindrical reactor by changing the position of the ultrasound horn and the boundary conditions (reflecting or absorbing) on the reactor walls. They found that changing the type of the horn walls exerts small effects on the pressure amplitude in the reactor. However, they did not consider the damping effect of cavitation bubbles on the propagation of waves. Yasui et al. [101] used similar FEM simulations to investigate the effect of boundaries on the pressure amplitude. The effect of ultrasound pressure on the vibration of walls and their deflections can be investigated by means of FEM as shown by Louisnard et al. [102]. In the following, first, the linear wave propagation in simple benchmark geometries to verify the numerical approach is investigated. Thereafter, the same phenomenon in complex geometries of a conical reactors is explained. The pursued target is to numerically investigate laboratory scale, three dimensional reactors with a complicated geometry. The approach includes investigation of different frequencies, boundary conditions as well as scale up of the reactor with a fast and robust numerical method.

3.1.1. Geometries, boundary conditions and physical properties

Simple geometries as benchmarks

Three different configuration are selected as benchmarks. The goal is to compare the FEM results with the FDM results which are presented in the work of Dähnke and Keil [17]. These types include: a cylindrical vessel with a simple circular resonator located at its bottom, a cylindrical

tube with three ultrasonic horns placed in an equilateral triangle in the same cross section around the tube and a cylindrical vessel with an ultrasonic horn located inside the liquid. For further information about the geometries, see Ref. [17]. The target of these simulations is to visualize the so called "shielding effect" of bubbles on the wave propagation. This phenomenon causes damping of the wave in the vicinity of the ultrasound source due to bubbles. Thus, three geometries at two different frequencies of 25 and 50 kHz for four different values of bubbles volume fraction as β= 0, 10^{-5}, 10^{-3} and 10^{-1} are investigated. The boundary conditions for the simulations in the frequency domain are set as follows:

1. The lateral walls of the reactors are assumed to reflect the sound waves and the Neumann boundary condition, $\partial P/\partial n = 0$ is applied.

2. A Dirichlet-type boundary condition with $P = 0$ applies at all bottom walls of the first and third reactors.

In addition, to see the effect of acoustic streaming in this linear model, a simple axisymmetric model is created and the flow field inside a horn type reactor is investigated. The result of velocity field is compared with experimental results of Dahlem et al. [75].

Conical reactors

The specific reactor under consideration was originally designed to produce barium sulphate particles from barium chloride and potassium sulphate by precipitation in aqueous solution. The experimental set-up used for this work is described in more details in [103] in which the irradiation source has a frequency of 20 kHz. To investigate the sensitivity of the applied models to the frequency of the acoustic wave, two additional frequencies, 10 kHz and 30 kHz are also considered in the simulations. These frequencies have been proved to be well suited for chemical reactions of this type [72, 103]. The use of these frequencies justifies neglecting the thickness of the Teflon walls, since this thickness is small in comparison with the wavelengths concerned [1]. The geometry of the reactor was optimized to concentrate the ultrasound and thus the cavitational activity in the mixing zone of the educt feed channels. A schematic representation of the reactor is presented in Fig. 3.1. The ultrasonic horn is positioned vertically at the top of the mixing chamber and is shown as a circular surface. The solid cross section in the figure shows the plane

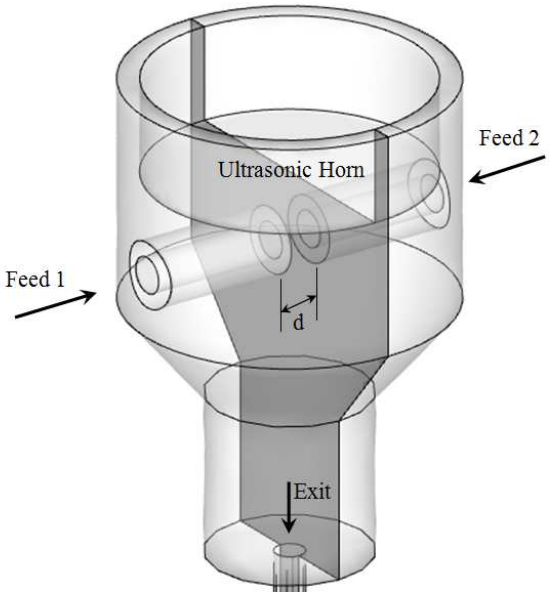

Figure 3.1.: Schematic representation of the reactor; $d = 2$ mm, geometry no. 1 and $d = 15$ mm, geometry no. 2. Solid cross section shows the plane used for 2-D contour plots.

in which the contour plots are presented in the results chapter. The incoming capillary tubes supply $BaCl_2$ and K_2SO_4, which are dissolved in water as carrier fluid.

Two different geometrical configurations have been investigated. The distinguishing feature is the distance between the impinging jets at the openings of the two educt feeding channels, and therefore the size of the mixing zone as well as the shear rate in the flow close to this zone. While reducing the gap ($d = 2$ mm) results in higher shear rates and faster mixing, it can be expected that the solid material in this region causes scattering and decreases the cavitational activity. For all of the simulations, the following boundary conditions were applied to the geometries:

1. The lateral walls of the steel horn, as well as the walls of the feeding and exit channels, are considered as rigid reflecting walls, although it has been observed that they exert a small effect on the pressure distribution [100]. It is assumed that all of these walls reflect the sound waves and that the Neumann boundary condition, $\partial P/\partial n = 0$ applies.

2. A Dirichlet-type boundary condition with $P = 0$ applies at all of the remaining walls of the reactor and at the inlet and exit cross sections of the feeding channels that constitute pressure-release boundaries. These reactor walls are made of Teflon to absorb the ultrasound waves.

3. The source of ultrasound is the horn shown in Fig. 3.1. A fixed pressure amplitude P_{amp} is imposed here; this value is related to the ultrasound power P_{US} as shown in [99] by

Table 3.1.: Physical properties applied in linear simulations.

γ	D (m^2/s)	σ (N/m)	ρ (kg/m^3)	c (m/s)
1.4	1.9×10^{-5}	0.0725	1000	1500

$$P_{amp} = \sqrt{\frac{2\rho c P_{US}}{A}}\,, \tag{3.1}$$

in which the area of the actuator surface is denoted by A.

The remaining physical properties required for the simulations are indicated in table 3.1.

3.1.2. Procedure of the linear analysis

In a first step, the homogeneous linear wave equation is solved for the specified geometries without considering bubbles, in order to investigate the effect of the frequency, boundary conditions, amplitude and power of the ultrasonic source on the acoustic field.

In the second step, the effect of bubbles is investigating at different levels of attenuation. In this step, it is assumed that the bubbles are homogeneously distributed in the medium. The goal is to show the effect of bubbles with constant volume fraction in the entire reactor on the attenuation of the wave. Different values of the bubble volume fraction in the range from 10^{-5} to 10^{-1} are considered. It is supposed that considering higher values for the volume fraction of bubbles is not reasonable, since the acoustic energy would then be completely absorbed because of scattering effects of the bubbles.

In the third step, the variation of the bubble volume fraction is determined on the basis of an equilibrium model, that is, a linear relationship between the pressure and the bubble volume fraction, taken from [60, 104]. This is realized for the real conical reactors only. Here, it is assumed that

$$\beta = 2 \times 10^{-9} P\,. \tag{3.2}$$

Because of the difference in the extent of attenuation with changing bubble volume fraction, a new pressure field has to be obtained. The process is repeated until a steady state is reached. For the sake of simplicity, in this approach the dynamics of the bubbles (their collapse and induced convection) is neglected. However, for low bubble concentrations, this simplification is justified as an engineering approach [19]. Furthermore, in the present configuration the effect of

convection is limited to a small region close to the feed nozzles where the fluid velocity is high. In the simulations, a threshold pressure of 10^5 Pa is assumed; this results in a volume fraction of $\beta = 2 \times 10^{-4}$. A maximum volume fraction of $\beta = 0.1$ is related to a pressure of 50 MPa. Therefore, an iterative scheme which is summarized as follows is required:

1. Solving the Helmholtz equation from Eq. (2.39),
2. calculating β from Eq. (3.2),
3. finding the number of bubbles per unit volume from Eq. (2.26) and the complex wave number from Eq.(2.45),
4. solving the modified Helmholtz equation from Eq. (2.39) and
5. finding the new values of β and going back to 1 until a steady state is reached.

3.1.3. Grid generation and grid study

For the first three simple geometries, quadrilateral elements are precise enough in simulating the linear wave equation without damping. The test cases are examined with different number of cells and no difference in the pressure amplitude predictions is observed.
For the complex geometries of the conical reactors, the applied three dimensional computational grids consist of tetrahedral elements. The discretization and solution are conducted by selecting linear second-order elements. The Helmholtz equation is solved with the use of the classical PDEs module included in the software. The complex wave number in this module is defined on the basis of different parameters including the geometry, the properties of the medium and the bubbles, as well as the variables obtained by means of the formulations explained in chapter 2. To avoid a numerical pollution effect [99, 100], the size of the elements is selected in such a way that the following criterion is satisfied for all of the simulations:

$$k \cdot h = const \ll 1\,. \tag{3.3}$$

Here, h denotes the average size of the edges of the elements. In the case of the highest frequency applied, 30 kHz, the wave number is equal to 125.66 m^{-1} and the average size of the elements is 0.3 mm; hence, the criterion is satisfied. However, to prove the grid independency, three different simulations have been performed and compared for different element sizes: 0.05 mm, 0.2 mm

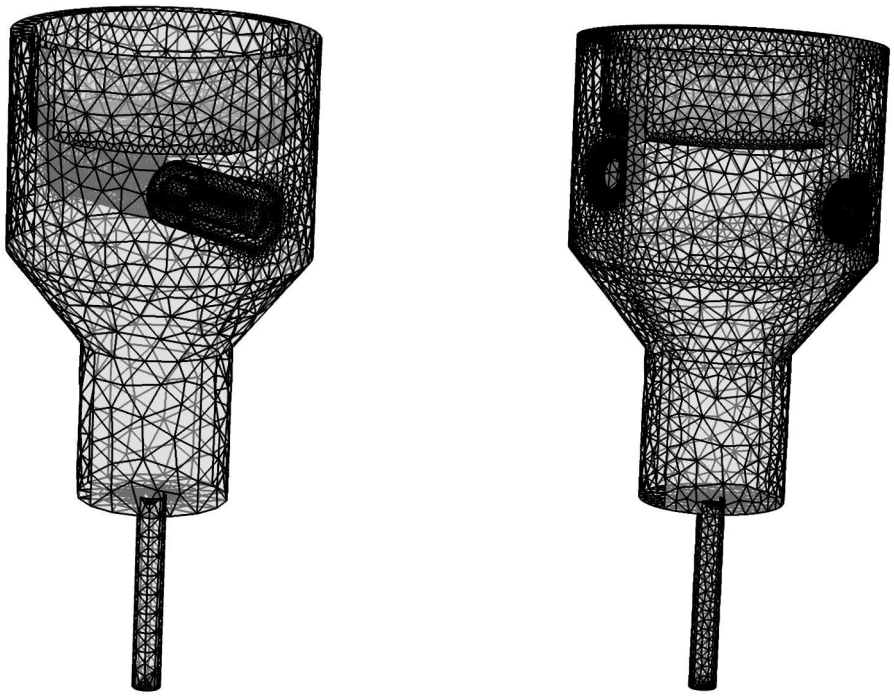

(a) Geometry no. 1 **(b)** Geometry no. 2

Figure 3.2.: Computational grids developed for conical reactors.

and 2 mm for geometry no. 1. The linear wave equation was solved for these cases and the variation of the normalized acoustic pressure on the central axis of the reactor (from the center of the horn to the exit section) was compared. The normalized acoustic pressure is defined as the ratio between the acoustic pressure at each point and the amplitude defined by Eq. (3.1). As shown by comparison, the results are independent of the selected element size. The simulations were performed on a computer equipped with the Linux red hat operating system, eight quad-core Intel Xeon CPUs and 20 GB of RAM. The time required for convergence varies from less than one minute for the case of the linear wave equation without damping to about 30 min for the case in which the damping is considered by applying the linear relationship given by Eq. (3.2). The convergence criterion for the Helmholtz equation is set to 10^{-6}. The specified configurations for the simulation parameters and the grids selected for the geometries are indicated in table 3.2. Finally, a grid with 96646 Degrees Of Freedom (DOF) for geometry no. 1 and 129088 DOFs for geometry no. 2 have been used.

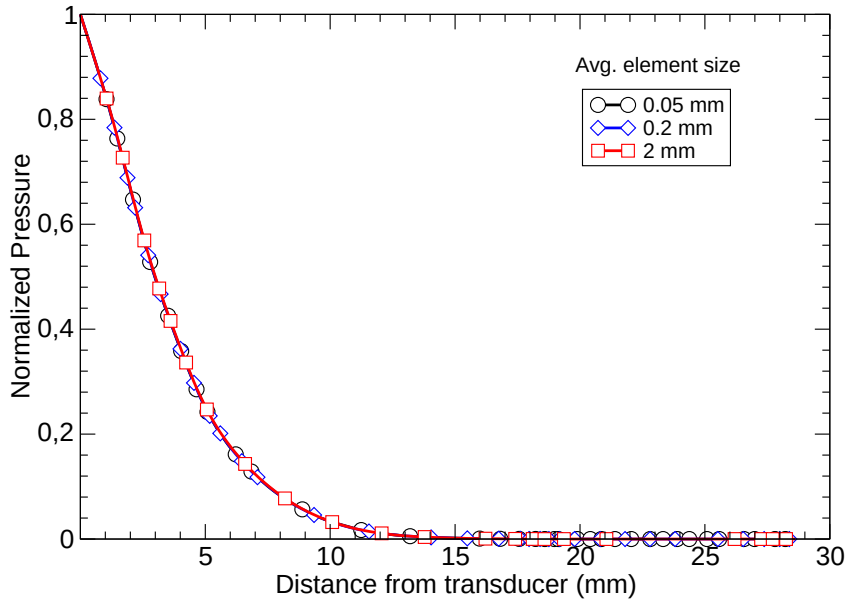

Figure 3.3.: Normalized acoustic pressure on the centerline of the reactor no. 1 for three different grid sizes. Ultrasound power: 20 W. Ultrasound frequency f= 20 kHz.

Table 3.2.: Specification of the simulation parameters, geometrical configurations and selected grids.

Geometry No.	Horn diam (mm)	Distance between tubes (mm)	Volume of the reactor (mm^3)	Ultrasound frequency (kHz)	Ultrasound power (W)	No. of DOFs	No. of tet. elements
1	13	2	2044	10, 20, 30	20, 110, 200	96646	63681
2	13	15	2419	10, 20, 30	20, 110, 200	129088	85479

3.2. Numerical set-up for nonlinear analysis

All simulations in this section are performed using OpenFOAM, a free software toolbox for continuum mechanics, specially for CFD. The basic idea of the nonlinear analysis is to consider the bubbles and their radial dynamics at microscale and simultaneously their structure due to pressure waves at macroscales. In this context, one may transfer the information obtained from a single bubble radial dynamics to a much bigger scale in a sonochemical reactor. Here, the main problem, is the difference between the time scales of a single bubble pulsation and the operating time of an acoustic source in a reactor. In addition, for the numerical simulation of the whole system, one cannot reduce the time scales to smaller values than microseconds. However, one should take the effects of oscillation of a single bubble into account, as it has been shown that the nonlinear theory predicts much higher values for damping of the waves in comparison with linear theory. Therefore, in this section, the goal is to combine the modeling approaches from a single bubble pulsation to acoustic pressure field variation in a laboratory scale.

For the first part, the pressure propagation equation in frequency domain is solved to obtain an initial pressure field and its gradients. Thereafter, a Lagrangian particle tracing method is used which treats each single bubble as a generic particle. The standard solvers of OpenFOAM are capable of modeling particles with constant diameter and therefore, one has to apply the bubbles radial dynamics equation into the solver for bubbles with varying radii. To find the structure formed by bubbles, it is required to sum up the forces on each individual particle which may be calculated from acoustic pressure distribution and other field variables, such as hydrodynamic pressure and liquid velocity. At each computational time step, which is much larger than one period of the acoustic wave, the radial dynamics equation is solved and the desired information is extracted and implemented in the wave propagation equation. This information includes the average radius and average volume of a single bubble as well as nonlinear estimations for viscous, thermal and radiation damping of a single bubble on the acoustic wave. Thereafter, the wave equation in frequency domain including the effect of nonlinear damping is solved and a pressure field is obtained which in the current time step is independent of time. Hence, the Helmholtz equation is solved to exclude the effect of pressure variation in time, but the pressure field is updated at each time step due to the new structure formed by bubbles. This combination is a novel approach in modeling pressure waves in acoustic cavitation and allows to reconstruct the

structure of bubbles in a sound field as well as their effect on the acoustic pressure field. This numerical method is computationally economic because the time could be discretized to flow field or bubbles translational motion time scales (typically millisecond or 10^{-4}sec). Furthermore, it is robust enough to compute the pressure wave propagation because it includes the mutual influence between bubbles and sound fields.

However, there are some notes about this method of simulation which should be clarified:

1. The most important deficiency of the method is assuming the periodicity of the single bubble radial dynamics during a computational time step. For instance, for a frequency of 50 kHz, the period of a complete acoustic cycle is 20 μs. However, the computational time step is typically 100 μs which is five time larger than the acoustic wave period. Therefore, the information from a single bubble radial dynamics in one acoustic period is derived and extended for the further periods. This deficiency would be bigger in case of higher frequencies of the wave. The assumption made here is based on testing plenty of cases with different initial radius for a single bubble under several acoustic pressure amplitudes. If the amplitude of acoustic pressure at a computational cell is less than the Blake threshold, then the radius of the bubble changes approximately around its equilibrium value. Therefore, one can assume that the bubble continues its oscillation for at least hundred cycles which is larger than the computational time step considered here. On the other hand, if the pressure amplitude exceeds the Blake threshold, the bubble experiences violent collapse. In this case, one can use the same averaging by assuming the periodicity of nonlinear oscillation of the bubble for tens of acoustic cycles.

   Although this assumption does not consider the physical effects such as non-spherical shape at the collapse time or bubble's breakup after collapse, it is precise enough at lower frequencies applicable in mixing type reactors (range of 20 kHz). Figure 3.4 shows some typical solutions of the KME for a bubble with initial radius of 5 μm at different frequencies and acoustic pressure amplitudes. The graphs depict that assuming repeating (even nonlinear) dynamics for bubbles radius is reasonable in case that the computational time step is considered about less than ten times of the acoustic period.

2. Secondly, it is shown that bubbles in a sound field influence both the real and the imaginary

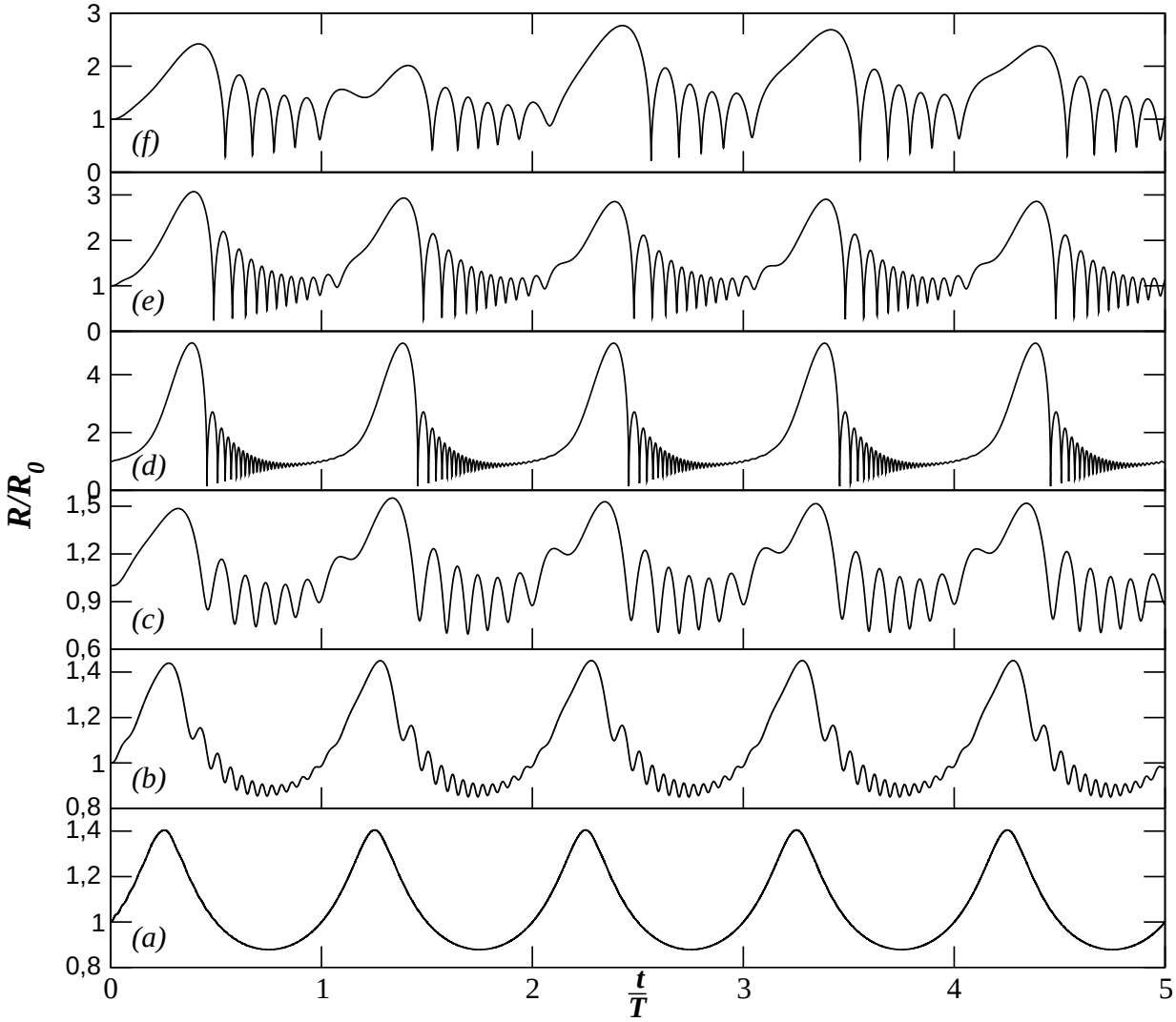

Figure 3.4.: Bubble radius variation for different amplitudes of pressure and wave frequency. (a) to (c): Pressure amplitude: 90 kPa and frequencies of 20, 50 and 100 kHz, respectively. (d) to (f): same frequencies but for an amplitude of 120 kPa.

parts of the wave number in the Helmholtz equation. This was explained previously in chapter 2. Thus, one needs a model to consider both of these effects which are available in complex wave number approximation of linear theory. For the nonlinear theory, however, this is not a straightforward task. Therefore, the approximation made by Louisnard [63] is used. According to his method, the effects of bubbles on real and imaginary parts of the wave number are decomposed by removing the imaginary part of the wave number from its original formulation and calculate the damping of the wave from nonlinear theory. Hence, the wave number of Eq. (2.45) is modified as

$$\mathfrak{Re}(k_m^2) = \frac{\omega^2}{c^2}\left(1 + \frac{4\pi c^2 N R_0}{\omega_0^2 - \omega^2}\right), \tag{3.4}$$

in which the imaginary part is removed. According to the model of Louisnard [63] the imaginary part of the wave number reads

$$\mathfrak{Im}(k_m^2) = -2\rho_l \omega N \frac{\Pi_{th} + \Pi_v + \Pi_r}{|P|^2}. \tag{3.5}$$

where the summation of the dissipations on the numerator of the RHS is computed for each individual bubble according to Eqs. (2.59-2.61). The model of Louisnard is modified by adding the radiation damping to this statement in the present work. However, there are two main differences between our modeling method and the approach of Louisnard:

a) Firstly, in applying the nonlinear damping models, he has considered a uniform distribution of bubbles wherever the acoustic pressure amplitude is higher than the Blake threshold. Therefore, one needs to consider a constant value for the number density of bubbles. Since this appears directly in the real and imaginary parts of the wave number, assuming different number density of the bubbles, leads to different values for the complex wave number.

   In the present method, since the position and other properties of any individual bubble are known, one can apply the nonlinear damping wherever a bubble exists. The advantage of this method is that one can observe the structure formed by bubbles by their Lagrangian tracing beside their nonlinear effects on the wave. However, the disadvantage is that high number of bubbles is required for more accurate simulation and the KME for each of them at each time step has to be solved. This increases

the computational effort significantly. To overcome this problem, an adaptive Runge-Kutta scheme for solving the radial dynamics equation is applied which increases the speed of computations considerably.

b) Secondly, mathematical operators (Laplacian, gradient and soforth) on complex fields are not prescribed in OpenFOAM. Therefore, the wave equation is decomposed from a single complex equation to two decoupled real and imaginary parts by assuming both pressure amplitude and wave number in the Helmholtz equation as complex variables. Assuming

$$P = P_r + iP_i\,, \tag{3.6}$$

and

$$k^2 = \mathfrak{Re}(k_m^2) + i\mathfrak{Im}(k_m^2) = K_r + iK_i\,, \tag{3.7}$$

and knowing that the Laplacian is a linear operator, one can decompose the Helmholtz equation (Eq. (2.39)) into two coupled equations as

$$\nabla^2 P_r + K_r P_r - K_i P_i = 0\,, \tag{3.8}$$

and

$$\nabla^2 P_i + K_r P_i + K_i P_r = 0\,. \tag{3.9}$$

The magnitudes of K_r and K_i are obtained from Eqs. (3.4) and (3.5), respectively. As it can be seen, these two equations are coupled in the source terms. Two field variables are defined with their own boundary conditions in OpenFOAM. After computing both fields, the magnitude of the real part is used for solving the radial dynamics equation.

3.2.1. Geometries, boundary conditions and physical properties

To verify the numerical method implemented in OpenFOAM, generic cases with simple geometries are considered. According to experiments [72, 103], in sonochemical reactors used for mixing, the frequency of the ultrasonic wave is in the range of kHz. In defining test cases, the frequency of 20 kHz is set as reference. The liquid is water in which the speed of sound is about

1500 m/s. Therefore, the length of the wave (λ) equals to 7.5 cm. Thus, the length of the 1D domain is 10 cm and for the 2D test case, a 10 cm$\times$10 cm square is considered. The reason for these selections is that the produced standing wave can experience both nodes and antinodes inside the domains. Schematic representations of the selected domains as well as the boundary conditions applied to them are presented in Fig. 3.5.

The boundary conditions for the flow field are prescribed values of velocity, turbulent kinetic energy and turbulent dissipation rate and zero gradient for the other parameters at the inlet. The momentum equation for the bulk liquid in the second 1D test case is solved to see the influence of acoustic streaming. In other cases, since only the effect of acoustic pressure gradient is of interest the flow field is not calculated. At the walls, the no slip boundary condition is imposed. The exit section of the 1D model is an outflow in which all gradients are set to zero except for the hydrodynamic pressure.

To solve the wave equation in the frequency domain, all the lateral walls of the geometries are supposed to absorb the ultrasound waves. Thus, they are modeled using Dirichlet type boundary condition with $P = 0$ in the Helmholtz equation.

In the 1D simulation, the left end of the domain is the ultrasound source which has a fixed pressure amplitude P_a= 10 kPa. This value is adopted to ensure the linear oscillations of the bubble radius and therefore, the results of the numerical simulation can be compared with analytical expressions. Analytical solutions exist only for this range of pressure amplitudes in which the oscillation of the bubble is considered as linear. The right end is set as a pressure release boundary, that is a Dirichlet boundary condition with $P = 0$. However, for the second 1D test case, the amplitude of pressure is set as P_a= 150 kPa to ensure that the bubble shows nonlinear behavior in its path of motion.

For the first 2D simulation, the upper boundary has a fixed pressure amplitude P_a= 10 kPa and the other ones are pressure release boundaries. For the second 2D case, the pressure amplitude is calculated from the external power applied to the sonotrode and physical and geometrical properties. In addition, the free surface and the side walls are pressure release boundaries while the side of the sonotrode and the bottom wall are assumed to reflect the wave. The remaining physical properties required for the simulations are indicated in table 3.3. Several simulations are conducted to check the grid independency of the results. Because of the simple geometrical

Table 3.3.: Physical properties applied in nonlinear simulations.

γ	ρ_b (kg/m^3)	σ (N/m)	ρ_l (kg/m^3)	μ (Pa.s)
1.4	1.2	0.0725	1000	0.001

configurations, the results of the wave equation and flow field were almost similar for different number of grid points. Finally, 10000 cells for the 1D test case and 200×200 cells for the first 2D geometry test case are adopted.

For the final test case, a 3D 6 cm×6 cm×6 cm domain is created and a circular sonotrode with frequency of 20 kHz is located at its bottom. This configuration exhibits a pressure antinode at the center of the box. The structure of bubbles obtained from simulations is compared with experimental results of Mettin et al. [8]. After grid independency check for the wave equation simulation, a grid with 60×60×60 cells is selected for the 3D box test case.

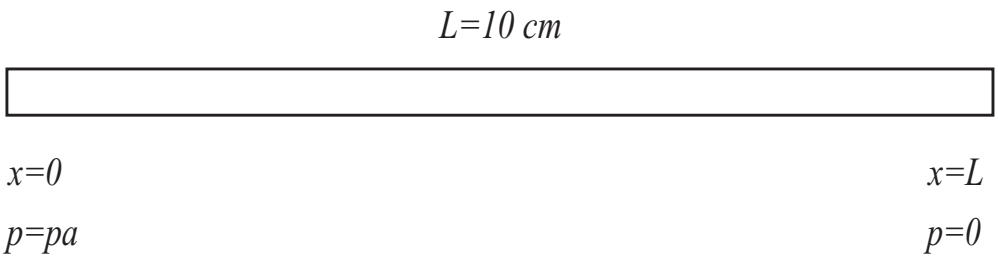

(a) 1D generic model

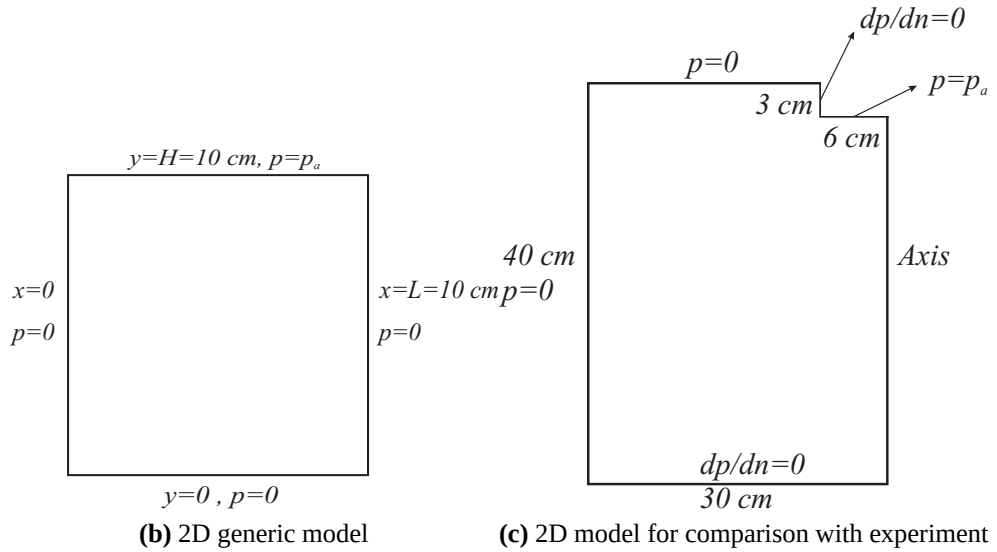

(b) 2D generic model **(c)** 2D model for comparison with experiment

Figure 3.5.: Geometries considered as the test cases with their boundary conditions and dimensions. (a): 1D, (b): 2D to be compared with analytical solution and (c): 2D to be compared with experiments.

3.2.2. Procedure of the nonlinear analysis

The procedure of nonlinear analysis can be summarized as follows:

1. The wave equation in frequency domain, Eq. (2.38), is solved and an initial pressure distribution is obtained.

2. The flow field is solved considering the acoustic streaming source term.

3. The motion of any single bubble due to the gradient of the pressure field (primary Bjerknes force) and other forces on the bubble is computed (Sec. 2.3).

4. Radial dynamics of each bubble is considered and average values for radius and volume of the bubble are calculated and modification of real and imaginary parts of the wave number wherever any bubble exist is done.

5. Eqs. (3.8) and (3.9) are solved to modify the pressure field by considering the effect of bubbles.

6. Finally, the procedure begins to repeat from 2 with a new perssure field at the next computational time step.

For the verification test cases, some of the steps are ignored. For instance, for the cases in which a single bubble motion (1D and 2D cases with low pressure amplitude) is of interest, the flow field and damping of the wave are ignored. Moreover, for the 1D case with high pressure amplitude and flow field, the effect of acoustic streaming is also negligible. The result of this case is a relationship between acoustic amplitude at each point and the volume of a single bubble. This relationship may be justified to find an equilibrium model for variation of the volume fraction of the bubbles and the acoustic pressure amplitude which is useful for linear theory. Previously (and also here for the linear analysis), it is considered as a linear function [20, 60, 104].
The final step is applying the same procedure to a 2D reactor with a large number of bubbles. In this case, all of the described steps are included in the simulation. The results of bubbles structure are compared with experiments, for example the ones performed by Moussatov et al. [105].

4. Results: Linearized approximations

All models are wrong, but some models are useful.

"George P. E. Box"

4.1. Simple geometries as benchmarks

4.1.1. Simulation of wave propagation

The results of simulating linear wave propagation for simple benchmark geometries described in Sec. 3.1.1 are shown in Figs. 4.1- 4.6. A comprehensive analysis of the geometries and pressure distributions is done using FDM in the work of Dähnke and Keil [17]. Since the pressure distributions obtained by FEM in the present thesis are similar to the aforementioned reference, the main results are reported here. It can be concluded from these analyses that:

1. For all three reactors, increasing the volume fraction of bubbles results in damping of pressure amplitude. This damping is more significant in case of higher values of β, i.e., larger than 10^{-3}. It is clear that for $\beta = 10^{-5}$, the influence of bubbles on wave propagation is negligible. This value is of the order of initial bubbles volume fraction before ultrasonic excitation [106]. Therefore, in the next steps of the analyses for real conical reactor, the minimum value of β as 10^{-4} is set.

2. A value of 10% is an upper limit for volume fraction of bubbles. For this value, regardless of the wave frequency and geometry of the reactor, pressure is completely damped in the vicinity of the ultrasound source. Thus, an upper limit of 10^{-1} is set in further simulations.

3. Increasing the wave frequency leads to more probable cavitation zones in the reactors. This effect is much more significant for the first and third reactors. In other words, for the

A part of this chapter has been published as: R. Jamshidi; B. Pohl; U. Peuker; and G. Brenner, Numerical investigation of sonochemical reactors considering the effect of inhomogeneous bubble clouds on ultrasonic wave propagation. *Chemical Engineering Journal*, 189-190(0):364–375, 2012.

second configuration, putting three ultrasound sources around a circle results in interfering waves and increasing the frequency for this set-up is not efficient.

4. The difference in the vertical position of the ultrasound source for the first and third reactors (leaving all other conditions unchanged) results in different pressure distributions. For the first reactor, pressure fluctuations are visible both in radial and axial directions, while for the third reactor the peaks of pressure amplitude are observed at different axial coordinates. Therefore, positioning the ultrasound source is of great importance in creating active cavitation zones.

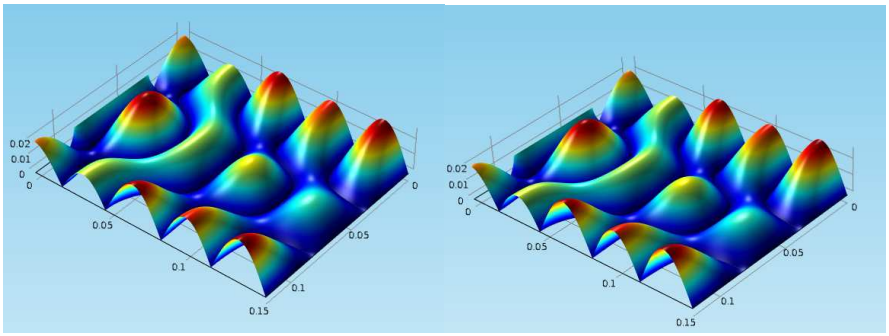

(a) $\beta = 0$ **(b)** $\beta = 10^{-5}$

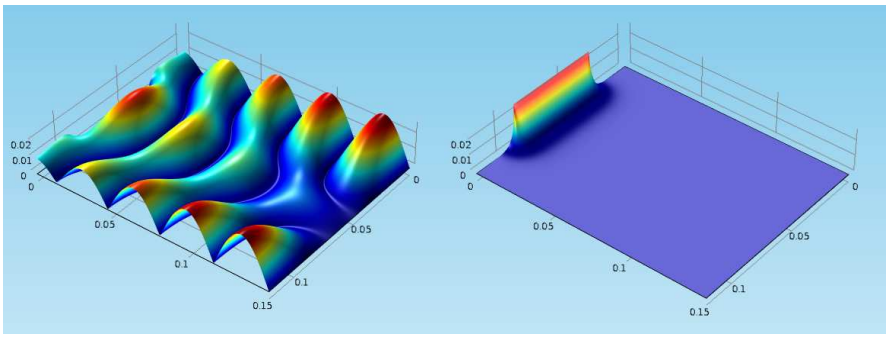

(c) $\beta = 10^{-3}$ **(d)** $\beta = 10^{-1}$

Figure 4.1.: Normalized pressure distribution in the mid-plane of the first reactor, wave frequency f= 25 kHz.

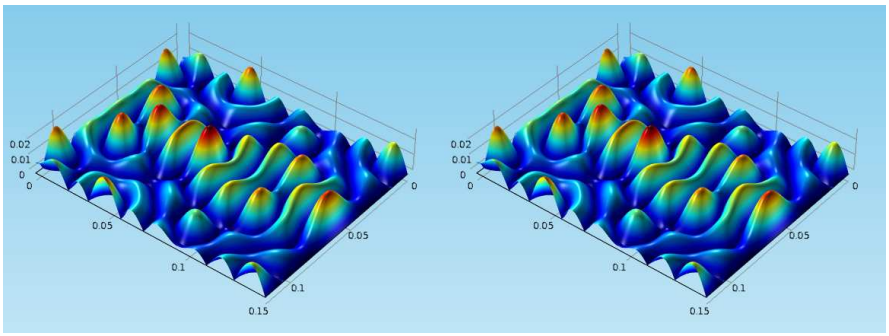

(a) $\beta = 0$ **(b)** $\beta = 10^{-5}$

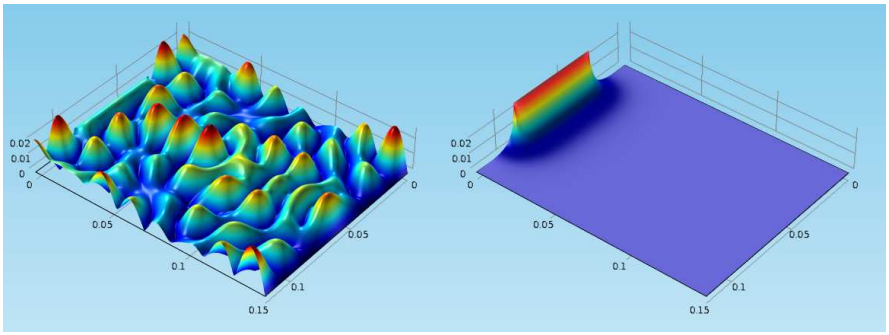

(c) $\beta = 10^{-3}$ **(d)** $\beta = 10^{-1}$

Figure 4.2.: Normalized pressure distribution in the mid-plane of the first reactor, wave frequency f= 50 kHz.

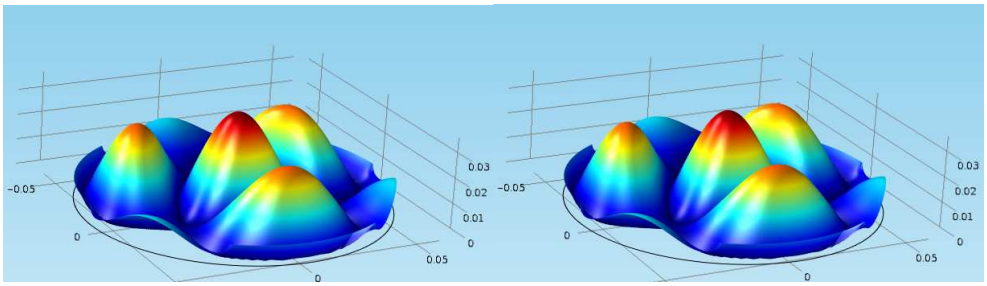

(a) $\beta = 0$ **(b)** $\beta = 10^{-5}$

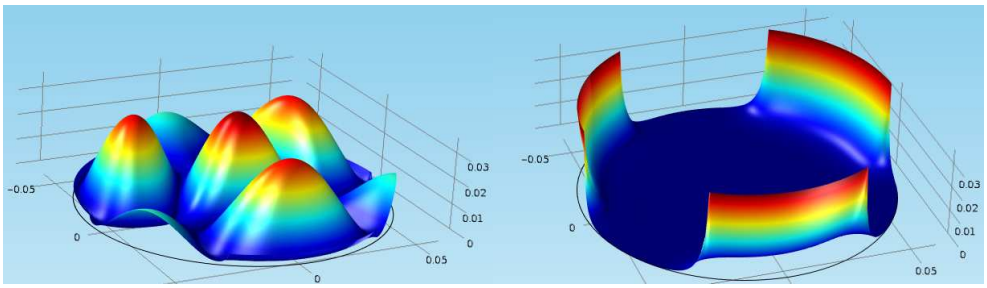

(c) $\beta = 10^{-3}$ **(d)** $\beta = 10^{-1}$

Figure 4.3.: Normalized pressure distribution in the mid-plane of the second reactor, wave frequency f= 25 kHz.

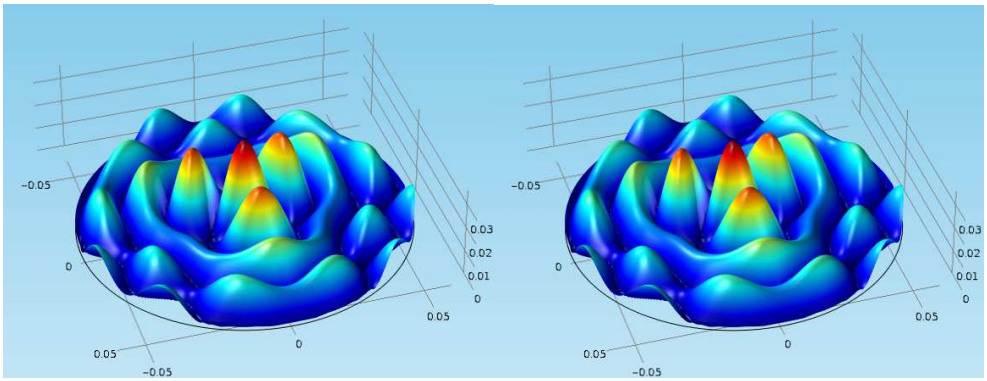

(a) $\beta = 0$ **(b)** $\beta = 10^{-5}$

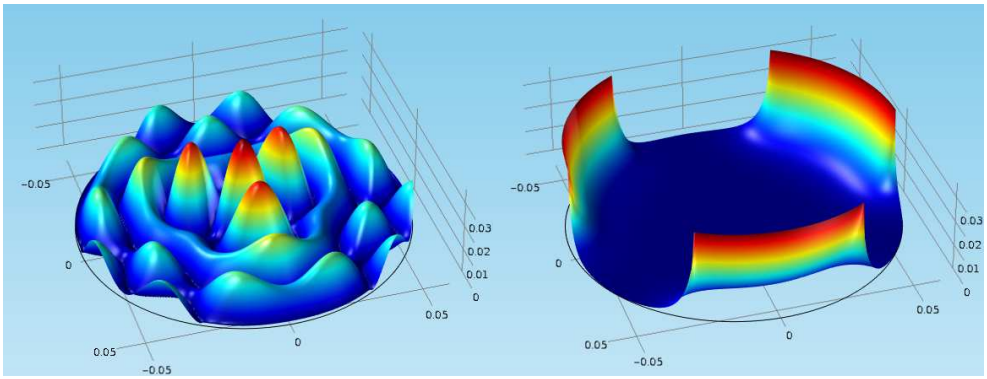

(c) $\beta = 10^{-3}$ **(d)** $\beta = 10^{-1}$

Figure 4.4.: Normalized pressure distribution in the mid-plane of the second reactor, wave frequency f= 50 kHz.

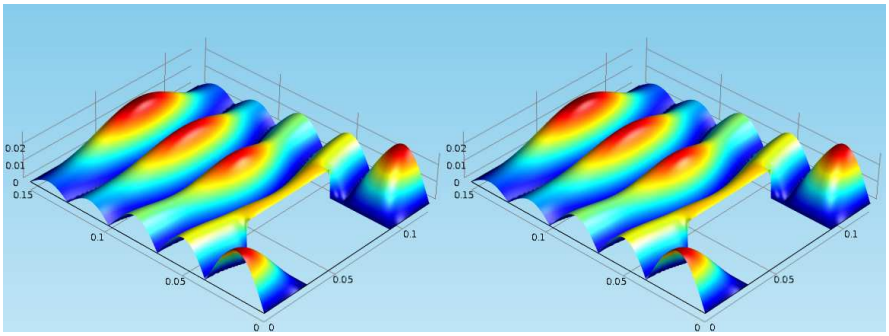

(a) $\beta = 0$ **(b)** $\beta = 10^{-5}$

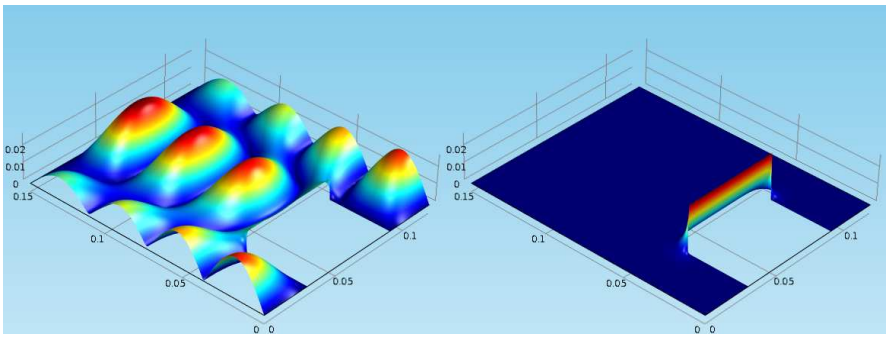

(c) $\beta = 10^{-3}$ **(d)** $\beta = 10^{-1}$

Figure 4.5.: Normalized pressure distribution in the mid-plane of the third reactor, wave frequency f= 25 kHz.

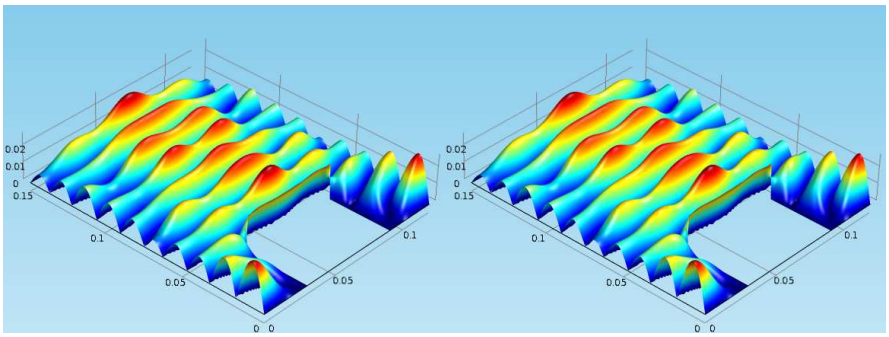

(a) $\beta = 0$ **(b)** $\beta = 10^{-5}$

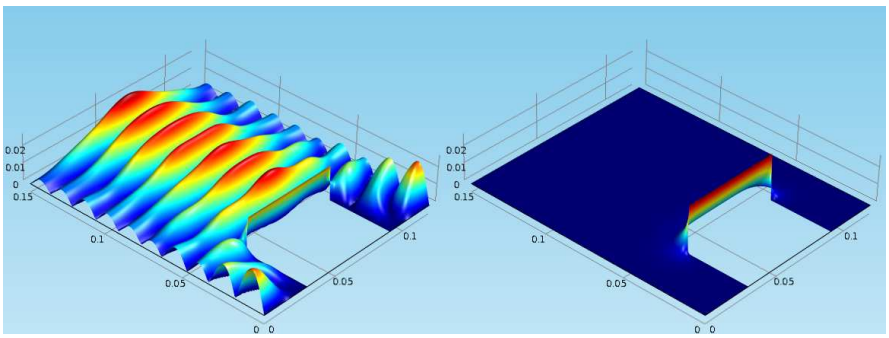

(c) $\beta = 10^{-3}$ **(d)** $\beta = 10^{-1}$

Figure 4.6.: Normalized pressure distribution in the mid-plane of the third reactor, wave frequency f= 50 kHz.

4.1.2. Simulation of acoustic streaming

The axisymmetric model of the horn-type reactor consists of walls with no slip boundary conditions. Moreover, the free surface is set as a boundary with zero gradient of pressure and there is no in and outflow for the reactor. The liquid is initially stagnant and the flow is only due to acoustic source. Figure 4.7 shows the velocity streamlines in the reactor obtained by FEM analysis (Right). The visualization of the results in experiment is done with Particle Imaging Velocimetry (PIV) technique and is shown on the left. There are two big contra-rotating vortices as stated by [75] which are also captured in the simulation. It can be seen that the simulation can reproduce the flow field inside the horn-type reactor in a reasonable way. However, it should be noted that in case of a reactor with external convective source, the source term of acoustic streaming is negligible for low frequencies. This can be investigated by looking at the set of Eqs. (2.83) and (2.84). For instance, in water for a frequency of 20 kHz and a pressure amplitude of 1 bar, the source term is about 4.5×10^{-5} N/m^3. This magnitude is negligible compared to the other forces, for instance, gravitational force $\rho_l g$. However, this force is considered in further calculations for the nonlinear analyses.

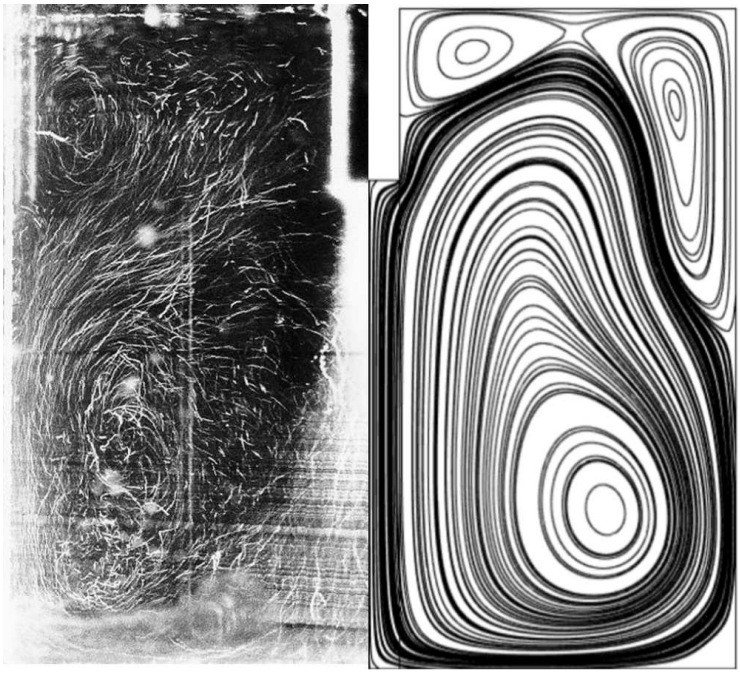

Figure 4.7.: Velocity streamlines due to acoustic streaming. Right: simulation results. Left: Experimental results reproduced from Ref. [75], with permission from Elsevier.

4.2. Pressure distribution in conical reactor

4.2.1. Pressure distribution without attenuation due to bubbles

In this section, results obtained for a simplified, linear model by neglecting the attenuation caused by the bubbles are presented. In Fig. 4.8, the variation of the normalized acoustic pressure along the half-length of the centerline of the reactor is shown for different operating conditions, that is, the minimum and maximum of the frequency and power. The results show that the pressure amplitude is almost independent of the frequency and is exactly of the same scale as the square root of the power, as defined in Eq. (3.1). The pressure level is damped within about 15 mm from the source because of the absorption by the confining walls, although the pressure amplitude approaches zero slightly faster for geometry no. 1. The reason for this result is the fact that the steel tubes, which cover about 5% of the whole volume of the reactor in geometry no. 1, are located near the transducer and reflect the wave in the region with high pressure amplitude. Consequently, a portion of the acoustic energy is restricted to the vicinity of the transducer; this effect results in a more pronounced damping of the wave. In presence of bubbles, the difference between two geometries my be greater, but for the linear case, there is no significant difference between the two geometrical configurations, except for a steeper decrease in the wave amplitude. In Fig. 4.9, the regions with a pressure level above 10^5 Pa are shown for geometry no. 1; this value is approximately equal to Blake threshold for transient cavitation to start. The acoustically activated volume increases with increasing amplitude of the ultrasound. For the following rea-

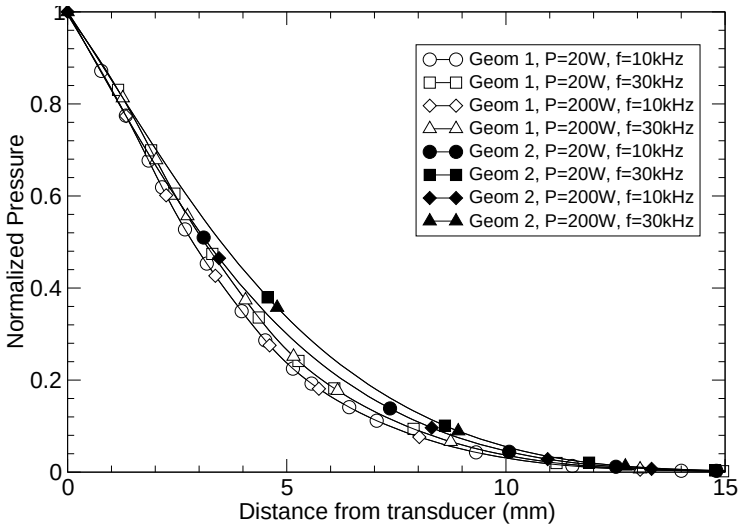

Figure 4.8.: Normalized pressure on the half-length of the central axis of the reactor for different geometrical configurations, power levels and frequency of ultrasound.

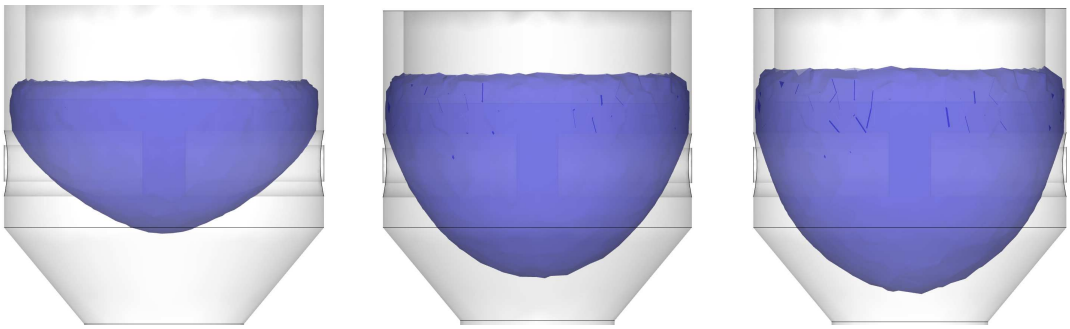

(a) $20W$ **(b)** $110W$ **(c)** $200W$

Figure 4.9.: Zones with pressure above 10^5 Pa for geometry no.1 at different values of the ultrasound powers, frequency= 20 kHz.

sons, however, this observation does not imply that an increase in the power of the ultrasound actuator will improve the effect of the ultrasound in the reactor. For some reactors, the first reason is the expected accumulation of the bubbles in the mixing region of the educts, rather than throughout the entire reactor. The second reason is the significant damping of the wave propagation by the bubbles (shielding effect). A higher pressure value causes a higher volume fraction of bubbles and thus more pronounced damping of the pressure. Hence, a balance is observed between the presence of bubbles and their effects that is considered in subsequent sections.

Effect of different boundary conditions, geometry scale-up and higher frequencies

As stated before, the linear wave model is useful in investigation different parameters affecting the pressure distribution for complex geometries. Therefore, different boundary conditions, frequencies and scaled geometries are consider in this section for the conical reactor. To consider the effect of frequency, the frequencies of 10 and 30 kHz are set as low ones and 50 and 100 kHz as high ones. Figures 4.10-4.12 show the distribution of pressure in the conical reactor with absorbing boundary conditions for different frequencies. It can be seen that at low frequencies, even up to 50 kHz, the pattern of pressure remains unchanged. However, for the frequency of 100 kHz the pressure amplitude experiences a peak at 5 mm distance from the source. Moreover, the pressure distribution is completely different from the other cases and is less uniform. It is deduced from these figures that the boundary conditions of the reactor have significant effect on the wave pattern.

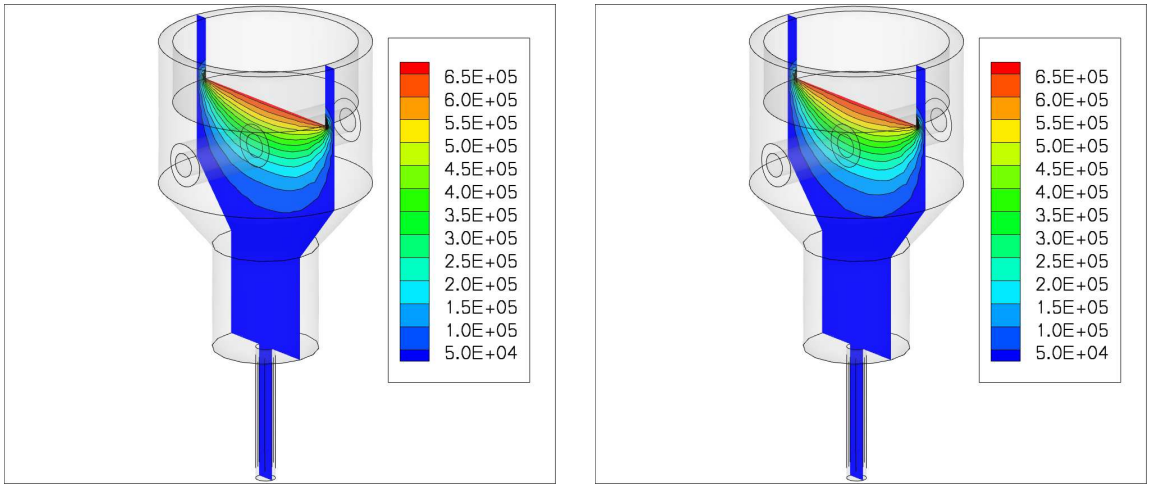

(a) f= 10 kHz **(b)** f= 30 kHz

Figure 4.10.: Effect of absorbing boundary conditions on wave propagation for low frequencies.

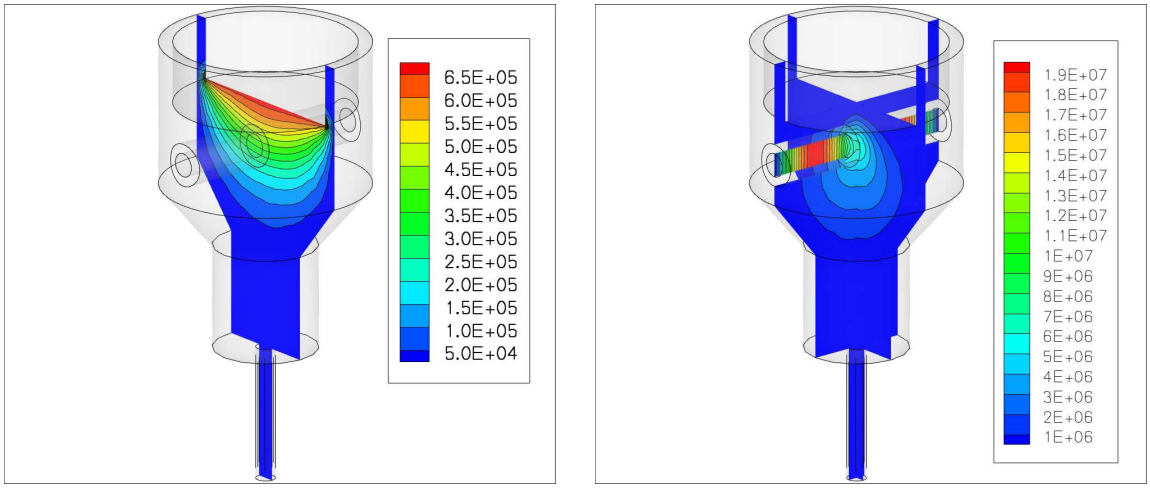

(a) f= 50 kHz **(b)** f= 100 kHz

Figure 4.11.: Effect of absorbing boundary conditions on wave propagation for high frequencies.

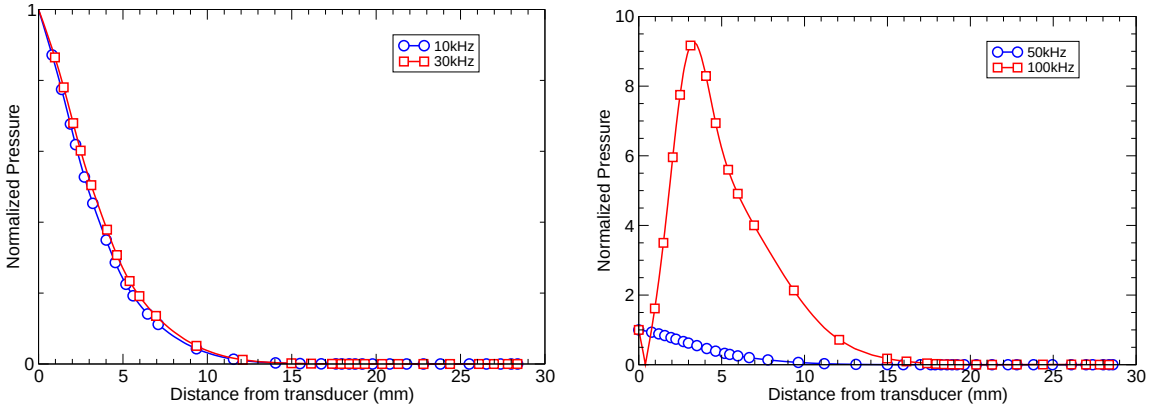

(a) Low frequencies **(b)** High frequencies

Figure 4.12.: Variation of normalized pressure along the centerline of the reactor with absorbing walls.

To investigate the sensitivity of the wave propagation to the boundary conditions, the same analysis is conducted by changing the boundary types from absorbing to reflecting. The results are shown in Figs. 4.13-4.15. It can be seen that even for low frequencies, reflecting boundary conditions lead to bigger zones of probable cavitation. The typical wave pattern with slightly reduced pressure amplitude close to the ultrasound source is not observed here. The graph of Fig. 4.15 depicts that hard walls help in creating high pressure regions in the reactor at low frequencies. The final note is about the position of the pressure peak. This can be observed, by comparing Figs. 4.12b and 4.15a. Both cases experience a pressure peak of about 8 times of the ultrasound source amplitude. However, the position of this peak is different. It can be concluded that by changing the properties of the walls, high pressure regions can be reached even at low frequencies.

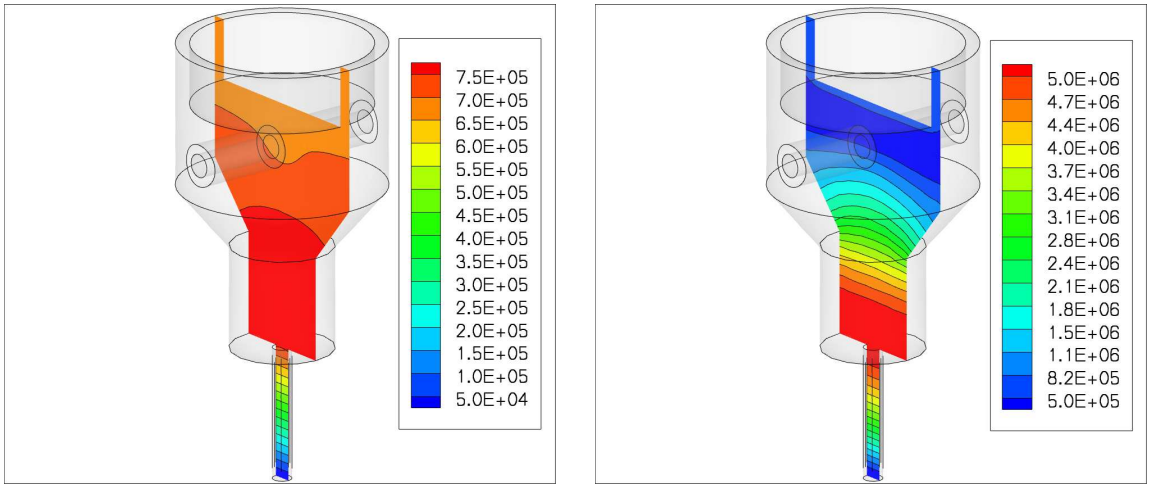

(a) f= 10 kHz **(b)** f= 30 kHz

Figure 4.13.: Effect of reflecting boundary conditions on wave propagation for low frequencies.

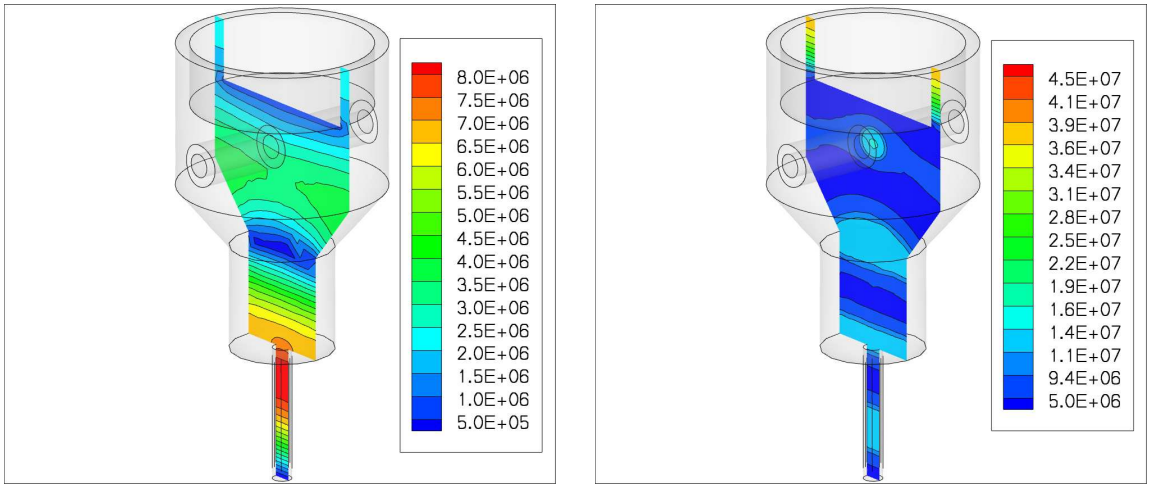

(a) f= 50 kHz **(b)** f= 100 kHz

Figure 4.14.: Effect of reflecting boundary conditions on wave propagation for high frequencies.

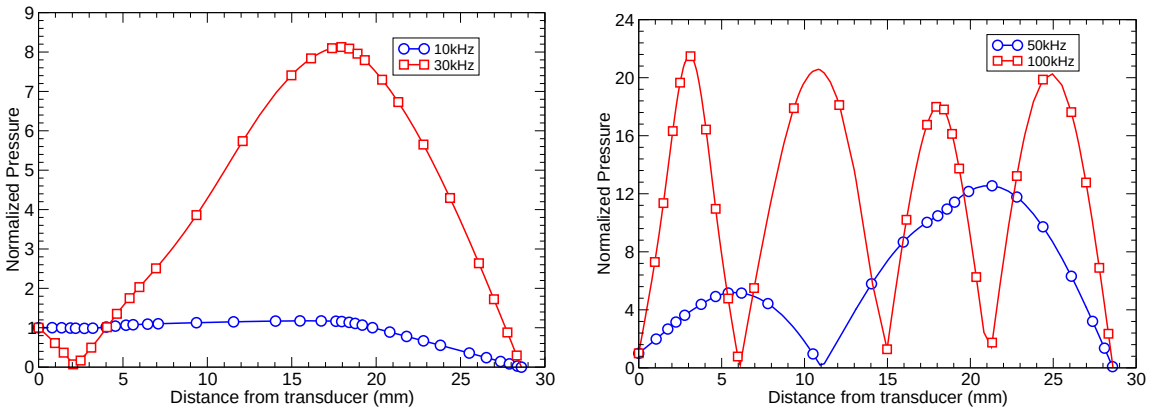

(a) Low frequencies **(b)** High frequencies

Figure 4.15.: Variation of normalized pressure along the centerline of the reactor with reflecting walls.

The final part of the linear wave analysis without damping of bubbles is the scale-up of the reactor geometry. The geometry of the reactor is scaled 10 times with the same dimensions for the ultrasound source. The results are shown in Figs. 4.16-4.18 for different frequencies and boundary conditions. It can be seen from the pressure distribution that the effect of boundary conditions are not as significant as for the smaller reactor. The reason is the larger distance from the transducer to the lateral walls of the reactor. In addition, the peaks of pressure on the centerline of the reactor have much smaller magnitudes compared to the previous cases. Hence, even in case of reflecting walls and increased frequency, the transducer is not able to create large zones of probable cavitation. Therefore, for bigger reactors, one cannot expect to have high efficiency of ultrasonication by increasing the wave frequency and using hard walls. The only solution is using bigger transducers which has its own technological problems in manufacturing and operating.

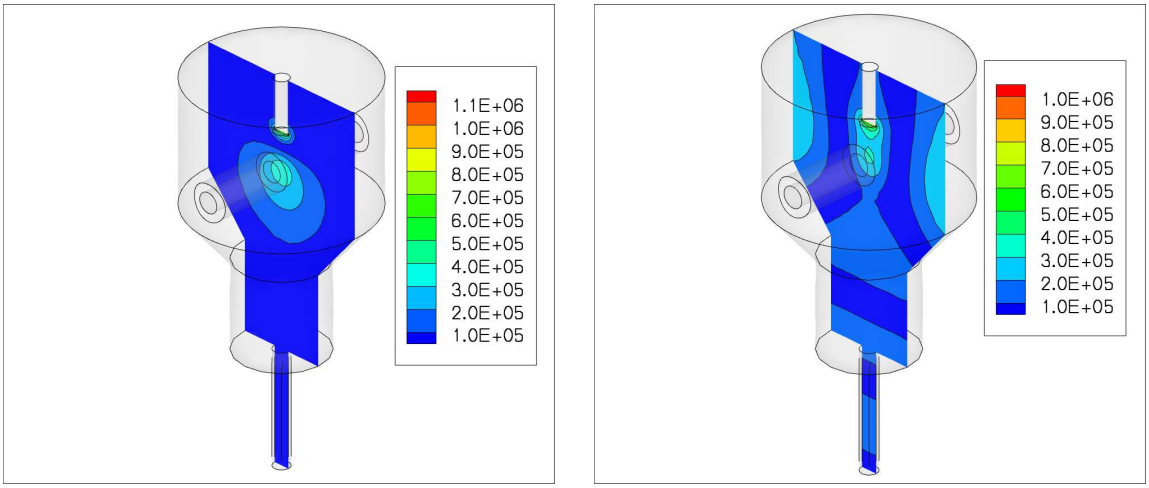

(a) P= 20 W, Dirichlet BCs. **(b)** P= 20 W, Neumann BCs.

Figure 4.16.: Pressure distribution in the mid-plane of the 10 times scaled reactor. Frequency f= 10 kHz.

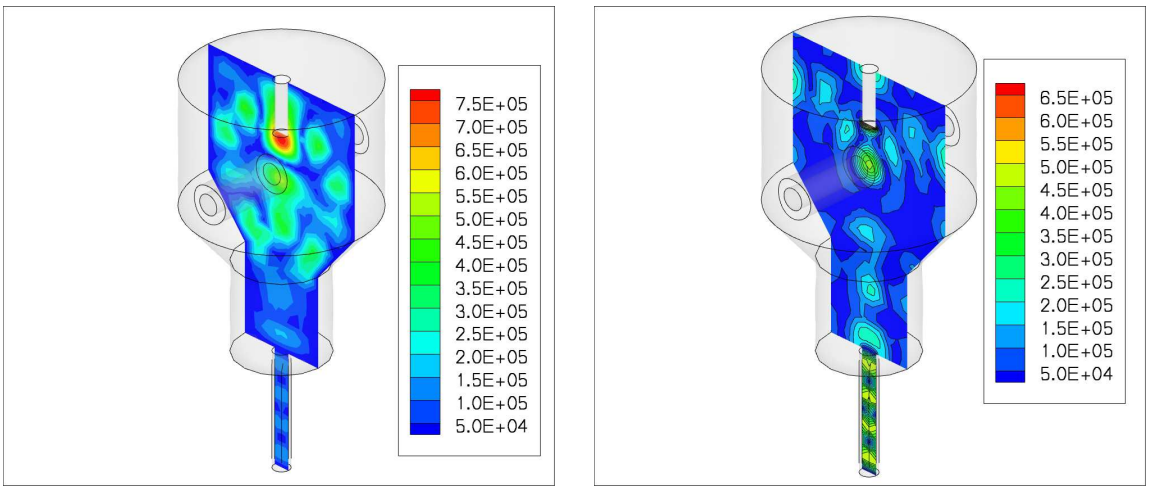

(a) P= 20 W, Dirichlet BCs. **(b)** P= 20 W, Neumann BCs.

Figure 4.17.: Pressure distribution in the mid-plane of the 10 times scaled reactor. Frequency f= 30 kHz.

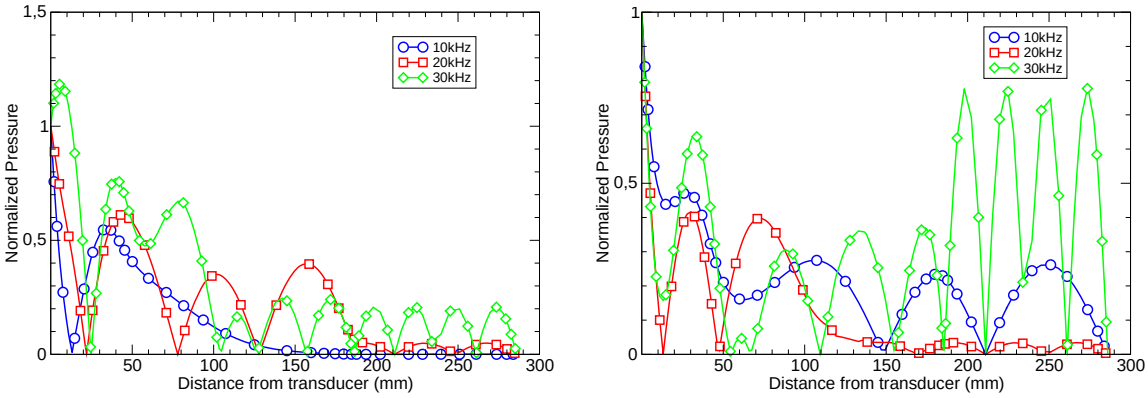

(a) P= 20 W, Dirichlet BCs. **(b)** P= 20 W, Neumann BCs.

Figure 4.18.: Variation of normalized pressure along the centerline of the 10 times scaled reactor.

4.2.2. Pressure distribution for homogeneous distribution of bubbles

Four different values are considered for the volume fraction of bubbles ($\beta = 10^{-4}, 10^{-3}, 10^{-2}, 10^{-1}$). Eq. (2.39) is solved for constant values of the attenuation obtained from a constant value of β. A monodisperse distribution of bubbles with a constant radius of 150 μm is considered. This value is the average size of the bubbles which is taken from the literature [107]. The wave number in Eq. (2.45) can be written in a slightly different form for analyzing the real and imaginary parts. After rearrangement, the following is obtained

$$k_m^2 = \frac{\omega^2}{c^2}\left(1 + \frac{A\beta}{A^2+B^2} - \frac{B\beta i}{A^2+B^2}\right), \tag{4.1}$$

in which

$$A = \frac{\omega_0^2 - \omega^2}{3(\frac{c}{R_0})^2}, \tag{4.2}$$

and

$$B = \frac{2b\omega}{3(\frac{c}{R_0})^2}. \tag{4.3}$$

Hence, the wave number consists of a real part, which represents the frequency of the wave for a constant speed of sound, and an imaginary part, which shows the damping effect. Therefore, the presence of bubbles contributes to the damping (the imaginary part of wave number) as well as the real part. The complex wave number can be written in trigonometric form as

$$k_m = \frac{\omega}{c} \quad \sqrt[4]{E^2+F^2}\left(cos(\frac{1}{2}tg^{-1}(\frac{F}{E})) - sin(\frac{1}{2}tg^{-1}(\frac{F}{E}))i\right), \tag{4.4}$$

where

$$E = 1 + \frac{A\beta}{A^2+B^2}, \tag{4.5}$$

and

$$F = \frac{B\beta}{A^2+B^2}. \tag{4.6}$$

In Fig. 4.19.a, the variation of the wave number is plotted as a function of the frequency for different values of β. In Fig. 4.19.b, the variation of the dimensionless wave number is plotted as function of β for different frequencies. As can be seen from the figure, the wave number exhibits

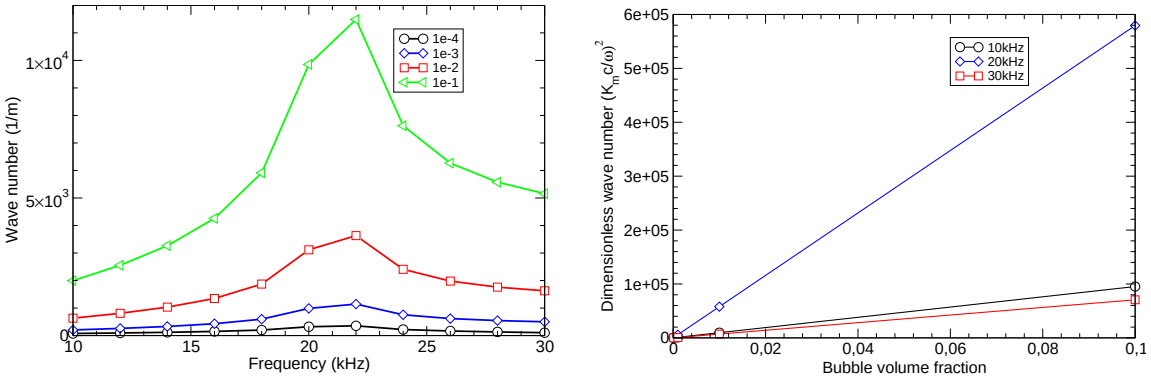

(a) Wave number versus frequency. **(b)** Dimensionless wave number versus β.

Figure 4.19.: Complex wave number.

a maximum at 22 kHz under the conditions which prevail in the present case. Furthermore, the magnitude of the wave number increases as β increases. Under the current conditions, the values of A and B in Eq. (4.1) are small, and the first term of the RHS of Eq. (4.5) is negligible for higher values of β. In this case, Eq. 4.4 can be simplified to

$$k_m = \frac{\omega}{c}\frac{\sqrt{\beta}}{\sqrt[4]{A^2+B^2}}\left(cos(\frac{1}{2}tg^{-1}(\frac{B}{A})) - sin(\frac{1}{2}tg^{-1}(\frac{B}{A}))i\right) . \tag{4.7}$$

From this simplified form of the equation, it is concluded that the wave number is approximately proportional to $\sqrt{\beta}$, as already mentioned in [55]. However, for low values of β, the simplification imposed in the derivation of Eq. (4.7) is no longer valid. This limitation is obvious from Fig. 4.19.b, where the dimensionless wave number is plotted as a function of β. Furthermore, the fraction of the imaginary part due to the presence of bubbles is independent of the volume fraction of bubbles. The second result also pertains to the fraction of the imaginary part, which is plotted as a function of the frequency in Fig. 4.20. This fraction differs slightly for different values of β. The imaginary part that varies as $sin((1/2)tg^{-1}(E/F))$ can also be approximated by $sin((1/2)tg^{-1}(B/A))$, which is not a function of β. The steep slope of the curve is related to the resonant frequency under the actual conditions. From Fig. 4.20, it is clear that the damping effect is small at lower frequencies, and that the wave can propagate. However, for frequencies above the resonant frequency, the damping effect is dominant.

The analysis explains the trend of the pressure levels shown in Fig. 4.21. Here, the variation of acoustic pressure along the central axis of the reactor for different values of β is considered. For $\beta = 10^{-4}$, it can be seen that the pressure amplitude does not differ significantly from that observed for the linear problem without bubbles. However, the pressure amplitude is obviously

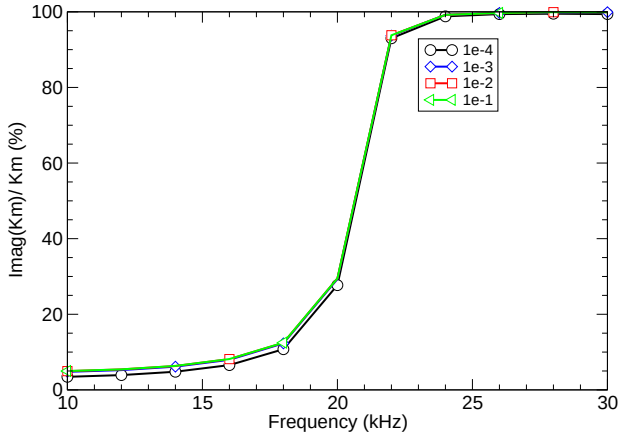

Figure 4.20.: Fraction of the imaginary part of the wave number versus frequency for different volume fractions of bubbles.

higher at a frequency of 20 kHz, in comparison with that observed at other frequencies. In the case of $\beta = 10^{-3}$ and a frequency of 20 kHz, large fluctuations of pressure are observed. This effect is due to the fact that the wave number is close to its maximum (as seen in Fig. 4.19.a) and the associated damping is slightly weaker than that observed at a frequency of 30 kHz. As a consequence, the pressure attains a peak value at about 3 mm below the transducer surface at 20 kHz. This is the zone in which the reacting streams impinge. For $\beta = 10^{-2}$, the fluctuation of the pressure observed at a transducer frequency of 10 kHz is more pronounced than for the other values. At a frequency of 30 kHz, the wave is completely damped in the vicinity of the horn. In the case of $\beta = 10^{-1}$, the damping is very pronounced at higher frequencies and the wave does not propagate at all. This effect has also been observed by other authors [17, 18, 19, 60, 104, 108, 109]. As β increases, the waves with lower frequency are amplified because of the positive effect of the bubbles on the magnitude of the wave number (Fig. 4.19); a small fraction of damping occurs in this region (Fig. 4.20). At a frequency of 10 kHz and a bubble volume fraction of $\beta = 10^{-1}$, the wave number is about 2000 m^{-1}. At this frequency, the damping, that is, the imaginary part of Eq. 4.1 is negligible as can be seen from Fig. 4.20. Thus, the pressure propagates at a wavelength of $\lambda = 2\pi/k_m = 3.1$ mm. This explains occurrence of 9 peaks in the pressure distribution along the centerline of the reactor which has a length of about 30 mm; as observed in Fig. 4.21.d. At higher frequencies, the variation is completely different because of the high extent of damping. This trend can be observed at a frequency of 30 kHz by increasing β.

The same phenomenon is illustrated in a different way in Fig. 4.22 in which regions of probable

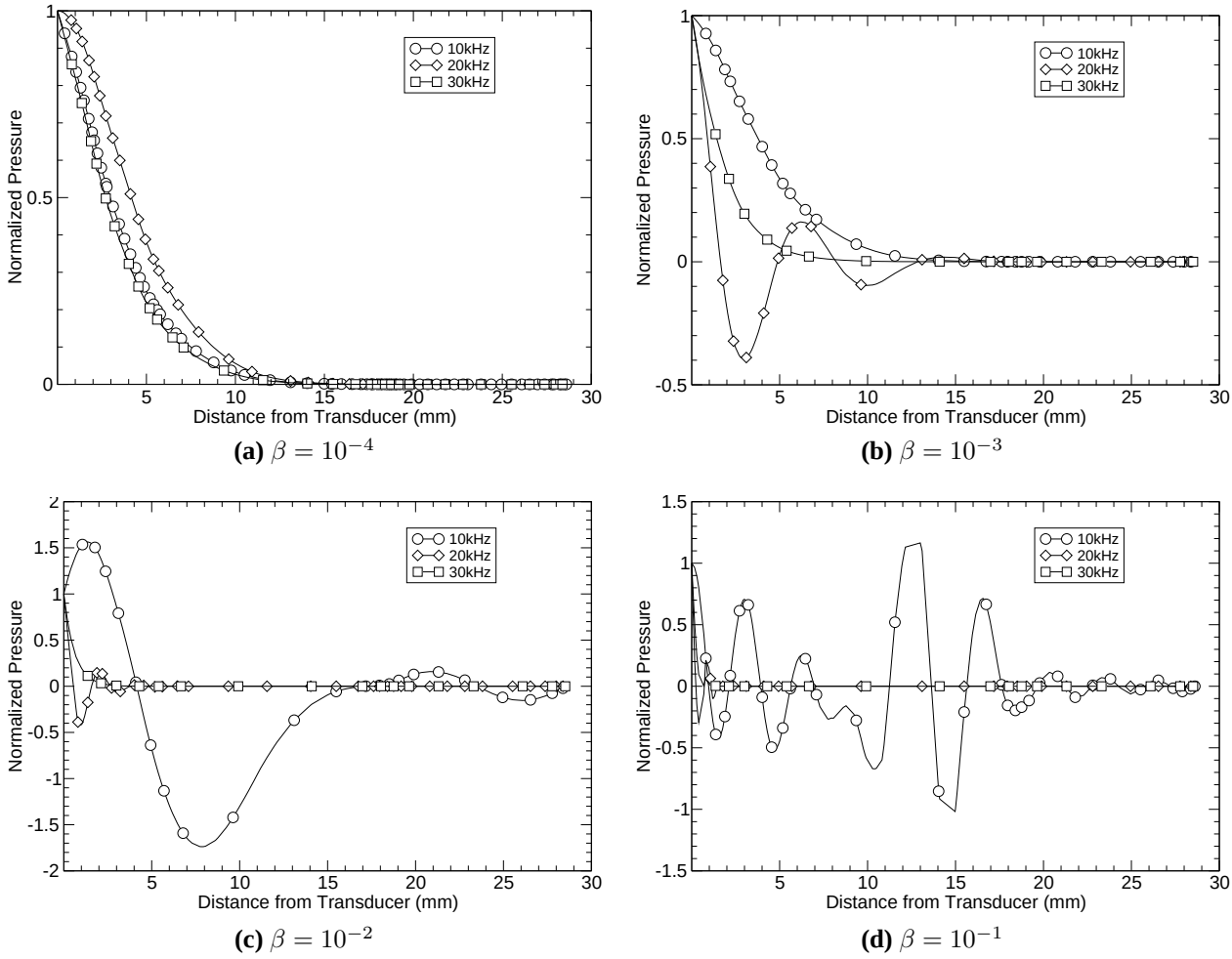

(a) $\beta = 10^{-4}$ **(b)** $\beta = 10^{-3}$

(c) $\beta = 10^{-2}$ **(d)** $\beta = 10^{-1}$

Figure 4.21.: Normalized pressure along the central axis of the reactor for geometry no.1, at different frequencies, ultrasound powers and volume fractions of bubbles.

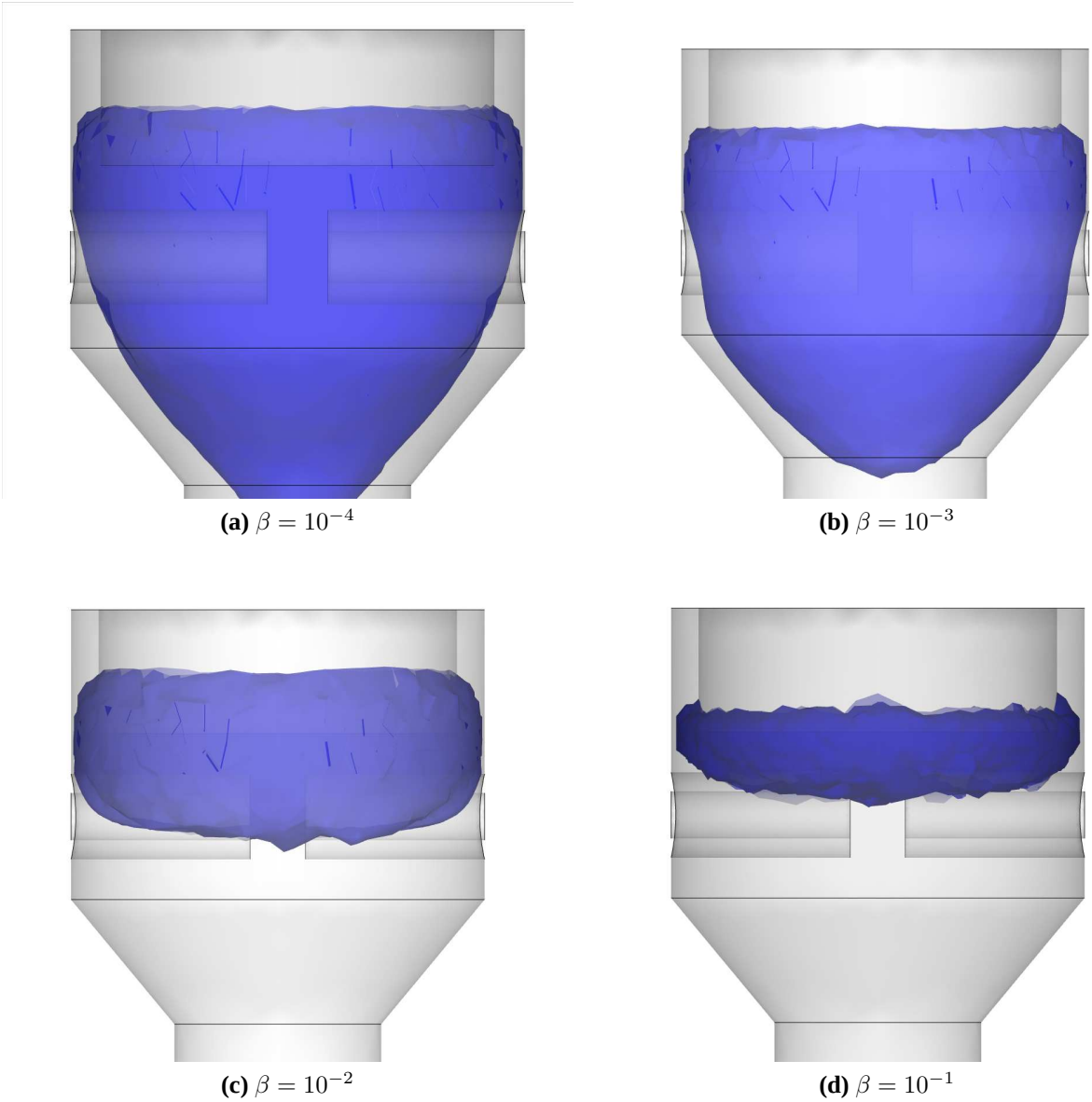

(a) $\beta = 10^{-4}$ **(b)** $\beta = 10^{-3}$

(c) $\beta = 10^{-2}$ **(d)** $\beta = 10^{-1}$

Figure 4.22.: Zones with pressure above 10^5 Pa for geometry no.1, ultrasound power: 200 W, frequency f= 20 kHz for different volume fractions of bubbles.

cavitation are shown for a frequency of 20 kHz. As can be seen from the figure, the damping effect grows as the volume fraction of bubbles increases, for a constant high frequency. The main objective of using ultrasound in sonochemical reactors is the creation of cavitation bubbles. As the volume fraction of bubbles increases, however, the associated damping also rises and therefore counteracts a further increase in cavitation. This mutual interaction should be considered with the application of an equilibrium-type equation, which has not yet been precisely defined. The results of the simulations with due consideration of this interaction are presented in the next section.

4.2.3. Pressure distribution for inhomogeneous distribution of bubbles

The method described in Sec. 3.1.2 is applied to both geometries. Since the volume fraction of bubbles depends on the pressure amplitude, the results can not be normalized, in the manner described in the previous sections. For geometry no. 1, the volume fraction of bubbles along the centreline is plotted in Fig. 4.23. For all power levels considered, the damping effect is still noticeable at a higher frequency. At a frequency of 20 kHz, a peak which is important for micromixing occurs in the β curve in the vicinity of the mixing zone in all cases. In Fig. 4.24, the bubble distribution along the middle cross section of the reactor (comparing with Fig. 3.1) is shown for three frequencies and for a power level of 20 W. For facilitating a comparison with the previously mentioned 10^5 Pa threshold, the line corresponding to this value is indicated in each subfigure. It is clear that a larger fraction of the reactor volume is filled with bubbles in the case of 20 kHz. This implies that the efficiency of applying ultrasound in creating bubbles is somehow optimized with the use of this configuration for the reactor (called a cavitational reactor) at this frequency. This conclusion has been qualitatively confirmed by experiment. The precipitation of nano-particles at this frequency and power level is more successful in terms of the uniformity and size of the particles [103].

Similar results for geometry no. 2 are shown in Figs. 4.25 and 4.26. Again, the damping effect is observed at the higher frequency of 30 kHz, and a peak is present in the curve for the volume fraction of bubbles at 20 kHz. However, it can be seen that the performance of the reactor in creating cavitational bubbles near the mixing zone is better at a frequency of 10 kHz. In the case of 10 kHz and 200 W in Fig. 4.25.c, there is a sharp increase in β for which the volume fraction reaches the order of 1% . This is a focal zone and occurs only at the centerline of the reactor. This region is located at a short distance downstream from the mixing zone of the incoming jets, as shown in Fig. 4.27. The occurrence of this region is associated with one of the antinodes of the pressure wave, which in turn is associated with the effect of the bubbles on the real part of the wave number at low frequencies, as described in Sec. 4.2.2. A more uniform bubble distribution is obtained for this geometry at a frequency of 10 kHz. Hence, if the reflecting effect of the educt walls vanishes, the oscillatory effect of the bubbles is manifested more clearly. For both geometries, a similar range of β results in the presence of the pressure field. As confirmed by experiment [103], however, the quality of mixing is impaired as the distance between the tubes

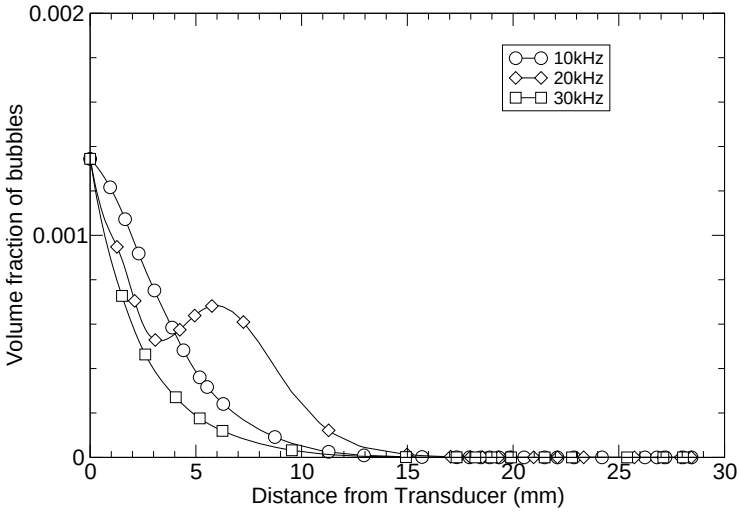

(a) 20 W

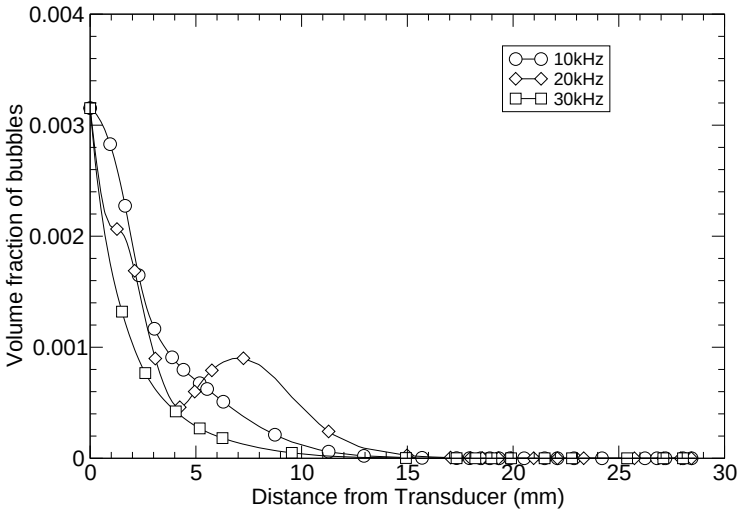

(b) 110 W

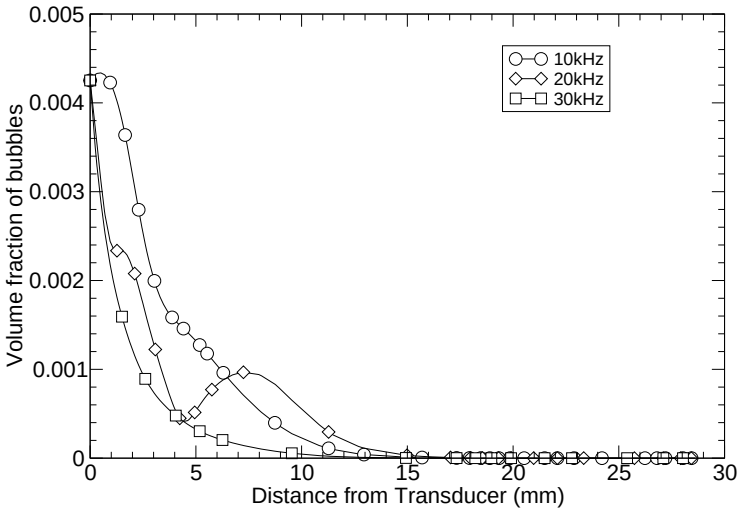

(c) 200 W

Figure 4.23.: Volume fraction of bubbles along the central axis of the reactor for geometry no. 1 at three different frequencies and three different values of ultrasound power.

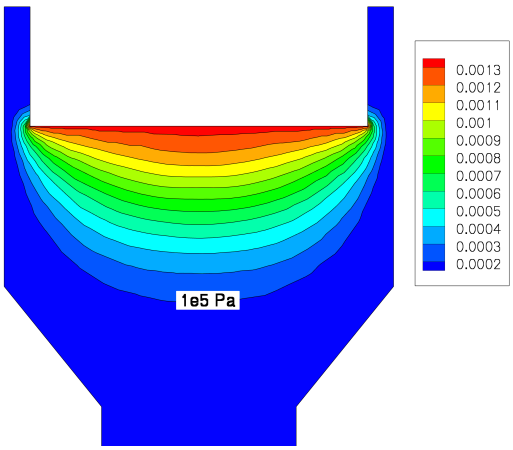

(a) 10 kHz

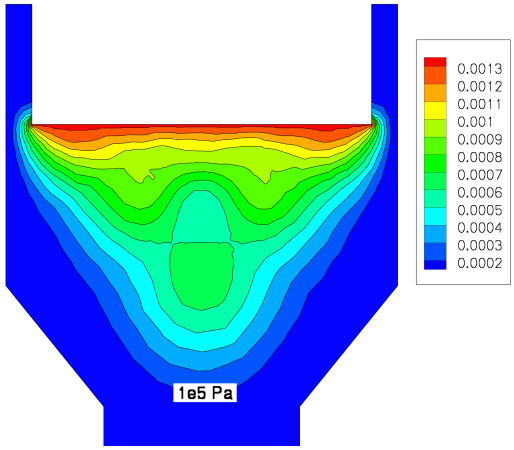

(b) 20 kHz

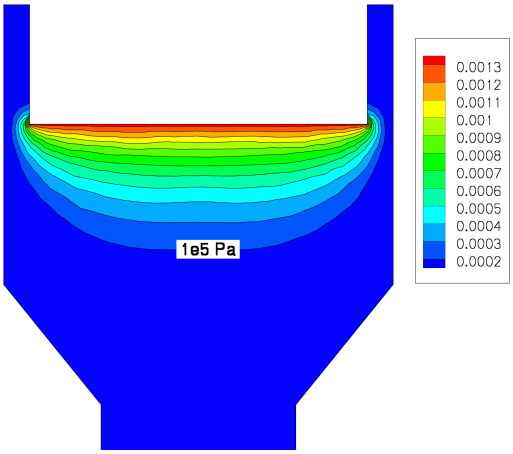

(c) 30 kHz

Figure 4.24.: Volume fraction of bubbles for geometry no. 1 on the middle cross section of the reactor at three different frequencies, ultrasound power= 20 W.

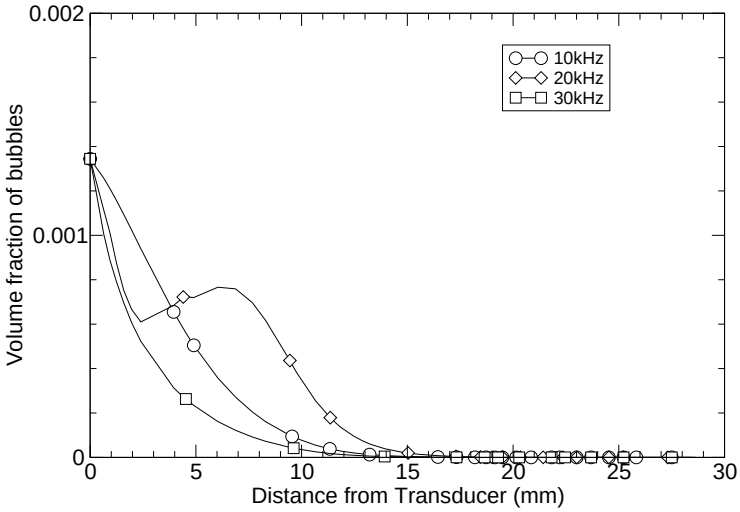

(a) 20 W

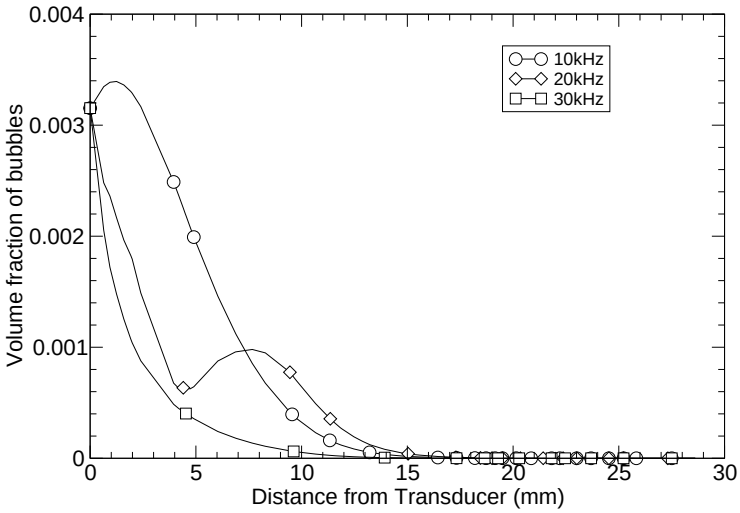

(b) 110 W

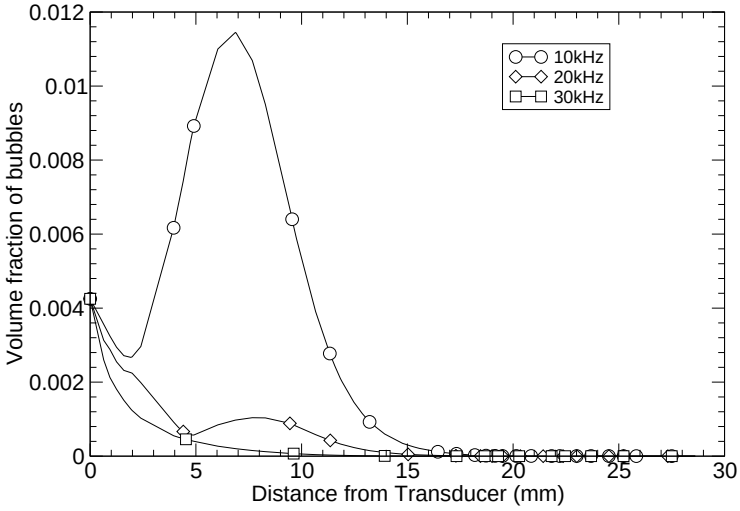

(c) 200 W

Figure 4.25.: Volume fraction of bubbles along the central axis of the reactor for geometry no.2, at three different frequencies and and three different values of ultrasound power.

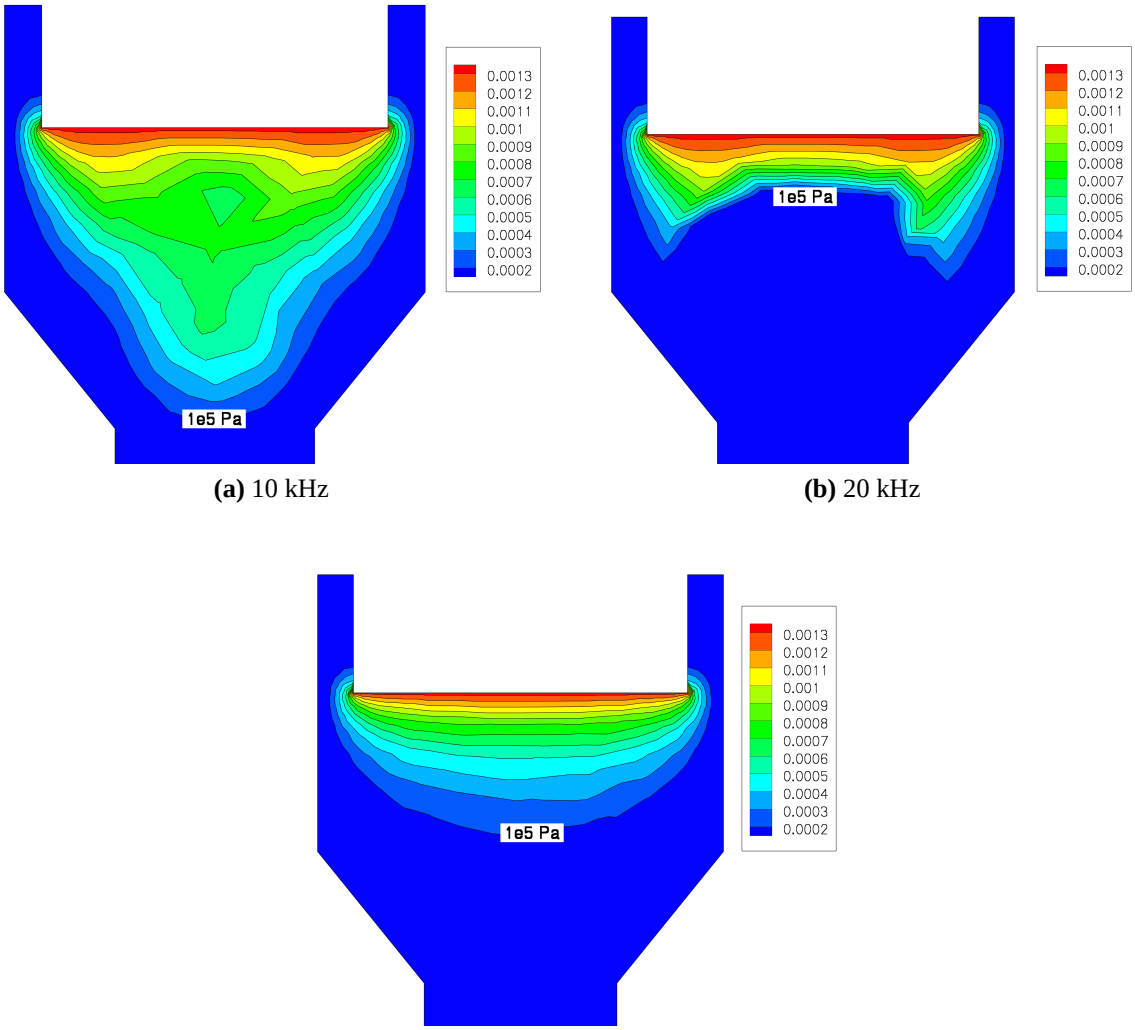

(a) 10 kHz

(b) 20 kHz

(c) 30 kHz

Figure 4.26.: Volume fraction of bubbles for geometry no. 2 on the middle cross section of the reactor at three different frequencies. Ultrasound power: 20 W.

increases. Hence, geometry no. 1 is better suited for this type of reactor, since the ultimate objective is to optimize the micromixing efficiency.

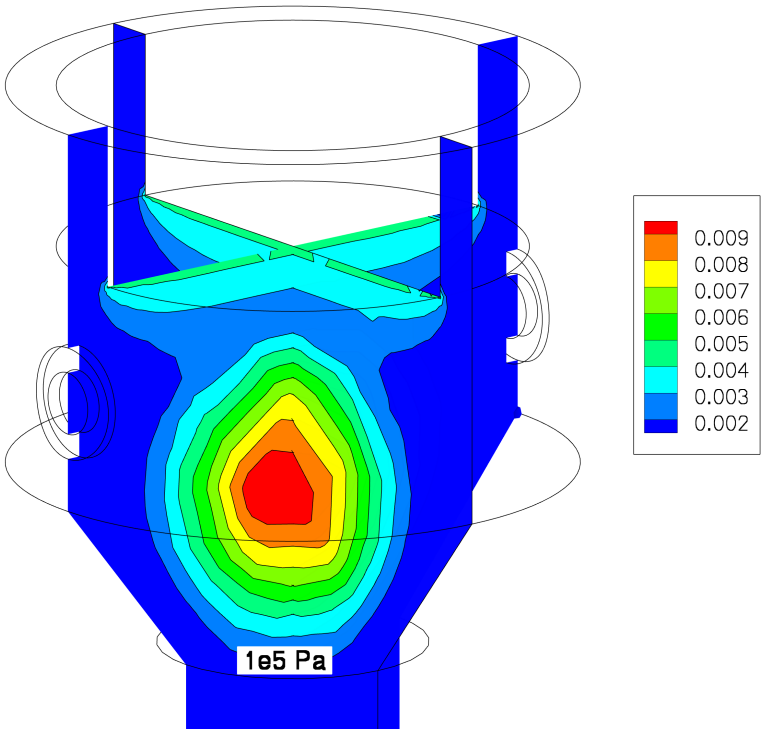

Figure 4.27.: Volume fraction of bubbles for geometry no. 2. Ultrasound power: 200 W. Frequency f= 10 kHz.

4.3. Flow field simulation in the conical reactor

As described in Sec. 3.1.1, more effective micromixing and precipitation of barium chloride and potassium sulphate in producing barium sulphate nano-particles, are the background of designing a conical shape for this reactor. Two feed tubes carry the reactant flows and the size and uniformity of the barium sulphate nano-particles at the exit tube is of interest. Therefore, studying the flow field inside the reactor is helpful in investigating the mixing zones. The basic idea of increasing the distance between the inflow tubes of the reactor is to avoid their interference with acoustic waves. The walls of these tubes are made of metal which reflects the wave and may leads to nonuniform acoustic activities. However, since better mixing of the flows is the main goal of designing the conical configuration for the reactor, one should consider the flow field as well. Therefore, for both configurations, the flow inside the reactor for four different volume flow rates of the reactants as q=0.8, 2.4, 4.0 and 6.0 lit/hr are simulated. These values are adopted from experiments [103]. The set of conservation mass (continuity) and momentum (Navier-Stokes) equations are solved for all of the cases using FEM and by considering water as the fluid. The inlet velocity is obtained by knowing the flow rate and the cross sectional area of the feed tubes and the boundary condition at exit section is ambient pressure. All of the walls of the reactor are set as no slip walls. Since the liquid is initially stagnant, the contours of velocity magnitude give reasonable information about the mixing of the flows. These contours are illustrated in Figs. 4.28 and 4.29 for different flow rates and configurations.

It can be deduced from the contours that the impinging between two flows is stronger in case of geometry no. 1. In addition, the zones inside the initially stagnant liquid which are influenced by the incoming flows are bigger compared to the ones in geometry no. 2. On the other hand, for the second configuration, the reactants are free to penetrate inside the whole geometry of the reactor and are not directly guided towards each other. Furthermore, it is revealed that increasing the flow rate, increases the zones with higher velocities for both geometries. However, another factor which influences the outcome of the reaction, is the residence time of the reactants. This parameter is defined as the time during which the reactants are inside the reactor and are able to create nano-particles. In steady state simulations of this section, it is not possible to specify this time. However, as it is observed in experiments [103], increasing the flow rates results in less residence time of the barium chloride and potassium sulphate inside the reactor. Therefore,

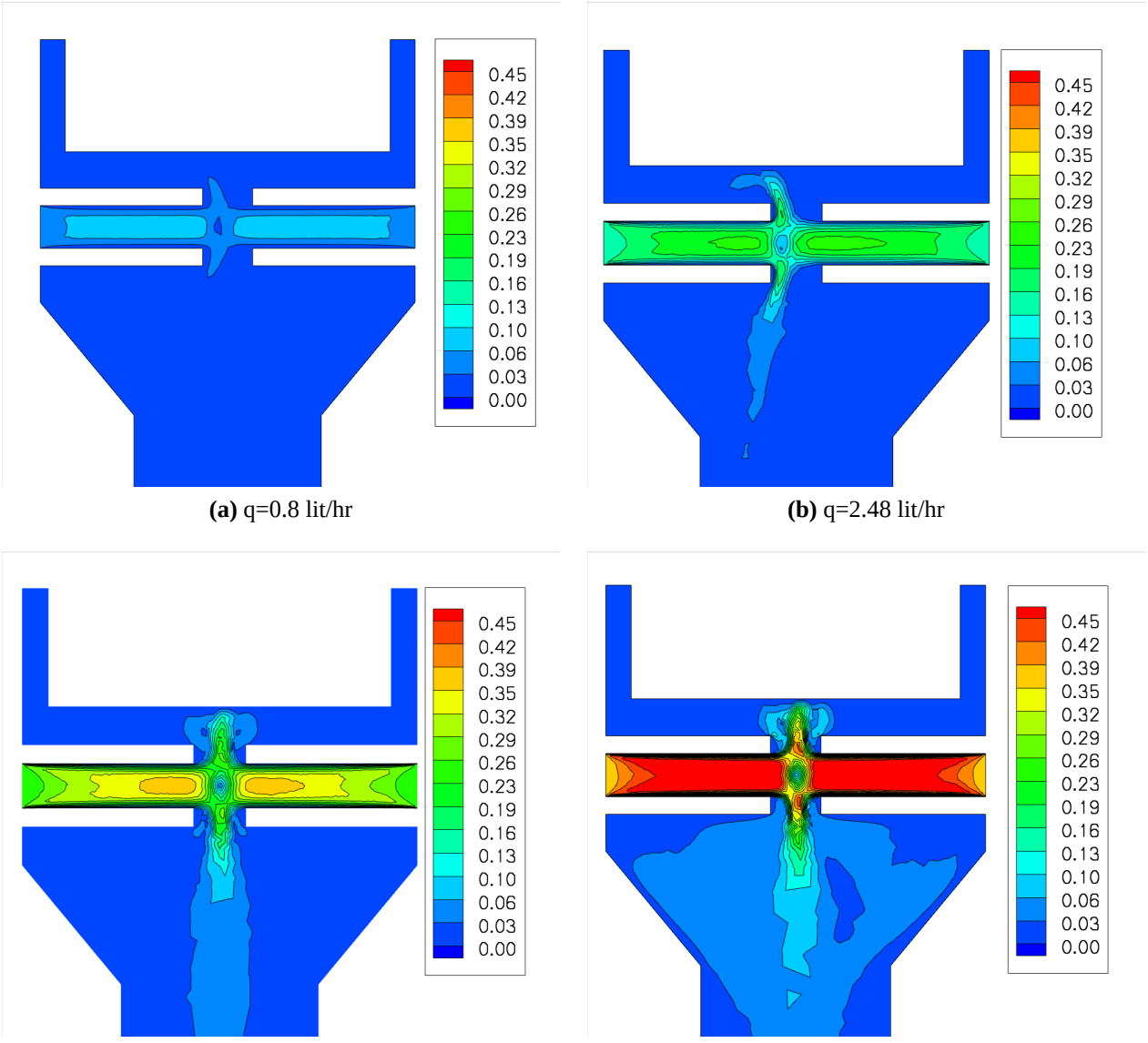

(a) q=0.8 lit/hr

(b) q=2.48 lit/hr

(c) q=4 lit/hr

(d) q=6 lit/hr

Figure 4.28.: Velocity contour at the middle cross section of geometry no.1 for different feed flow rates.

there should be an optimum flow rate in which the particles have enough time to react and mix properly. This analysis is performed using experiments by considering the size distribution of the products (both their size and uniformity). Finally, the flow rate of 4.0 lit/hr is found to be suitable for the micromixing process.

In this numerical simulation, the effects of acoustic streaming and also momentum transfer between liquid and bubbles are not considered. The coupling among these phenomena requires modeling bubbles as individual particles which is described in the nonlinear analysis of the next chapter.

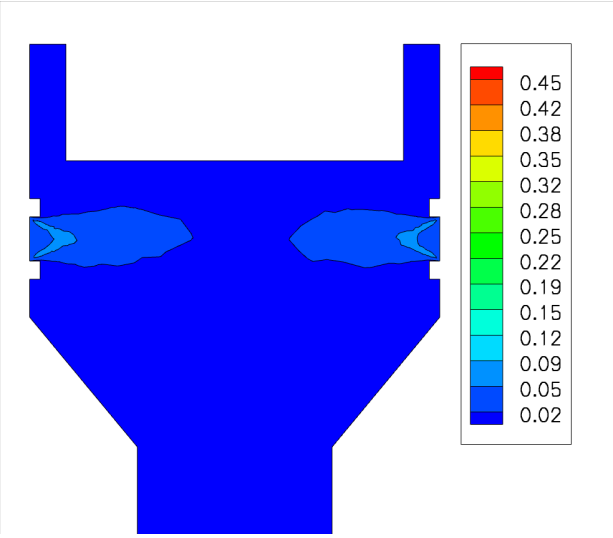

(a) q=0.8 lit/hr

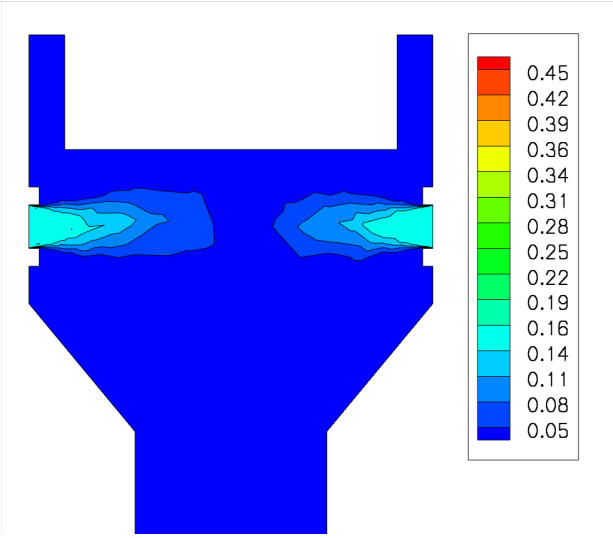

(b) q=2.48 lit/hr

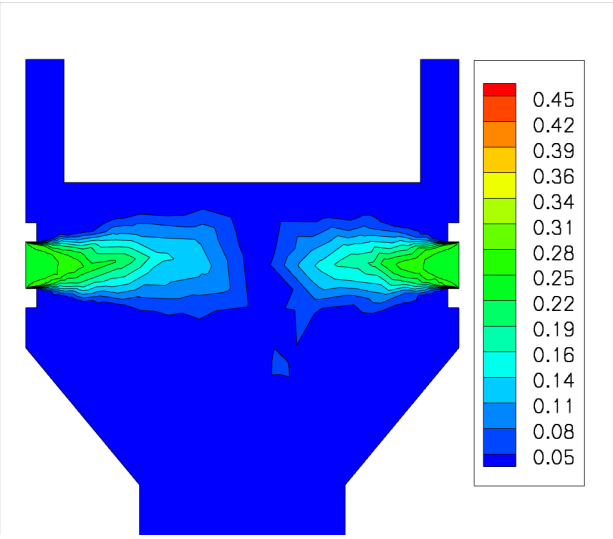

(c) q=4 lit/hr

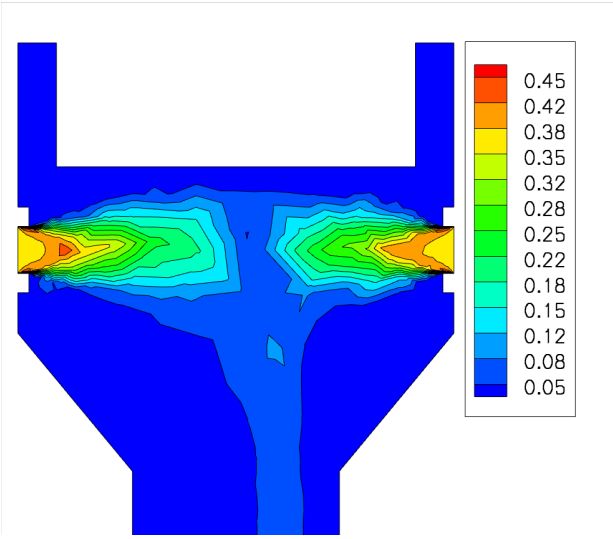

(d) q=6 lit/hr

Figure 4.29.: Velocity contour at the middle cross section of geometry no.2 for different feed flow rates.

5. Results: Nonlinear approximations

We often think that when we have completed our study of one, we know all about two, because 'two' is 'one and one'. We forget that we have still to make a study of 'and'.

"Arthur S. Eddington"

The background of the nonlinear analysis of acoustic cavitation in this thesis is based on three main questions:

1. Firstly, it is well-known that the linear models for wave propagation suffer from simplifying assumptions which lead to non-real cavitational activity in bubbly liquids. Therefore, the question arises that "How the nonlinearity of microbubbles pulsation could be introduced in wave propagation in a sophisticated model and thereafter in a simulation approach?"

2. Secondly, previous researches are confined to investigate bubbles as single particles (particle modeling) or wave propagation considering bubbles volume fraction as a field variable (continuum approach). Thus, one may ask: "Is it possible to couple these two approaches simultaneously using a numerical method?"

3. Finally, OpenFOAM as an open source package allows to investigate several aspects of a physical phenomenon in a unified solver. Accordingly, numerical implementation of different available models in sonochemistry in OpenFOAM is of interest in this work.

The following list shows different physical phenomena that are required to be implemented in one single numerical solver:

1. Acoustic pressure propagation independent of time

2. Flow field inside the bulk liquid due to external convective sources or acoustic streaming

A part of this chapter has been published as: R. Jamshidi; G. Brenner, An Euler-Lagrange method considering bubble radial dynamics for modeling sonochemical reactors. *Ultrasonics Sonochemistry*, 21(1):154–161, 2014.

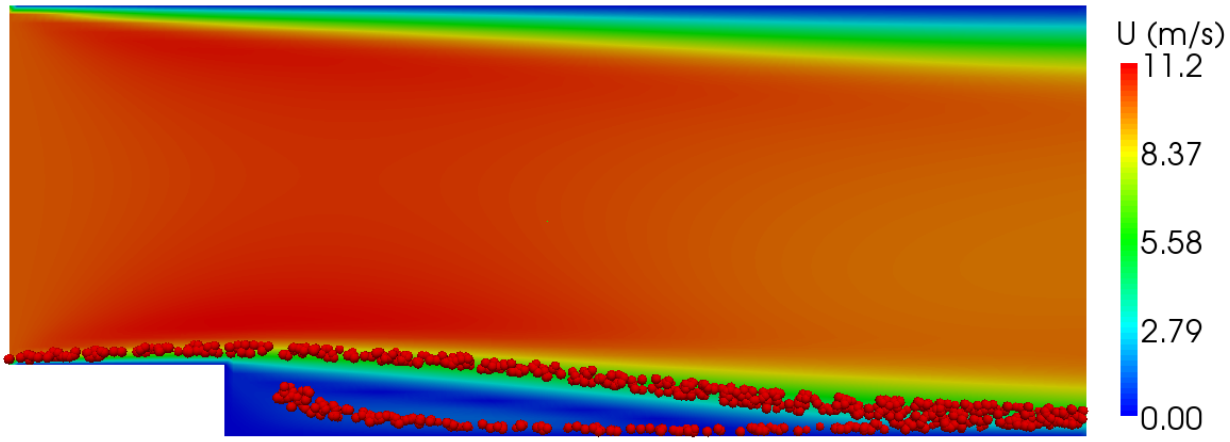

Figure 5.1.: Contour of velocity magnitude in a backward facing step test case. Bubbles with constant diameter of 1 mm are injected form the lower left corner of the inlet section. Inlet velocity=10 m/s.

3. Single bubble radial dynamics

4. Structure of a swarm of bubbles under the action of a sound field

5. Nonlinear influence of bubbles on acoustic pressure amplitude

Thus, in this chapter the step by step modeling approach and implementation of numerical method in OpenFOAM is verified using several generic test cases and validated by comparing the results with experimental observations.

5.1. Benchmarks for numerical implementations

5.1.1. Backward Facing Step (BSF)

The first step of the numerical approach is investigating the motion of bubbles due to an external convective source. Therefore, a 2D BFS case is defined in which water moves from left to right with an inlet velocity of 10 m/s. This velocity leads to a turbulent flow field which is solved using a PISO algorithm in OpenFOAM. Bubbles are constantly injected with a fixed diameter of 1 mm from lower left corner of the inlet section into the domain. It is expected that in absence of a sound field, the bubbles follow the streamlines of flow due to convection. Figure 5.1 illustrates that some of the bubbles start to recirculate inside the wake after the step. The others, due to the strong inertia of the flow field, are directly convected towards the exit section. This test case shows that the solver is capable to simulate a turbulent flow field and arbitrary point source of bubbles which inject bubbles at any time step into the domain.

5.1.2. Sudden expansion: convection of a single bubble with varying radius in a sound field

To investigate the radial dynamics of bubbles, simulation of the Helmholtz equation is also required to find the pressure amplitude in the computational domain. A 2D sudden expansion geometry (with a 8 cm $\times$5 cm rectangular geometry after the expansion) is defined as the test case. The liquid moves from left to right with an inlet velocity of 10 m/s. Four different sonotrodes are located at the walls of the model with an amplitude pressure of 1.3 bar and a frequency of 20 kHz. A single bubble with initial diameter of 2 μm is injected at the center of the inlet section. The bubble starts to move due to high velocity of the flow and experiences high pressure levels during its motion through the domain. Figure 5.2 depicts that the four sonotrodes create a high pressure region at the central zone of the domain. The bubble experiences a different value of pressure amplitude at each new position and consequently, a new diameter is calculated for the bubble according to KME. Therefore, the proportionality of the diameter of a single bubble with pressure amplitude can be investigated. The results are shown as the variation of acoustic pressure amplitude and bubble's diameter in Fig. 5.3. It can be seen that at high pressure zones, the bubble's diameter increases to about 1 mm. This analysis can be extended, for instance, for simulation of reactors with different sonotrodes which have different input powers and frequencies. In addition, it is useful in estimating the volume fraction of bubbles from a single bubble behavior and comparing the results with experimental measurements. This estimation will be represented later in Sec. 5.3.2

The final step of combining the transient and turbulent flow field solver with Lagrangian solver is introducing multiple bubbles rather than a single one. This is done by coupling the method of injecting a single bubble point source of Sec. 5.1.1 with the current solver. Instead of a point source, a line source is defined at the inlet section of the sudden expansion model and force ten bubbles to pass the high pressure zone created at the center of the domain. Figure 5.4 shows the structure formed by bubbles and their dimensions. It is depicted that near the ultrasound source, bubbles have larger diameters and when they pass the high pressure region, their sizes decrease. Since the injection line introduces ten bubbles at each time step, this trend repeats itself for different time steps. Therefore, the structure of Fig. 5.4 does not change considerably in time.

Up to now, the motion of multiple bubbles swarm due to external flow field is investigated.

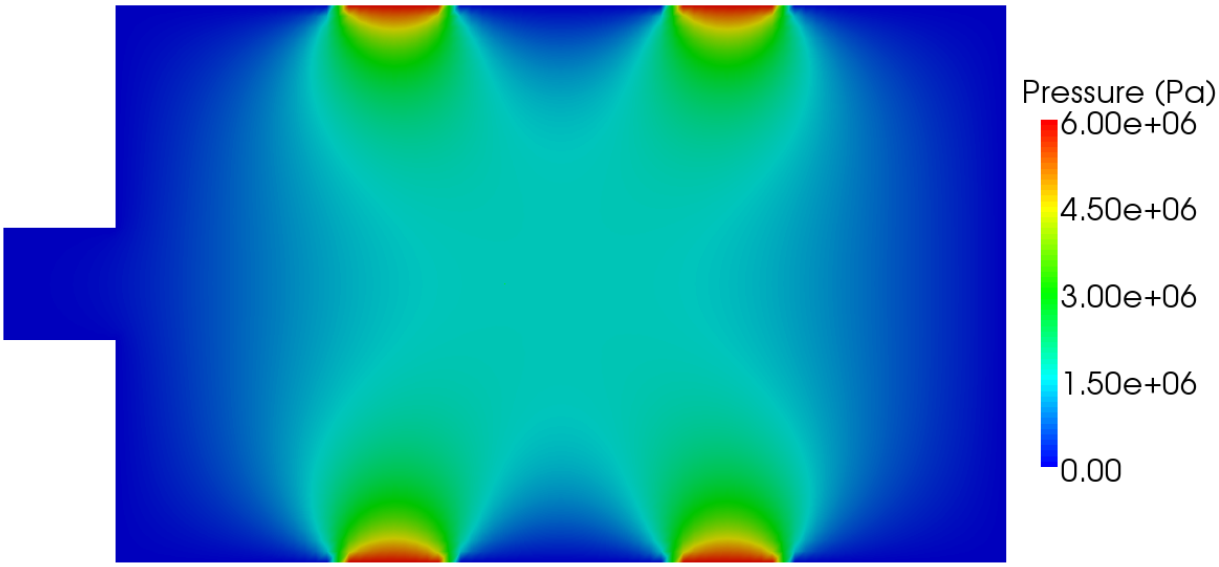

Figure 5.2.: Acoustic pressure distribution in the 2D sudden expansion test case. Inlet velocity= 10 m/s.

However, since the structure of bubbles under the action of ultrasound is strongly dependent to the acoustic pressure gradient, one should introduce the acoustic forces on each single bubble. This is done by applying the primary and secondary Bjerknes forces in the next sections.

5.2. Orders of magnitude of the forces on bubbles

There are six different forces on the LHS of Eq. (2.86) that are acting on the bubble. Assuming the displaced mass of the fluid by the bubble as $\rho_l V_b$, the orders of magnitude of the forces per displaced mass of the fluid are obtained as $|g|$ for the gravitational force, $\overline{U}/T_f$ for the inertia and the volume variation forces, $\overline{U}\nu/R_b^2$ for the drag force, $\nabla P_a/\rho$ for the primary Bjerknes force and $R_b^3/(T_f\Delta\mathbf{x})^2$ for the secondary Bjerknes force. In these relations, $\overline{U}$ denotes the order of the velocity magnitude of the bubble and the bulk of the medium, T_f is the time scale of the flow field and $\Delta\mathbf{x}$ is the typical distance between two bubbles. For common sonochemical reactors, the nuclei of bubbles have diameters of about 10^{-5}m. The reactors are usually filled with water as the bulk medium with a viscosity of $\nu = 10^{-6}\text{m}^2/\text{s}$ and the mean velocity of the flow field and its time scale are in the order of 1 m/s and 10^{-2}s, respectively. Therefore, it can be deduced that the drag force is much stronger than the other forces and depending on the gradient of the acoustic pressure, the primary Bjerknes force is also be of great importance. The secondary Bjerknes force would be of great importance in case the distance between two bubbles approaches zero and vanishes immediately by increasing the distance (proportional to $(\Delta\mathbf{x})^{-3}$).

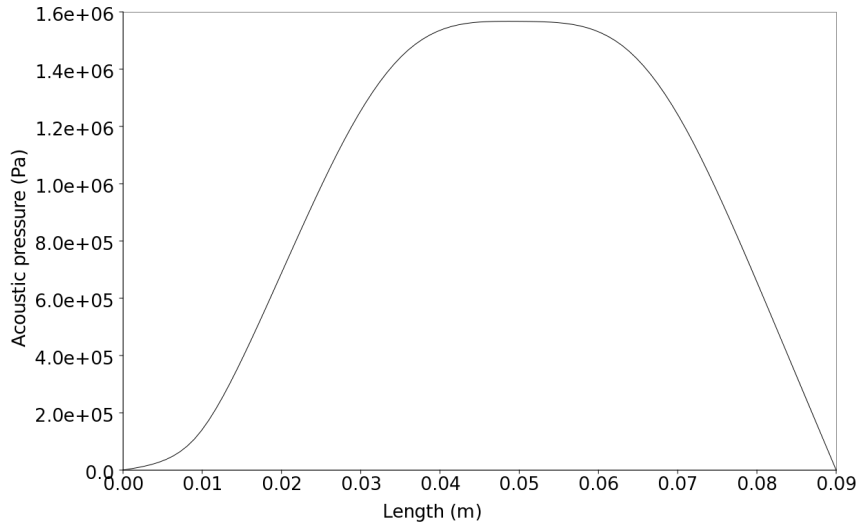

(a) Acoustic pressure

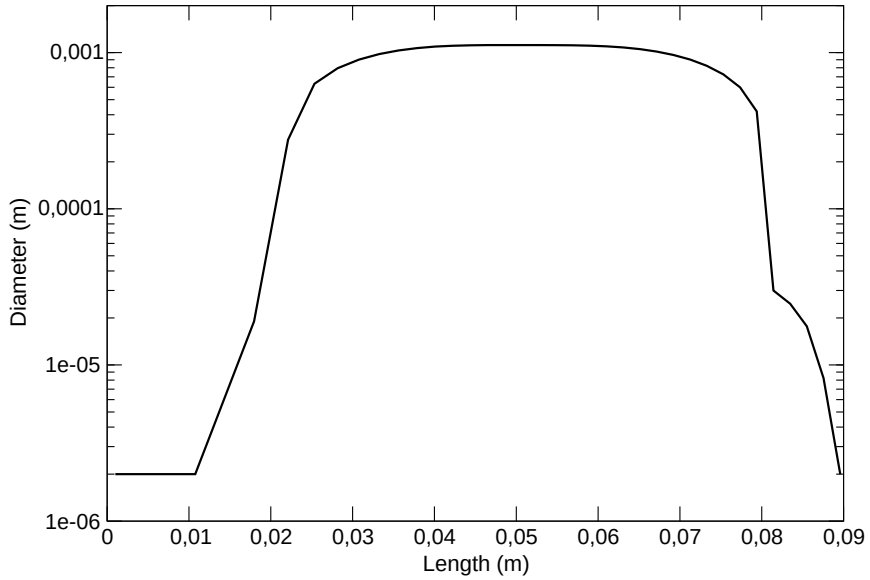

(b) Bubble diameter

Figure 5.3.: Variation of (a): acoustic pressure amplitude and (b): diameter of a single bubble on the centerline of the sudden expansion geometry. Bubble initial diameter: 2 μm. Inlet velocity= 10 m/s.

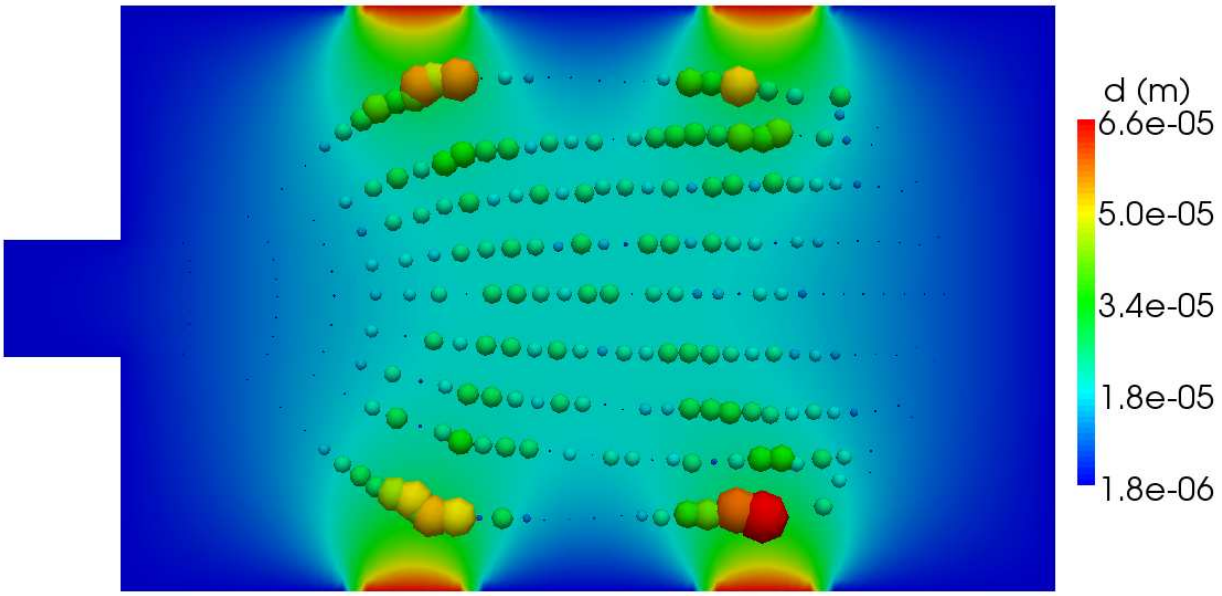

Figure 5.4.: Bubbles translational motion due to external convective source and radial motion due to acoustic field in the 2D sudden expansion test case. Initial diameter of bubbles: 2 μm. Inlet velocity= 10 m/s. Size of the bubbles are magnified to show the change of diameter at different positions.

From the above analysis, it is concluded that the two drag and primary Bjerknes forces play a substantial rule in determining the trajectories of the bubbles, especially for high pressure amplitudes in the nonlinear region. In case of an accumulation of bubbles in a small region (for instance around a pressure antinode), the secondary Bjerknes force is also significant. The averaged formulation for the drag force is similar to the Stokes' law and its implementation in OpenFOAM is straightforward. On the other hand, since the effect of the primary Bjerknes force on the bubbles trajectories is of importance in the present study, the implementation of this force in the Lagrangian approach is examined at first. To verify the numerical approach, 1D and 2D benchmarks with low pressure amplitudes are investigated. For these cases, analytical expressions are available for bubble's trajectory.

5.3. One-dimensional simulation

5.3.1. Single bubble motion- Linear oscillations

In case of an acoustic standing wave as $p(\mathbf{x},t) = p_0 - P_a(\mathbf{x})sin(\omega t)$, the average of the primary Bjerknes force in one acoustic cycle reads

$$\mathbf{F_{Bj1}} = -\frac{1}{2}V'\nabla P_a cos(\phi)\,, \tag{5.1}$$

in which $V' = 4\pi R_0^2 R'_a$ is the amplitude of the oscillation of the bubble volume and ϕ is the phase shift [40]. According to Leighton [69], larger bubbles with initial radius bigger than the resonant radius ($cos(\phi)$ >0) are attraced towards the pressure nodes and smaller bubbles with $R_0 < R_{res}$ ($cos(\phi)$ <0) move towards the pressure antinodes. The resonant radius is the radius of the bubbles if their resonance frequency is equal to the frequency of the external acoustic source. Equation (2.38) in 1D reduces to $P'' + k^2 P = 0$ and with the boundary conditions illustrated in Sec. 3.2.1, one can find a solution as

$$P_a(x) = \frac{P_a sin(k(l-x))}{sin(kl)}\,, k > 0, kl \neq n\pi, \tag{5.2}$$

for the amplitude of the acoustic pressure and its gradient as

$$\nabla P_a(x) = -\frac{P_a k cos(k(l-x))}{sin(kl)}\,. \tag{5.3}$$

On the other hand, the solution of Eq. (2.25) leads to the following relationships for the amplitude of the linear oscillations and the phase shift

$$R'_a = \frac{P_a(x)}{\rho R_0 \sqrt{(\omega_0^2 - \omega^2)^2 + (\alpha\omega)^2}}\,, \tag{5.4}$$

and

$$cos(\phi) = \frac{\omega^2 - \omega_0^2}{\sqrt{(\omega_0^2 - \omega^2)^2 + (\alpha\omega)^2}}\,. \tag{5.5}$$

Variation of the normalized acoustic pressure, its gradient and amplitude of bubble oscillation is illustrated in Fig. 5.5. To put all these parameters in one single graph, normalization is done for pressure as $P_a/P_a(x=0)$, for its gradient as $\nabla P_a/10^6\ pa/m$ and for radius as $R'(x)/R'_{max}$. It is obvious that the linear method is a reasonable approximation for this model.

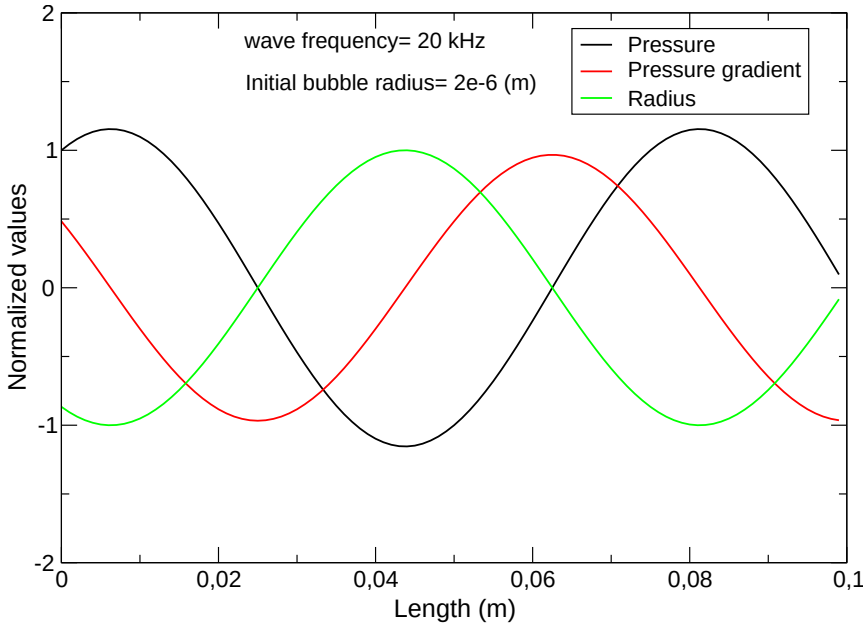

Figure 5.5.: Variation of normalized pressure amplitude, pressure gradient and bubble's radius in the 1D domain. Initial radius: 2 μm. Pressure source amplitude $P_a(x=0)$: 10 kPa. Normalization is done for pressure as $P_a/P_a(x=0)$, for gradient as $\nabla P_a/10^6\ pa/m$ and for radius as $R'(x)/R'_{max}$.

By substituting Eqs. (5.3-5.5) in Eq. (5.1), the primary Bjerknes force at each point of the domain is obtained. Finally, the equation of motion for a single bubble under the action of this force (neglecting the drag force) can be obtained as

$$\ddot{x} + A \cdot sin(2k(l-x)) = 0\,, \tag{5.6}$$

where A is a constant which can be written as

$$A = \frac{3}{4}\frac{kP_a^2(\omega_0^2-\omega^2)}{\rho\rho_b R_0^2 sin^2(kl)((\omega_0^2-\omega^2)^2+(\alpha\omega)^2)}\,. \tag{5.7}$$

In deriving Eq. (5.7), it is assumed that due to the small oscillations of the bubble, the mass of the gas inside the bubble remains constant. Equation (5.6) models a mass-spring system in which the spring constant is a function of space. Therefore, it is expected that in absence of the drag force, the bubble should oscillate around some focal points. This equation (5.6) can be solved with the use of elliptic integrals which at the end require numerical integration or by a backward Euler method (the 4^{th} order Runge-Kutta scheme reduces to the Euler method for this ODE). Here, the backward Euler method is used for numerical solution of the ODE.

The resonant radius of cavitation bubbles with an external wave frequency of 20 kHz is equal to 0.15 mm. Hence, two different cases, one with a radius smaller and one with a radius larger

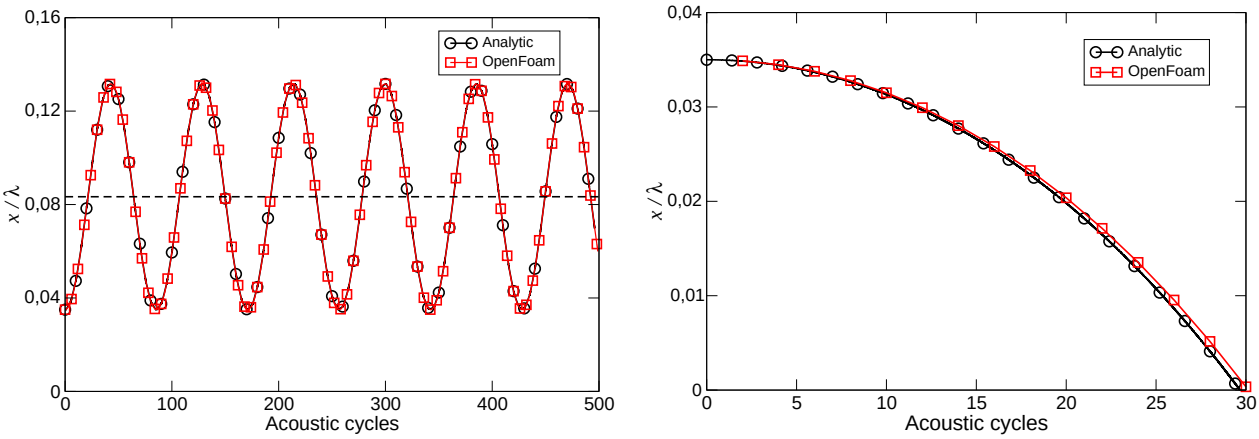

(a) $R_0 = 5$ μm **(b)** $R_0 = 0.5$ mm

Figure 5.6.: Normalized position of the bubble due to the effect of primary Bjerknes force. Nondimensionalization is done by dividing the position to the wavelength of the wave, λ. (a): $R_0 = 5$ μm and (b): $R_0 = 0.5$ mm. Dashed line shows the position of the nearest antinode.

than 0.15 mm are assumed to verify the numerical implementation. The bubbles with initial radii of 5 μm and 0.5 mm are located at x/L= 0.026 in the geometry of 1D model. Comparisons between the numerical simulation and the analytical solution for the motion of the bubble are shown in Figs. 5.6a and 5.6b. The bubble with initial radius of 5 μm starts to oscillate around the nearest antinode at x/L= 0.0625; while the other one tries to move toward the nearest pressure node outside of the domain. If the boundary condition at x= 0 is not defined in the model, the bubble starts to oscillate around a virtual point outside of the domain that is exactly located at the next node of the pressure field. Hence, a boundary condition is defined at x= 0 in a manner that if a bubble reaches to this point, it will stick to the wall. This definition also has a physical meaning because the bubbles tend to stick to the wall due to the effect of cohesion. The oscillation of the bubble with 5 mm in radius around the nearest pressure node inside the domain is also investigated and confirmed. The variation of the position has the same trend as Fig. 5.6-a and is not repeated. As it can be seen from the results, the finite volume method (FVM) predicts the position of the bubble precisely. It should be noted that in the FVM, the radius of the bubble is changing due to the solution of Eq. (2.46) at each time step and the primary Bjerknes force is obtained from Eq. (2.88) instead of Eq. (5.1). However, because the amplitude of the acoustic source is not significantly high, the amplitude of the oscillation of the radius is approximately 2% of the initial radius (Fig. 2.2-b). Therefore, the variation of the radius can not affect the RHS of Eq. (2.99) considerably.

5.3.2. Single bubble motion- Nonlinear oscillations and convection

An inlet velocity of 10 m/s is applied to the model of Sec. 5.3.1 to move the bubble from left to right. This value is adopted to ensure pushing the bubble to move along the domain without being hindered by the drag force. The drag force is the only force which is considered here to resist against the bubble motion due to the external convection source. If the Bjerknes force is activated, the bubble may oscillate around some specific points and is not able to experience all of the pressure amplitudes. The pressure amplitude at the inlet is set as 180 kPa to ensure the non-linear oscillation of the bubble. The initial diameter of the bubble is 1.5 μm. Here, the goal is to find the local volume fraction of bubbles which is defined as

$$\beta = \frac{4\pi}{3} N R^3 \,. \tag{5.8}$$

Both N (number of bubbles) and R (their radii) are functions of pressure amplitude. In some references, the value of N is specified and assumed as a constant number, such as the work of Louisnard [64] and Vanhille and Campos-Pozuelo [15]. Moreover, some authors have assumed that if the pressure amplitude increases, the volume fraction of bubbles rises linearly [19]. The former assumption does not see the change of N due to bubbles break up and fragmentation, for instance, after violent collapse. In addition, the latter does not separate the contributions of N and R in increasing the value of β. Since the variation of R with respect to pressure amplitude can be derived in this work using the KME at each computational cell, only a linear function is assumed for changing the number of bubbles with pressure. It is supposed that after the collapse of a bubble at higher pressures, it is fragmented to smaller bubbles. The higher the value of the pressure, the higher the number of children produced by the initial nuclei. Due to the lack of sufficient knowledge about the physical background, a linear function is applied here for this proportionality and the method of its application is described as the following.

The maximum radius of the bubble in one acoustic period is calculated by Eq. (2.46) to find the volume of a single bubble at each point. It is assumed that a bubble requires a space equal to its maximum volume during one cycle. For a bubble with an initial diameter of 1.5 μm, the threshold of transient cavitation is P_a= 184.5 kPa. At this pressure, the maximum radius of the bubble reaches to about 58 times of its initial radius (Fig. 5.7). Up to this point, as the bubbles are oscillating almost linearly, their volume fraction is negligible and does not increase drastically

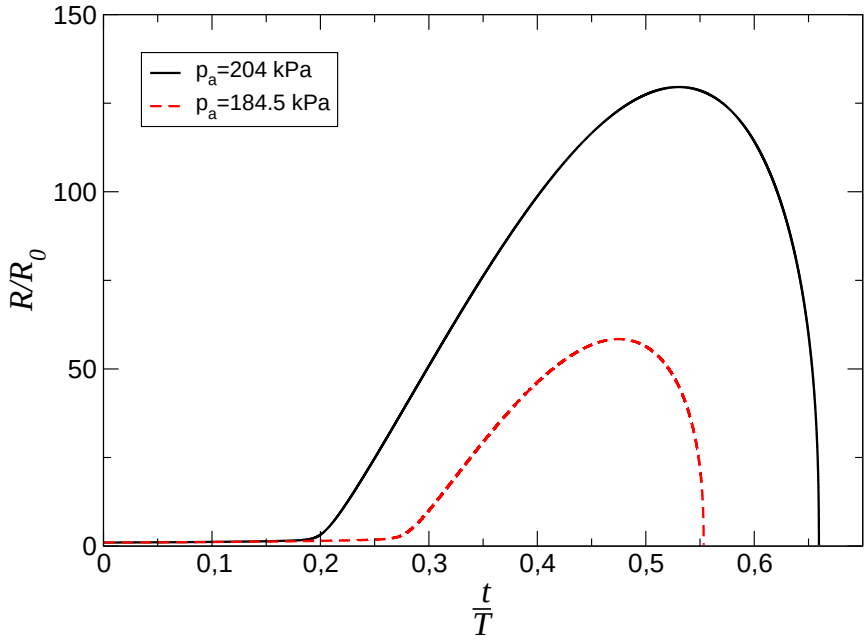

Figure 5.7.: Collapse of a bubble with initial diameter of 1.5 μm for two different acoustic pressure amplitudes. Wave frequency: 20 kHz.

with pressure. Thus, a small value of $\beta = 10^{-4}$ is considered for this pressure amplitude. This value is adopted since it is shown to have insignificant effect on wave propagation [19, 20]. By knowing this value and also the maximum volume of a single bubble, the number of bubbles per unit volume at the beginning of the transient cavitation region is estimated as 2.84×10^8. The same analysis can be done for a volume fraction of 10^{-1} as the upper limit for β and a pressure amplitude of P_a= 204 kPa. The upper limit for β is adjusted because the damping of the ultrasonic wave for larger values does not allow the wave to propagate. In addition, the coalescence among bubbles at larger volume fractions will be dominant which leads to a so-called "saturated cavitation" phenomenon. The pressure amplitude of 204 kPa is adopted because it is observed in the experiment as the initial amplitude of the coalescence-dominated cavitation [110]. At this pressure, a bubble experiences a radius approximately 130 times of its initial radius (Fig. 5.7), that is $R_{max} = 97.5$ μm. Therefore, a value of about 2.61×10^{10} is estimated for the number of bubbles per cubic meter. By conducting this analyses, a linear relationship is obtained between the number of bubbles and the pressure amplitude. This relationship as well as the variation of radius which is obtained from Eq. (2.46) can be applied to Eq.(2.26) to predict the volume fraction of bubbles.

The final results can be compared with the experimental results from Akulichev [110] and are shown in Fig. 5.8 in which the volume fraction is plotted as a function of the pressure amplitude.

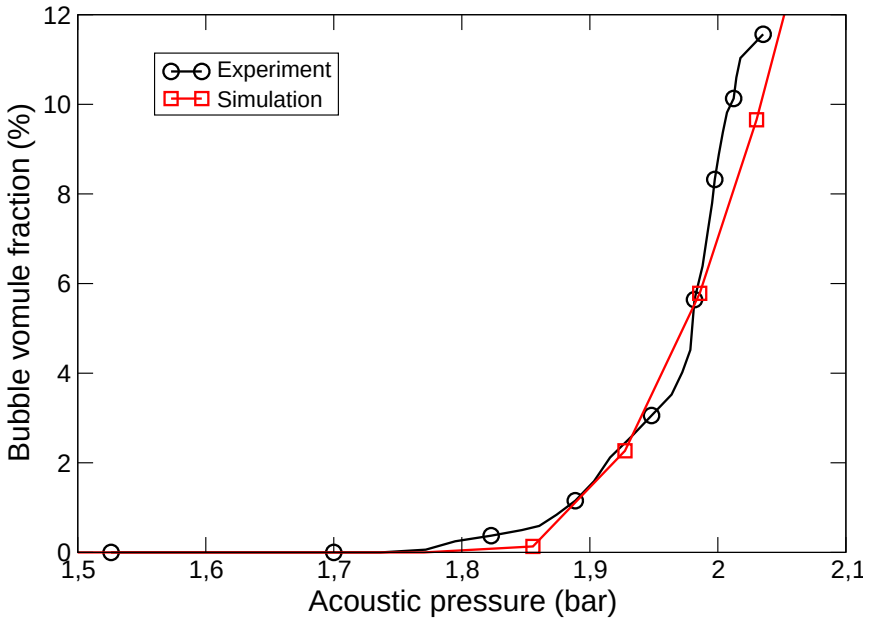

Figure 5.8.: Comparison between experimental and numerical results for bubble volume fraction versus pressure amplitude. Experimental data are from [110].

In the experiment, the volume fraction of bubbles is measured by inserting a capillary in the cavitation zone. The cavitation zone is located under a cylindrical ring transducer, exactly on the axis. The method measures the change of volume and is called dilatometric method (Rozenberg [111]). The result is a “quasi-steady” bubble density which could be used to calculate the volume fraction of bubbles. As can be seen, after a threshold, transient collapse of bubbles occurs and their volume fraction increases sharply. As it is illustrated, the FVM results show good agreement in predicting the trend of bubble volume fraction with experiments. It can be concluded that assuming a relation, even a linear one, between number of bubbles instead of their volume fraction and pressure amplitude leads to reasonable results. Nevertheless, the assumption made here could be modified by applying more complicated physical models on the population of bubbles in acoustic fields.

5.4. Two-dimensional simulation

5.4.1. Single bubble motion- Linear oscillations

In a 2D domain, Eq. (2.38) is written as $\partial^2 P/\partial x^2 + \partial^2 P/\partial y^2 + k^2 P = 0$. By applying the boundary conditions which are illustrated in Sec. 3.2.1, the solution of this equation is obtained as a Fourier series

$$P_a(x,y) = \sum_{n=1}^{\infty} \frac{4P_a}{n\pi sin\sqrt{k^2 - (\frac{n\pi}{l})^2}H} sin(\frac{n\pi x}{l}) sin\sqrt{k^2 - (\frac{n\pi}{l})^2}y\,. \tag{5.9}$$

Figure 5.9 shows the pressure distribution which is obtained by analytical approximation and numerical solution from OpenFOAM. The initial position of bubble is also shown in Fig. 5.9a.

The gradient of this pressure distribution is substituted in Eq. (5.1). By assuming $c_n = n\pi/l$ and $d_n = \sqrt{k^2 - (n\pi/l)^2}$, the equations of motion for a single bubble under the action of the primary Bjerknes force reads

$$\ddot{x}_b + B\sum_{n=1}^{\infty} \frac{sinc_n x_b sind_n y_b}{n\pi sind_n H} \sum_{n=1}^{\infty} \frac{cosd_n x sind_n y_b}{l sind_n H} = 0\,, \tag{5.10}$$

and

$$\ddot{y}_b + B\sum_{n=1}^{\infty} \frac{sinc_n x_b sind_n y_b}{n\pi sind_n H} \sum_{n=1}^{\infty} \frac{sinc_n x_b d_n cosd_n y_b}{n\pi sind_n H} = 0\,, \tag{5.11}$$

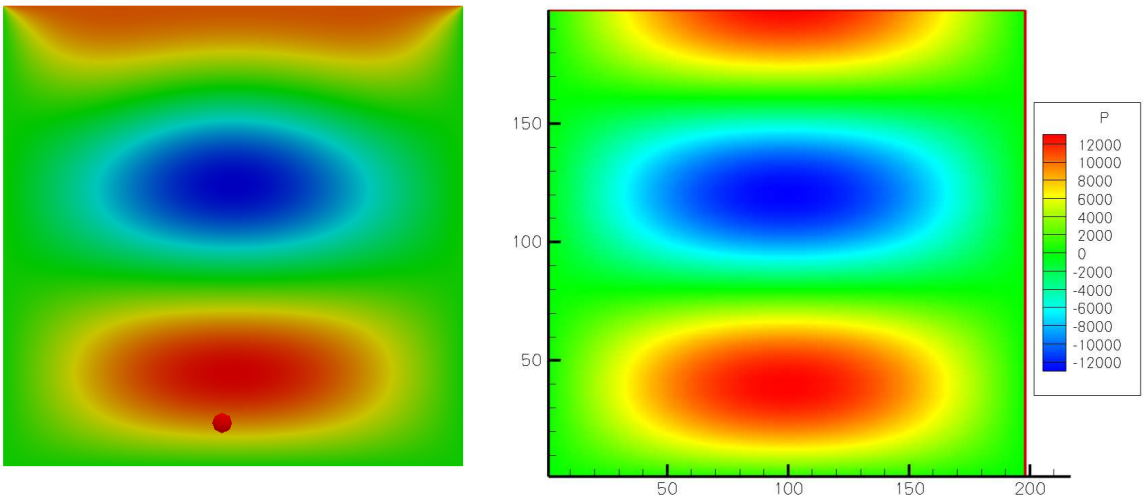

(a) OpenFOAM **(b)** Analytic

Figure 5.9.: Pressure distribution in the 2D domain by (a): numerical simulation and (b): analytical method. Acoustic source pressure amplitude: 10 kPa. Bubble initial radius: 5 μm.

where B is a constant as

$$B = \frac{24P_a^2(\omega_0^2 - \omega^2)}{\rho\rho_p R_0^2((\omega_0^2 - \omega^2)^2 + (\alpha\omega)^2)} \,. \tag{5.12}$$

The same assumptions as in the 1D case are applied in deriving these relations. Again, with the use of the backward Euler method, Eqs. (5.10) and (5.11) are solved and the motion of a single bubble is compared to the results obtained by FVM simulation. A bubble with the initial radius of 5 μm is placed at x/L= 0.5 and y/H= 0.1 in the geometry of the 2D model. The comparison between the numerical simulation and the analytical solution for the y-coordinate of the bubble position is shown in Fig. 5.10. It is observed that the bubble starts to oscillate around the nearest antinode at y/H= 0.275. Because of the symmetricity of the pressure around the line x/L= 0.5, the bubble has no motion in x-direction. It can be seen that the FVM gives reasonable results for predicting the position of the bubble in the 2D test case.

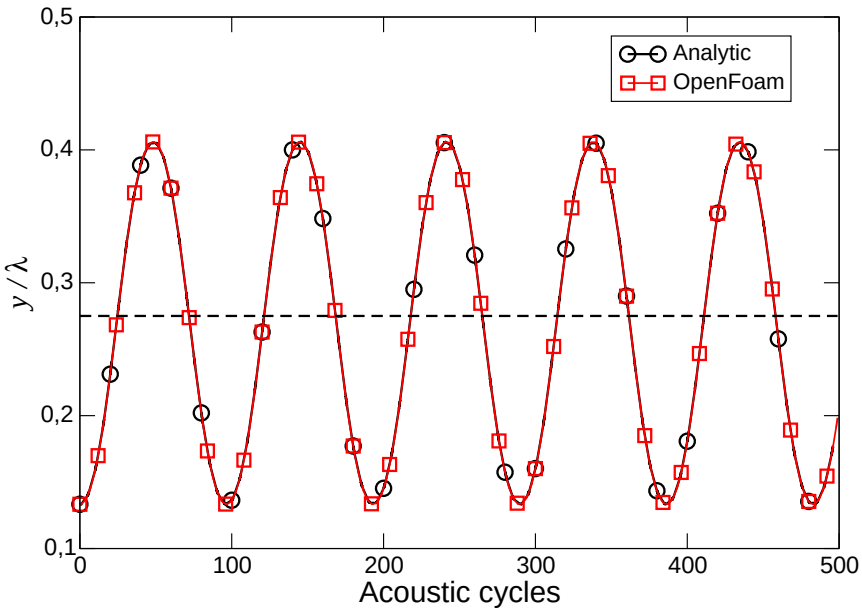

Figure 5.10.: Normalized position of the bubble due to the effect of primary Bjerknes force in a 2D domain. $R_0 = 5$ μm. The dashed line shows the position of the nearest antinode.

5.4.2. Multiple bubbles motion- Nonlinear oscillations

An axisymmetric 2D geometry with 24000 cells is considered to reproduce the conical structure formed by the bubbles in the vicinity of an ultrasound source, as observed in experiments [105]. In the experiment, a sonotrode with a diameter of 120 mm, a frequency of 20.7 kHz and an acoustic intensity (power per unit area of the sonotrode, $I = P_{US}/A$) of 8.2 W/cm^2 is placed in a tank.

The tank made of glass walls is filled with water and has dimensions of 60 cm$\times$100 cm$\times$40 cm. The cone bubble structure is captured using a digital photo camera which focuses on the cavitation zone. Although the tank is cubic in shape, assuming a cross section of a cylindrical tank in an axisymmetric 2D geometry leads to reasonable results for the structure made by bubbles. The reason is the large dimension of the tank compared to the small cylindrical sonotrode. In order to apply the value of ultrasound power to the acoustic source, the acoustic pressure amplitude in the simulation should be set as the boundary condition which is obtained from Eq. (3.1).

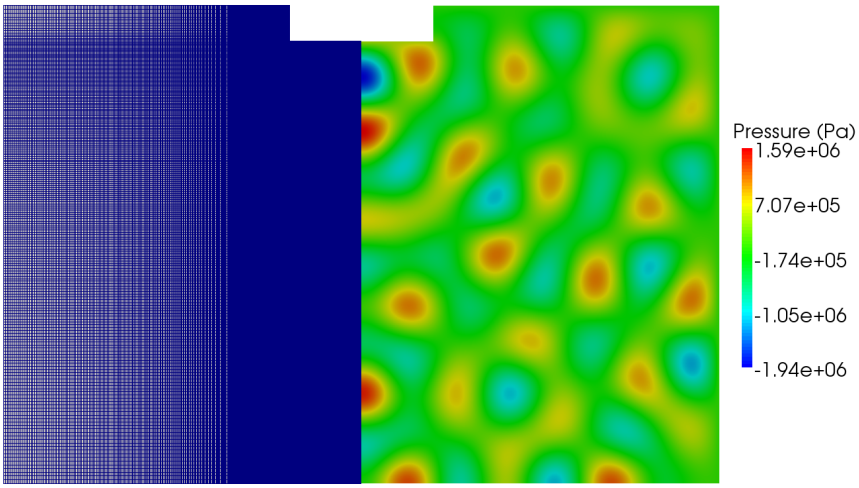

Figure 5.11.: 2D axisymmetric model. Left: Computational grid. Right: Acoustic pressure amplitude.

For the present configuration, the amplitude of pressure at the sonotrode is calculated as P_a= 4.96 bar. The result of pressure distribution as well as the grid generated for the geometry is shown in Fig. 5.11.

1200 bubbles with an initial radius of $R_0 = 2\ \mu$m are distributed uniformly inside the axisymmetric geometry in the vicinity of the sonotrode. The comparison between the results of simulation and the experimental observations is shown in Fig. 5.13. Although the bubbles show a chaotic unsteady motion, they accumulate around the pressure antinodes and also stick to the surface of the ultrasonic source as a quasi-steady structure. In addition, they are repelled from the pressure node and this leads to a conical shell with a highly populated base near the sonotrode, and a solitude zone inside the cone [64]. The influence of primary Bjerknes force is obvious in creating the conical structure of bubbles.

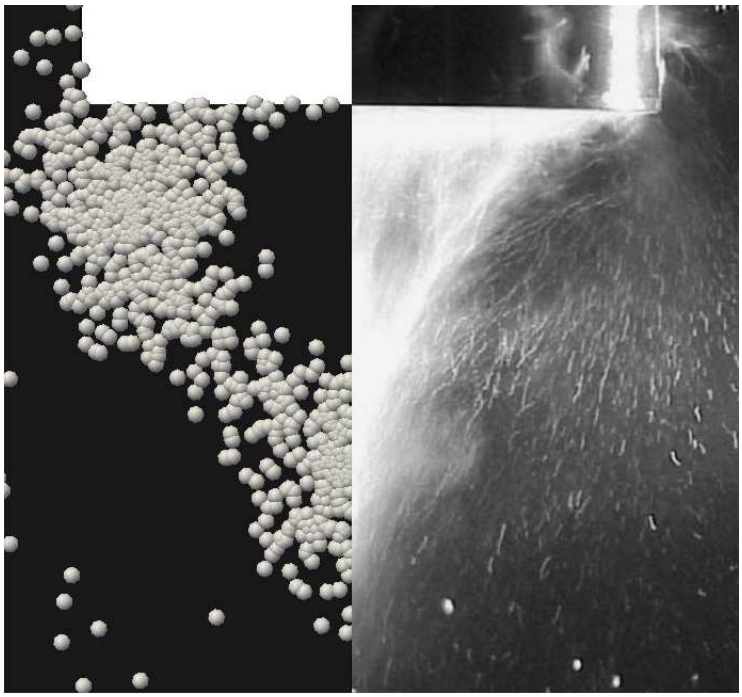

Figure 5.12.: Bubbles conical structure in the vicinity of the ultrasonic horn. 1200 bubbles with $R_0 = 2$ μm are located uniformly in a small region near sonotrode in the 2D-axisymmetric simulation (left). Right: reprinted from Ref. [105], with permission from Elsevier. Acoustic intensity=8.2 W/cm^2. Wave frequency f= 20.7 kHz.

5.4.3. Multiple bubbles motion- Nonlinear damping

To accomplish the numerical implementation, the nonlinear effect of bubbles on wave propagation are considered. According to the method described in Sec. 3.2, the bubbles influence both the real and imaginary parts of the wave number. Louisnard [63] states that the contribution of bubbles on the real part is negligible in case of inertial cavitation. To verify this statement, one may check the ratio between the two terms at the RHS of Eq. (3.4). This ratio is plotted for different number of bubbles per unit volume in Fig. 5.13. It is illustrated that except for high number of nuclei (more than 10 billions) the contribution of bubbles on the real part of the wave number is negligible. For higher frequencies, this assumption is more reliable because ω appears at the numerator of the first term of the RHS of Eq. (3.4) and at the denominator of its second term. Thus, for a common range of wave frequencies in sonochemistry, one can concentrate on investigating the effect of bubbles on imaginary part of the wave number (contribution to damping). Nonetheless, both effects are applied in this work to prepare the tool for further investigations or when the number of bubbles increases to billions per m^3.

To investigate the flow field, the source term of acoustic streaming is also applied to the solver.

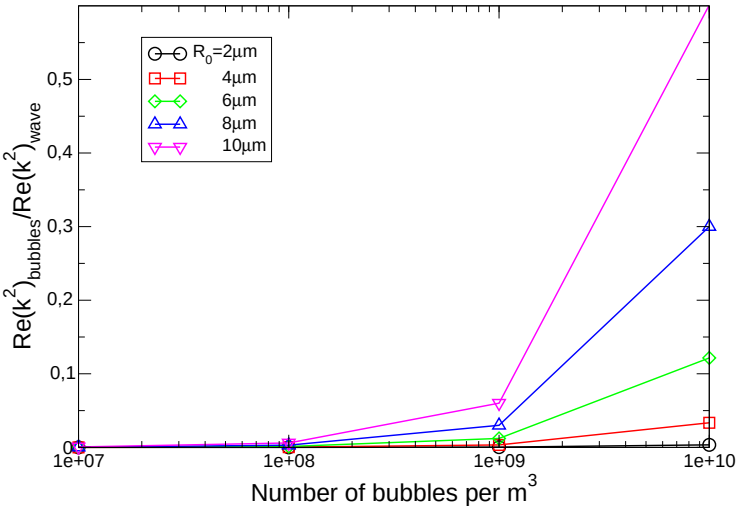

Figure 5.13.: Effect of bubbles on real part of wave number. Wave frequency f= 20 kHz.

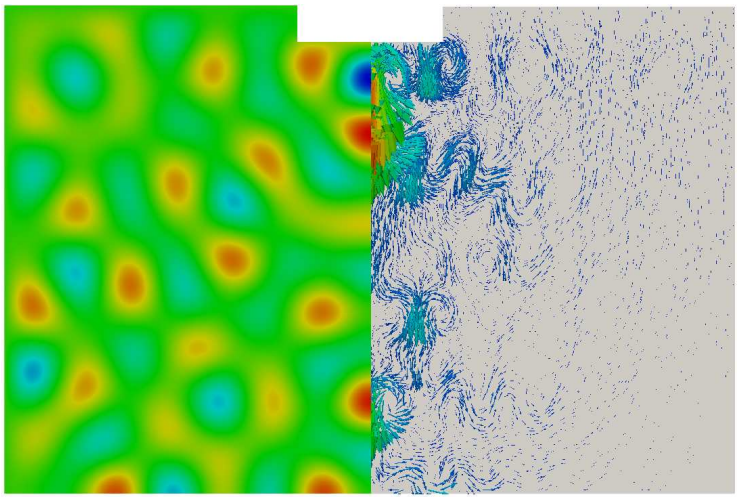

Figure 5.14.: Flow field inside reactor due to acoustic streaming. Left: Pressure amplitude. Right: Velocity vectors.

As described before, this source term is negligible with respect to other sources such as external convective source or momentum source due to coupling between bubbles and the bulk liquid. Nevertheless, the flow field only due to acoustic streaming is examined. Figure 5.14 shows the pressure amplitude as well as the velocity vectors of the fluid due to acoustic source. The proportionality of the liquid velocity due to acoustic streaming with pressure amplitude is clear from the figure (Eq. 2.83). The structure made by the bubbles is shown in Fig 5.15 for two different sequences at t= 7 ms and 30 ms after turning the sound source on. It can be seen that the bubbles near the sonotrode form the conical structure as before but with slightly different shape. Sticking to the surface of the sonotrode, accumulating around the antinodes and escaping from the solitude zone between the sonotrode and the nearest antinode is visible in the structure of bubbles.

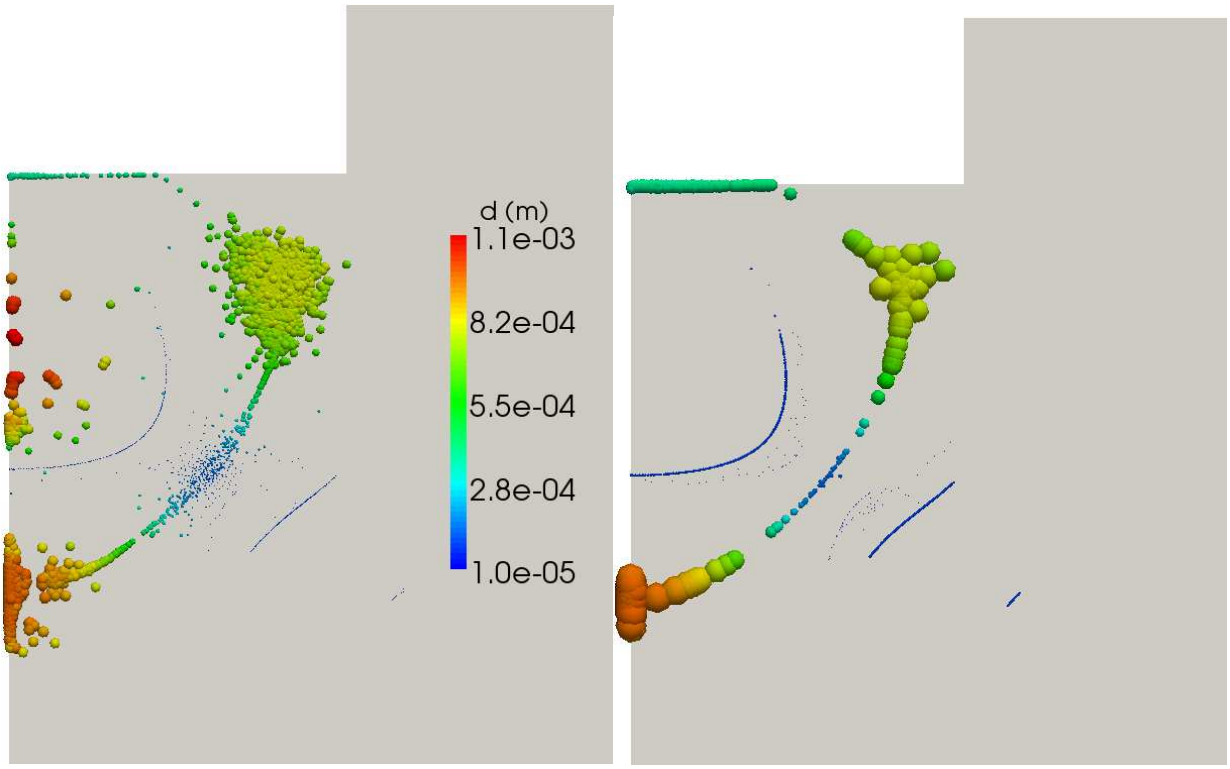

(a) 7 ms **(b)** 30 ms

Figure 5.15.: Bubbles structure near the horn. (a): t= 7 ms (b): t= 30 ms. Bubble initial radius: 5 μm.

Bubbles who are activated by sound and experience inertial cavitation, accumulate around high pressure zones. The other ones who have smaller size move towards the nodes of the pressure field. They are visible as thin blue lines in the figure. Accumulation of bubbles near the high pressure zones is due to the strong pressure gradient which appears in the primary Bjerknes force. However, two other phenomena, namely the collision among bubbles and repulsive secondary Bjerknes force, lead the bubbles to scape from high pressure zones. This compromise results in an oscillatory motion of bubbles around an antinode. This oscillatory motion may be investigated by considering the velocity vectors of bubbles near an antinode of pressure. Figure 5.16 illustrates such vectors. It can be seen that some bubbles are moving towards the antinode while the others are escaping from it. The reason of the latter is the repulsive effect of secondary Bjerknes force and also collision with other bubbles. This small oscillations around high pressure zones are visible by focusing on a small region. The order of velocity magnitude (10 m/s) reveals that in the scale of computational time step, the motion of bubbles are not observable (around 1 mm). At the next time step, since the forces on each bubble change both in magnitude and direction, another velocity vector is obtained. This velocity could result in an attraction or escaping from the

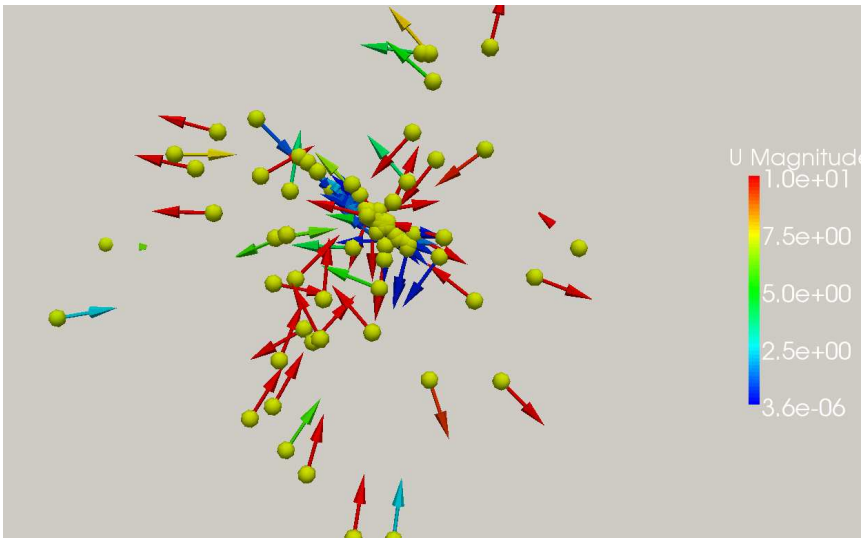

Figure 5.16.: Velocity vectors of bubbles near a pressure antinode.

antinode or even stagnation of the bubble. Therefore, bubbles structure remains quasi-stationary when one look at the large scale of the whole reactor rather than the small scale of tiny bubbles. The motion of inertial bubbles towards the antinodes of pressure is not restricted to the vicinity of the sound source. By increasing the number of bubbles, similar trend is observed for the whole reactor. Therefore, 10000 bubbles are introduced to the whole geometry. The bubbles structure is shown in Fig. 5.17 in which the pressure distribution is also visible. The bubbles who are activated by sound, accumulate around high pressure zones and oscillate there. Other smaller bubbles oscillate around the nodes and are visible by thin blue lines in the figure.

To see the effect of bubbles on the liquid flow, the source terms related to the bubble motion are added to the flow field equations. The result is illustrated as velocity vectors of liquid in Fig. 5.18. The flow field has a trend similar to the case without coupling. However, there are two important observations that should be mentioned here: First, velocities are much higher with respect to the case without coupling. The liquid velocity reaches to the order of centimeters per second which is a typical value for sonochemical reactors. Thus, in case of large number of bubbles, the momentum exchange between the two phases is more significant with respect to acoustic source. Second, the fluid velocity reaches to its maximum near the sound source. The reason is the cooperative effects of high pressure amplitude (acoustic source) and accumulation of large bubbles in that region.

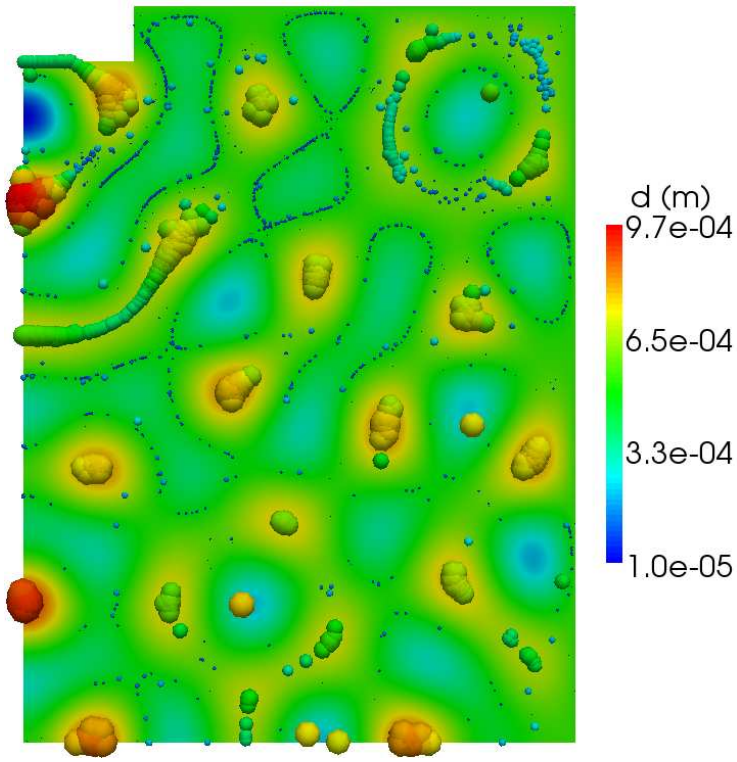

Figure 5.17.: Bubbles structure inside the whole reactor. t= 10 ms.

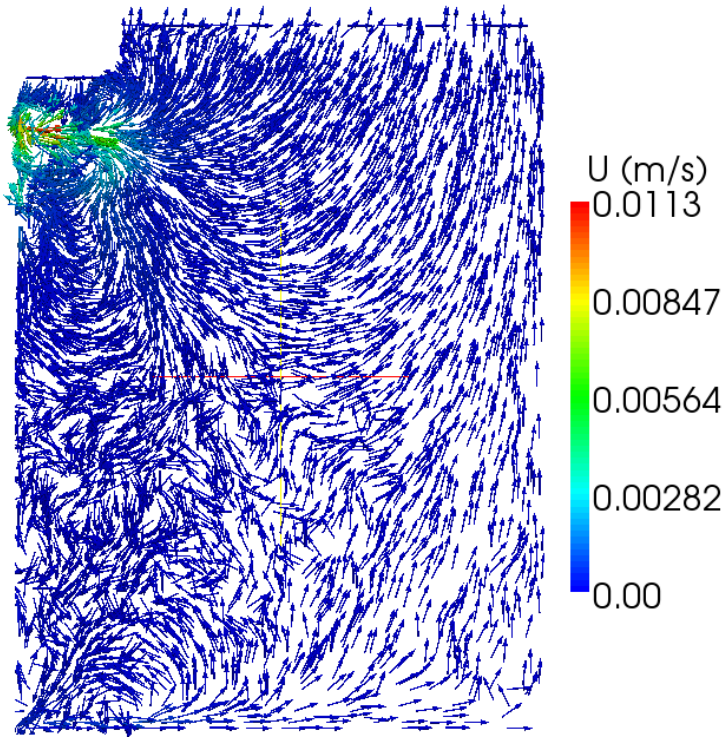

Figure 5.18.: Velocity vectors of the liquid due to four way coupling modeling. t= 10 ms.

5.5. Three-dimensional simulation

The final step of verification of the solver is simulating a 3D reactor. The cubic reactor described in Sec. 3.2.1 is filled with stagnant water and a sonotrode is located at the bottom of the reactor. This results in a standing wave with an antinode at the center of the geometry. The structure of bubbles is captured using high speed cameras and the so-called Acoustic Lichtenberg Figures (ALF) of the bubbles is presented in Ref. [8]. To compare our simulation results with experiment, 30 bubbles are injected at each time step on the surface of a sphere with a radius of 2 cm centrally located inside the reactor. Figure 5.19 shows the comparison in which the motion of bubbles towards the central antinode is captured by simulation. The bright lines in the experiment are the streamers which start from invisible nuclei of bubbles and move due to the primary Bjerknes force towards the antinode of the pressure field. The black lines in the simulation results are the paths of bubbles (streaklines) during time. The velocities of bubbles obtained from simulation cannot be compared with experimental results. However, the quasi-steady structure simulated here is a helpful tool in estimating the distribution of bubbles and their structure in sonochemical reactors.

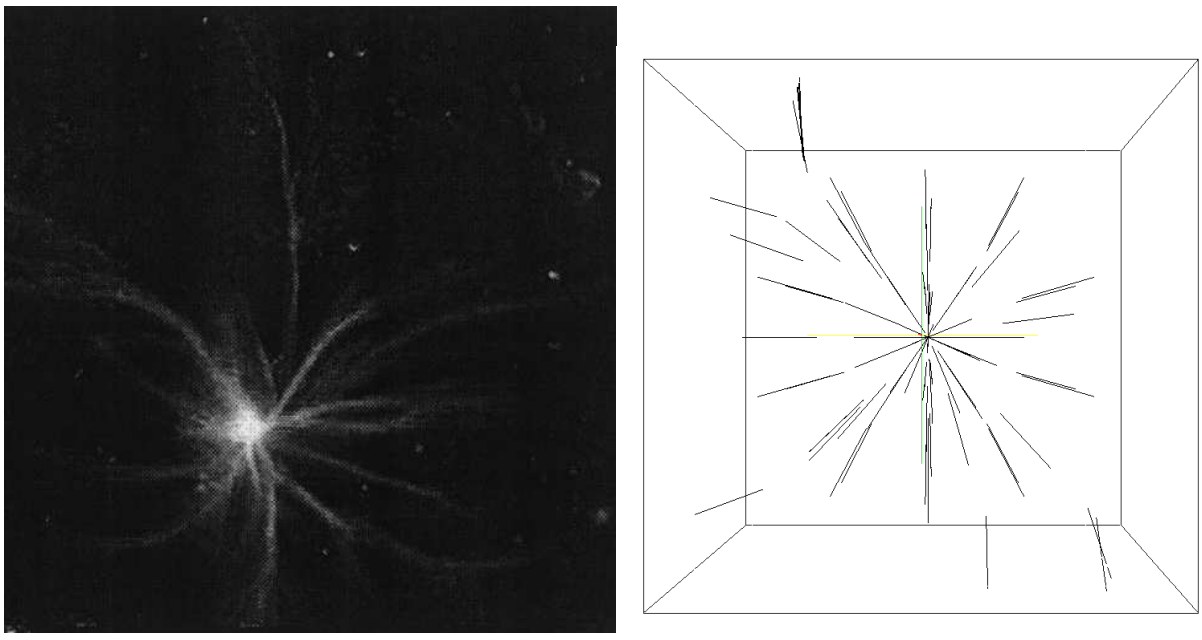

(a) Experiment **(b)** Simulation

Figure 5.19.: Bubbles structure at the middle of the cubic reactor. (a): experimental snapshot reprinted from Ref. [8], with permission from Elsevier and (b): simulation. Bubble initial radius: 5 μm. Acoustic pressure source amplitude P_a= 130 kPa.

6. Summary and recommendation for future work

Nothing in life is to be feared, it is only to be understood. Now is the time to understand more, so that we may fear less.

"Marie Curie"

In this thesis, the ultrasonic wave propagation in sonochemical reactors has been analyzed using numerical methods. The studies are categorized to linearized and nonlinear approximation methods. The linear study of the phenomena is based on assuming a volume fraction for bubbles. The nonlinear investigation includes the determination of the structure of cavitation bubbles using a Lagrangian approach and applying the attenuating effect of individual bubbles on pressure amplitude using nonlinear damping models.

To consider the nonlinear damping of bubbles, a new method is presented to find the nonlinear damping considering the compressibility of the bubbly liquids. The damping of the wave due to viscous, thermal and radiation losses resulting from the nonlinear oscillation of a single bubble in a compressible liquid is computed numerically. It is observed that the radiation damping cannot be neglected in the case of transient cavitation of bubbles. Besides that, it is revealed that the thermal damping has stronger influence than expected in previous studies. Moreover, it is shown that the rates of change of different modes of energies which contribute to bubble phenomena, are the secondary effects that dissipate power to the liquid. By applying the introduced damping factors to the wave propagation equation in the frequency domain, the attenuation coefficient inside the complex wave number can be modified. The result is a better explanation of the sudden damping of the acoustic pressure in sonochemical reactors.

In the linear analysis, the effect of cavitation bubbles on wave propagation is based on three different assumptions in order to demonstrate the sensitivity of the models in predicting cavitation: a linear wave without consideration of bubbles, linear wave with a constant volume fraction of bubbles and a linear wave with an assumed linear relationship between the volume fraction of bubbles and the acoustic pressure amplitude. The Helmholtz equation was applied for

modeling the wave propagation inside the reactor. Using the COMSOL Multiphysics software, different frequencies and input power levels of the sound source were examined. To verify the implemented numerical methods, several benchmarks were defined and the method was finally applied to analyze an industrial reactor with a conical shape.

Results of the verification benchmarks illustrated that by increasing the volume fraction of bubbles to about 10%, the waves cannot propagate through the reactor. This result is applicable to any reactor configuration and for different frequencies. Moreover, pressure amplitudes are very sensitive to the acoustic properties of the reactor walls. It was revealed that to activate bigger zones in a sonochemical reactor, it is better to manufacture the walls from materials which reflect the wave. In addition, using linear methods, the acoustic streaming could also be investigated. The streamlines of the flow are compared with PIV results of experiments and it is depicted that the linear models for pressure distribution are precise enough for modeling flows due to acoustic sources.

Furthermore, results of the linearized method for the conical reactor indicate that both the frequency and power of the ultrasound actuator may be optimized with respect to the location and strength of cavitation. Since the linear analysis is computationally economic in predicting wave propagation, it can help in predicting different design parameters of the reactors. Therefore, effects of different frequencies, types of reactor walls and geometries are considered using this method. It is found that the process-parameter combination of 20 kHz and 20 W yielded better results in terms of the bubble distribution for conical reactor with feeding tubes inside the reactor (geometry number 1). Moreover, it is illustrated that the effect of reactor geometry on wave pattern is different for different frequencies. At higher frequencies such as 30 kHz, the damping effect of the bubbles is dominant and the presence of reflecting tubes is of no consequence. However, at lower frequencies of about 10 kHz, the effect of bubbles is more significant if the wave is not restricted by reflecting walls. On the other hand, the result of mixing of the incoming flows by comparing the size and uniformity of the nano-particles at the exit section, depicts that a shorter distance between feeding tubes is more favorable.

In the nonlinear analysis, the translational motion of cavitational bubbles under the action of an ultrasonic field or other momentum sources is investigated numerically including bubble radial dynamics. The summation of the forces on any individual bubble is calculated and using the

FVM, the velocities and positions of the bubbles are updated in a Lagrangian frame. To verify the implemented method in the OpenFOAM software, benchmarks are considered and it is shown that the FVM, predicts the motion of the bubbles in a precise way. However, as the radial dynamics of the bubbles undergoes complex variations in the case of high amplitudes of the acoustic source, the method is compared with experiments. Results show that the method can be applied to complex geometries with high number of nuclei to investigate the structure of bubbles inside sonochemical reactors. Moreover, the increment of the bubble volume fraction by increasing the acoustic pressure amplitude is verified. It is illustrated that by finding an appropriate relation between the number of bubbles and the pressure amplitude, the experimental results can be reproduced by numerical simulations. The structure of bubbles in 2D and 3D simulations is also in agreement with experimental observations. It is depicted that in the case of high acoustic amplitude pressure, the Bjerknes force is predominant and plays the main role in creating the bubbles structure. By increasing the number of initial nuclei in the approach, more physical aspects of the phenomena will be revealed.

The damping effect of the bubbles on wave propagation is investigated using a Lagrangian approach. This is be done by transferring information between bubbles as the disperse phase and the acoustic pressure field. The result is an updated new pressure field which may result in a new structure of bubbles. The effect of acoustic streaming is added as a source term to the equation of motion of the flow.

Finally, a numerical tool is developed in the OpenFOAM software which is able to investigate:

- acoustic pressure distribution,
- flow field due to acoustic streaming, external convection and momentum exchange with dispersed phase,
- motion of bubbles and their structure under the action of a sound field or other convective sources,
- bubble radial dynamics at each computational time step and
- nonlinear coupling between bubbles in a Lagrangian frame with acoustic pressure as a field variable.

This numerical tool may be used for larger reactors with more complicated geometries and higher number of bubbles at the start of the simulation. In this context, parallel computations are required for simulation of the microbubbles and pressure waves pattern in 3D geometries. The solver assumes that for frequencies in the range of kHz, the considered computational time step is fine enough to justify the repeatability of radial dynamics of the bubbles. However, for higher frequencies, the computational time step has to be decreased which leads to higher computational effort.

There are plenty of unknowns to be discovered, modeled and simulated in multi-bubble sonochemistry. Regarding modeling, the main topic which may be addressed is the damping of the acoustic wave due to bubbles. The nonlinear damping approach presented in this thesis, still suffers from simplifications. For better understanding of the damping, the conservation laws of mass and momentum should be written for a compressible liquid and the radial dynamics of the bubbles should be considered with less simplifications. Therefore, the Gilmore equation is a more precise model for predicting the radial dynamics. Since this equation deals directly with the enthalpy rather than an expansion of enthalpy as a series of pressure, it gives a better physical representation of the damping of the wave. However, the mathematical treatment of the procedure as well as physical interpretation of the new damping terms are not easy tasks.

The influence of other bubbles on the radial motion of an individual bubble is another important issue. Several attempts toward modeling such a coupling are performed and published, e.g. in Hay et al. [28], Harkin et al. [29], Fuster and Colonius [45], Doinikov and Zavtrak [112], Doinikov [113], Wang [114] and Pelekasis et al. [115]. However, most of the models are based on several assumptions such as inviscid, incompressible potential flow around bubbles, 1D motion of bubbles, considering only two bubbles and neglecting compressibility and the effect of translational motion on radial dynamics. A combination of all of these issues is not realized.

Introducing a distribution for number of bubbles rather than assuming a constant value is another topic which requires experimental results. In this context, several phenomena which influence the bubble population density should be covered by the models. These include bubbles coalescence, nucleation, break up and fragmentation. These events are much more complicated in presence of a sound field in comparison with other bubbly flows in industries. Therefore, experiments are required to illustrate the effects of these phenomena and to apply them in the available models.

Regarding the numerical simulation of acoustic cavitation in sonochemistry, several topics may be addressed to modify the present algorithms. Firstly, the radial dynamics equation is solved with an adaptive Runge-Kutta method in this thesis. Nonetheless, most of the computational time required for the simulation is due to the computation of the radial dynamics of bubbles. Faster algorithms for solving the ODE of radial dynamics may be applied in OpenFOAM to reduce the computational time.

Secondly, tracing millions of bubbles with varying radii in a 3D complicated geometry with unstructured grid is not a straightforward numerical task. Thus, parallel computation is required in this case. By considering the interaction among bubbles, parallelization of the code would be demanding. The reason is that the information of any single bubble may be stored in a CPU different from the ones for another bubble. Therefore, transferring data through interfaces should be optimized in parallel programming of the Lagrangian solver.

Finally, the coupling of the real and imaginary parts of the presuure amplitude in this thesis is done in an explicit way. More robust numerical solvers may be applied for coupling the two parts to increase the convergence rate.

A. Appendix

A.1. List of Tables

2.1. Physical properties set for the test case. 34

3.1. Physical properties applied in linear simulations. 57
3.2. Specification of the simulation parameters, geometrical configurations and selected grids. 60
3.3. Physical properties applied in nonlinear simulations. 67

A.2. List of Figures

1.1. Different types of cavitation [6]. 1
1.2. Conical Bubble Structure (CBS) below a sonotrode [7]. 2
1.3. Interaction among physical phenomena inside a sonochemical reactor. 2

2.1. Geometry of a bubble with coupled pulsation and translation. 12
2.2. Variation of radius of a 5 μm bubble excited by a 20 kHz wave. (a): normalized acoustic pressure, (b): comparison between linear theory (Eq. (2.25)) and Eq. (2.13) for P_a= 10 kPa and (c) Variation of bubble radius for P_a= 120 kPa. . . 17
2.3. Temporal scales of relevant physical phenomena inside a sonochemical reactor. . 20
2.4. Nonlinear damping of the wave versus normalized acoustic pressure amplitude for $N = 1$. The vertical dashed line shows the Blake threshold. 35
2.5. Variation of Π_v for amplitudes lower than the Blake threshold. 37
2.6. Variation of Π_r for amplitudes lower than the Blake threshold. 38
2.7. Collision between two bubbles in a 2D configuration. 47

3.1. Schematic representation of the reactor; $d = 2$ mm, geometry no. 1 and $d = 15$ mm, geometry no. 2. Solid cross section shows the plane used for 2-D contour plots. 56
3.2. Three dimensional tetrahedral elements developed for conical reactors. 59
3.3. Normalized acoustic pressure on the centerline of the reactor no. 1 for three different grid sizes. Ultrasound power: 20 W. Ultrasound frequency f= 20 kHz. . 60
3.4. Bubble radius variation for different amplitudes of pressure and wave frequency. (a) to (c): Pressure amplitude: 90 kPa and frequencies of 20, 50 and 100 kHz, respectively. (d) to (f): same frequencies but for an amplitude of 120 kPa. 63
3.5. Geometries considered as the test cases with their boundary conditions and dimensions. (a): 1D, (b): 2D to be compared with analytical solution and (c): 2D to be compared with experiments. 67

4.1. Normalized pressure distribution in the mid-plane of the first reactor, wave frequency f= 25 kHz. 71
4.2. Normalized pressure distribution in the mid-plane of the first reactor, wave frequency f= 50 kHz. 71
4.3. Normalized pressure distribution in the mid-plane of the second reactor, wave frequency f= 25 kHz. 72
4.4. Normalized pressure distribution in the mid-plane of the second reactor, wave frequency f= 50 kHz. 72
4.5. Normalized pressure distribution in the mid-plane of the third reactor, wave frequency f= 25 kHz. 73
4.6. Normalized pressure distribution in the mid-plane of the third reactor, wave frequency f= 50 kHz. 73
4.7. Velocity streamlines due to acoustic streaming. Right: simulation results. Left: Experimental results reproduced from Ref. [75], with permission from Elsevier. . 74
4.8. Normalized pressure on the half-length of the central axis of the reactor for different geometrical configurations, power levels and frequency of ultrasound. . . . 75
4.9. Zones with pressure above 10^5 Pa for geometry no.1 at different values of the ultrasound powers, frequency= 20 kHz. 76

4.10. Effect of absorbing boundary conditions on wave propagation for low frequencies. 77

4.11. Effect of absorbing boundary conditions on wave propagation for high frequencies. 77

4.12. Variation of normalized pressure along the centerline of the reactor with absorbing walls. 77

4.13. Effect of reflecting boundary conditions on wave propagation for low frequencies. 79

4.14. Effect of reflecting boundary conditions on wave propagation for high frequencies. 79

4.15. Variation of normalized pressure along the centerline of the reactor with reflecting walls. 79

4.16. Pressure distribution in the mid-plane of the 10 times scaled reactor. Frequency f= 10 kHz. 81

4.17. Pressure distribution in the mid-plane of the 10 times scaled reactor. Frequency f= 30 kHz. 81

4.18. Variation of normalized pressure along the centerline of the 10 times scaled reactor. 81

4.19. Complex wave number. 83

4.20. Fraction of the imaginary part of the wave number versus frequency for different volume fractions of bubbles. 84

4.21. Normalized pressure along the central axis of the reactor for geometry no.1, at different frequencies, ultrasound powers and volume fractions of bubbles. 85

4.22. Zones with pressure above 10^5 Pa for geometry no.1, ultrasound power: 200 W, frequency f= 20 kHz for different volume fractions of bubbles. 86

4.23. Volume fraction of bubbles along the central axis of the reactor for geometry no. 1 at three different frequencies and three different values of ultrasound power. . . 88

4.24. Volume fraction of bubbles for geometry no. 1 on the middle cross section of the reactor at three different frequencies, ultrasound power= 20 W. 89

4.25. Volume fraction of bubbles along the central axis of the reactor for geometry no.2, at three different frequencies and and three different values of ultrasound power. 90

4.26. Volume fraction of bubbles for geometry no. 2 on the middle cross section of the reactor at three different frequencies. Ultrasound power: 20 W. 91

4.27. Volume fraction of bubbles for geometry no. 2. Ultrasound power: 200 W. Frequency f= 10 kHz. 92
4.28. Velocity contour at the middle cross section of geometry no.1 for different feed flow rates. 94
4.29. Velocity contour at the middle cross section of geometry no.2 for different feed flow rates. 95

5.1. Contour of velocity magnitude in a backward facing step test case. Bubbles with constant diameter of 1 mm are injected form the lower left corner of the inlet section. Inlet velocity=10 m/s. 98
5.2. Acoustic pressure distribution in the 2D sudden expansion test case. Inlet velocity= 10 m/s. 100
5.3. Variation of (a): acoustic pressure amplitude and (b): diameter of a single bubble on the centerline of the sudden expansion geometry. Bubble initial diameter: 2 μm. Inlet velocity= 10 m/s. 101
5.4. Bubbles translational motion due to external convective source and radial motion due to acoustic field in the 2D sudden expansion test case. Initial diameter of bubbles: 2 μm. Inlet velocity= 10 m/s. Size of the bubbles are magnified to show the change of diameter at different positions. 102
5.5. Variation of normalized pressure amplitude, pressure gradient and bubble's radius in the 1D domain. Initial radius: 2 μm. Pressure source amplitude $P_a(x = 0)$: 10 kPa. Normalization is done for pressure as $P_a/P_a(x = 0)$, for gradient as $\nabla P_a/10^6\ pa/m$ and for radius as $R'(x)/R'_{max}$. 104
5.6. Normalized position of the bubble due to the effect of primary Bjerknes force. Nondimensionalization is done by dividing the position to the wavelength of the wave, λ. (a): $R_0 = 5$ μm and (b): $R_0 = 0.5$ mm. Dashed line shows the position of the nearest antinode. 105
5.7. Collapse of a bubble with initial diameter of 1.5 μm for two different acoustic pressure amplitudes. Wave frequency: 20 kHz. 107
5.8. Comparison between experimental and numerical results for bubble volume fraction versus pressure amplitude. Experimental data are from [110]. 108

5.9. Pressure distribution in the 2D domain by (a): numerical simulation and (b): analytical method. Acoustic source pressure amplitude: 10 kPa. Bubble initial radius: 5 μm. 109
5.10. Normalized position of the bubble due to the effect of primary Bjerknes force in a 2D domain. $R_0 = 5$ μm. The dashed line shows the position of the nearest antinode. 110
5.11. 2D axisymmetric model. Left: Computational grid. Right: Acoustic pressure amplitude. 111
5.12. Bubbles conical structure in the vicinity of the ultrasonic horn. 1200 bubbles with $R_0 = 2$ μm are located uniformly in a small region near sonotrode in the 2D-axisymmetric simulation (left). Right: reprinted from Ref. [105], with permission from Elsevier. Acoustic intensity=8.2 W/cm^2. Wave frequency f= 20.7 kHz. 112
5.13. Effect of bubbles on real part of wave number. Wave frequency f= 20 kHz. 113
5.14. Flow field inside reactor due to acoustic streaming. Left: Pressure amplitude. Right: Velocity vectors. 113
5.15. Bubbles structure neat the horn. (a): t= 7 ms (b): t= 30 ms. Bubble initial radius: 5 μm. 114
5.16. Velocity vectors of bubbles near a pressure antinode. 115
5.17. Bubbles structure inside the whole reactor. t= 10 ms. 116
5.18. Velocity vectors of the liquid due to four way coupling modeling. t= 10 ms. . . . 116
5.19. Bubbles structure at the middle of the cubic reactor. (a): experimental snapshot reprinted from Ref. [8], with permission from Elsevier and (b): simulation. Bubble initial radius: 5 μm. Acoustic pressure source amplitude P_a= 130 kPa. . . 117

A.3. Nomenclature

Latin letters

A	Area (m^2), dimensionless constant
b	damping factor (1/s)
B	dimensionloss constant, birth rate (1/s)
c	speed of sound (m/s), constant number (1/m)
$C_{1,2}$	dimensionloss constant
C_v	specific molar heat capacity at constant volume (j/(mol.K))
d	constant number (1/m)
D	thermal diffusivity of the gas inside bubble (m^2/s), death rate (1/s)
e	restitution coefficient, dimensionless
E	dimensionless constant
f	frequency (Hz)
F	dimensionless constant
$\mathbf{F}$	force (N)
$\mathbf{g}$	gravitational acceleration (m/s^2)
h	liquid enthalpy (kj/kg), average element size (m)
H	liquid enthalpy at bubble's surface (kj/kg), Height (m)
i	imaginary unit
I	acoustic intensity (W/m^2)
k	wave number (1/m), thermal conductivity (W/(m.K)), turbulent kinetic energy (m^2/s^2)
K	liquid kinetic energy (j), wave number (1/m)
l	length (m)
m	physical mass (kg)
n	surface normal vector (m), dimensionless constant
N	number of bubbles
p	pressure (Pa)
P	pressure amplitude independent of time (Pa), power (W)
$\overline{P}$	complex conjugate of pressure amplitude (Pa)

$P_i()$	Legendre polynomials
Q	heat energy (j)
r	radial coordinate (m)
R	bubble radius (m)
t	physical time (sec)
T	acoustic wave period (sec), temperature (K)
u	translational velocity (m/s)
$\vec{u}$	average velocity of mixture (m/s)
$\overline{u}$	average velocity of liquid in turbulent flow (m/s)
$\mathbf{U}$	velocity vector (m/s)
v	radial velocity (m/s)
V	volume (m^3)
w	growth or dissolution rate (m/s)
$x_{i,j}$	general spatial coordinates (m)
y	spatial coordinate in y direction (m)

Greek letters

α	thermal diffusivity of gas (m^2/s), absorption coefficient of wave (1/m)
β	volume fraction of bubbles
γ	specific heat ratio of gas
δ	thermal boundary layer thickness (m)
ϵ	turbulent dissipation rate (m^2/s^3), small dimensionless perturbation parameter
ζ	bulk viscosity (Pa.s)
η	dimensionless isothermal or adiabatic index
θ	circumferential coordinate (rad)
λ	wave length (m)
μ	dynamic viscosity of liquid (Pa.s)
ν	kinematic viscosity (m^2/s)
Π	dissipated power (W)
ρ	density (kg/m^3)
σ	surface tension (N/m), dimensionless constant
τ	characteristic time (sec)
ϕ	velocity potential (m^2/s), phase shift (rad)
Φ	complex dimensionless parameter
χ	dimensionless parameter
ω	wave frequency (rad/s)

Subscripts

amp	amplitude of acoustic source
a	amplitude
$A.S.$	acoustic streaming
AM	added mass
b	bubble
B	Blake threshold
Bj	Bjerknes
$cell$	computational cell
$diff$	diffusive heat transfer
dyn	dynamic
D	drag
f	fluid
g	gas
G	gravitational
h	hydrodynamic
i	imaginary part
in	entring
l	liquid
m	complex
mix	mixture
n	digit number
out	exiting
r	radiation, real part
th	thermal
T	temperature, turbulence
US	ultrasound
v	viscous
vol	volume variation
ϵ	turbulent dissipation rate
0	equilibrium, resonance, undisturbed situation
∞	infinity

Abbreviations

ALF	Acoustic Lichtenberg Figures
BC	Boundary Condition
BCS	Bubble Conical Structure
BFS	Backward Facing Step
CFD	Computational Fluid Dynamics
DNS	Direct Numerical Simulation
DOF	Degrees Of Freedom
FDM	Finite Difference Method
FEM	Finite Element Method
FVM	Finite Volume Method
KME	Keller-Miksis Equation
LHS	Left Hand Side
MoM	Method of Moments
$MUSIG$	Multiple Size Group
ODE	Ordinary Differential Equation
PIV	Particle Imaging Velocimetry
RHS	Right Hand Side
RPE	Rayleigh-Plesset Equation

Operators

Δ	difference
∇	nabla
Σ	summation
∂	partial derivation
$\langle\rangle$	averaging

B. Bibliography

[1] Vinayak S. Sutkar, Parag R. Gogate, and Levente Csoka. Theoretical prediction of cavitational activity distribution in sonochemical reactors. *Chemical Engineering Journal*, 158(2):290 – 295, 2010.

[2] H. Monnier, A. M. Wilhelm, and H. Delmas. Effects of ultrasound on micromixing in flow cell. *Chemical Engineering Science*, 55(19):4009–4020, 2000.

[3] N. Riley. Acoustic streaming. *Theoretical and Computational Fluid Dynamics*, 10:349–356, 1998.

[4] W. Bonrath. Ultrasound supported catalysis. *Ultrasonics Sonochemistry*, 12:103–106, 2004.

[5] Parag R. Gogate, Prashant A. Tatake, Parag M.Kanthale, and Aniruddha B.Pandit. Mapping of sonochemical reactors: Review, analysis, and experimental verification. *AIChE Journal*, 48(7):1542–1560, 2002.

[6] W. Lauterborn and C. D. Ohl. Cavitation bubble dynamics. *Ultrasonics Sonochemistry*, 4:65–75, 1997.

[7] C. Campos-Pozuelo, C. Granger, C. Vanhille, A. Moussatov, and B. Dubus. Experimental and theoretical investigation of the mean acoustic pressure in the cavitation field. *Ultrasonics Sonochemistry*, 12:79–84, 2005.

[8] R. Mettin, S. Luther, C.-D. Ohl, and W. Lauterborn. Acoustic cavitation structures and simulations by a particle model. *Ultrasonics Sonochemistry*, 6:25–29, 1999.

[9] B. D. Storey and A. J. Szeri. A reduced model of cavitation physics for use in sonochemistry. *Proceedings of the Royal Society of London A*, 457:1685–1700, 2001.

[10] A. Kumar, P. R. Gogate, and A. B. Pandit. Mapping the efficacy of new designs for large scale sonochemical reactors. *Ultrasonics Sonochemistry*, 14(5):538 – 544, 2007.

[11] J. Lee, M. Ashokkumar, K. Yasui, T. Tuziuti, T. Kozuka, A. Towata, and Y. Iida. Development and optimization of acoustic bubble structure at high frequencies. *Ultrasonics Sonochemistry*, 18:92–98, 2011.

[12] P. R. Gogate, I. Z. Shirgaonkar, M. Sivakumar, P. Senthilkumar, N. P. Vichare, and A. B. Pandit. Cavitation reactors: Efficiency assessment using a model reaction. *AIChE journal*, 47(11):2526–2538, 2001.

[13] W. Lauterborn, T. Kurz, R. Geisler, D. Schanz, and O. Lindau. Acoustic cavitation, bubble dynamics and sonoluminescence. *Ultrasonics Sonochemistry*, 14:484–491, 2007.

[14] R. Dangla and C. Poulain. When sound slows down bubbles. *Physics of Fluids*, 22, doi: 10.1063/1.3415496:041703–1,041703–4, 2010.

[15] C. Vanhille and C. Campos-Pozuelo. Nonlinear ultrasonic waves: Two-dimensional simulations in bubbly liquids. *Ultrasonics Sonochemistry*, 18(2):679–682, 2011.

[16] P. R. Gogate and A. B. Pandit. Engineering design method for cavitational reactors: I. sonochemical reactors. *AIChE journal*, 46(2):372–379, 2000.

[17] S. Dähnke and F. J. Keil. Modeling of three-dimensional linear pressure field in sonochemical reactors with homogeneous and inhomogeneous density distribution of cavitation bubbles. *Industrial and Engineering Chemistry Research*, 37:848–864, 1998.

[18] S. Dähnke and F. Keil. Modeling of tsound fields in liquids with a nonhomogeneous distribution of cavitation bubbles as a basis for the design of sonochemical reactors. *Chemical Engineering and Technology*, 21:873–877, 1998.

[19] S. W. Dähnke and F. J. Keil. Modeling of linear pressure field in sonochemical reactors considering an inhomogeneous density distribution of cavitation bubbles. *Chemical Engineering Science*, 54:2865–2872, 1999.

[20] R. Jamshidi, B. Pohl, U. A. Peuker, and G. Brenner. Numerical investigation of sonochemical reactors considering the effect of inhomogeneous bubble clouds on ultrasonic wave propagation. *Chemical Engineering Journal*, 189-190:364–375, 2012.

[21] A. A. Doinikov. Equations of coupled radial and translational motions of a bubble in a weakly compressible liquid. *Physics of Fluids*, 17:128101–1–4, 2005.

[22] L. L. Foldy. The multiple scattering of waves. *Physcal Review*, 67(3-4):107–119, 1945.

[23] L. Van Wijngaarden. On the equation of motion for mixtures of liquid and gas bubbles. *Journal of Fluid Mechanics*, 33:465–474, 1968.

[24] L. Van Wijngaarden. One-dimensional flow of liquids containing small gas bubbles. *Annual Review of Fluid Mechanics*, 4:369–394, 1972.

[25] R. E. Caflisch, M. J. Miksis, G. C. Papanicolaou, and L. Ting. Effective equations for wave propagation in bubbly liquids. *Journal of Fluid Mechanics*, 153:259–273, 1985.

[26] A. A. Doinikov. Translational motion of a spherical bubble in an acoustic standing wave of high intensity. *Physics of Fluids*, 14:1420–1425, 2002.

[27] R. Mettin and A. A. Doinikov. Translational instability of a spherical bubble in a standing ultrasound wave. *Applied Acoustics*, 70(10):1330 – 1339, 2009.

[28] T. A. Hay, M. F. Hamilton, Y. A. llinskii, and E. A. Zabolotskaya. Model of coupled pulsation and translation of a gas bubble rigid particle. *Journal of the Acoustical Society of America*, 125:1331–1339, 2009.

[29] A. Harkin, T. J. Kaper, and A. Nadim. Coupled pulsation and translation of two gas bubbles in a liquid. *Journal of Fluid Mechanics*, 445:377–411, 2001.

[30] W.H. Besant. *A treatise on hydrostatics and hydrodynamics*. Deighton, Bell, 1859.

[31] Lord Rayleigh. On the pressure developed in a liquid during the collapse of a spherical cavity. *Philosophical Magazine*, 34:94–98, 1917.

[32] M. S. Plesset. The dynamics of cavitation bubbles. *Journal of Applied Mechanics*, 16:277–282, 1949.

[33] A. Lin, B. D. Storey, and A. J. Szeri. Inertially driven inhomogeneities in violently collapsing bubbles: the validity of the rayleigh-plesset equation. *Journal of Fluid Mechanics*, 452:145–162, 2002.

[34] F. R. Gilmore. The growth or collapse of a spherical bubble in a viscous compressible liquid. Technical report, California institute of technology, Hydrodynamics laboratory report No. 26, 1952.

[35] J B. Keller and I. I. Kolodner. Damping of underwater explosion bubble oscillations. *Journal of Applied Physics*, 27:1152–1161, 1956.

[36] J. B. Keller and M. Miksis. Bubble oscillations of large amplitude. *Journal of the Acoustical Society of America*, 68:628–633, 1980.

[37] A. Prosperetti. The equation of bubble dynamics in a compressible liquid. *Physics of Fluids*, 30:3626–3628, 1987.

[38] A. Prosperetti and A. Lezzi. Bubble dynamics in a compressible liquid. part I. first-order theory. *Journal of Fluid Mechanics*, 168:457–478, 1986.

[39] A. Lezzi and A. Prosperetti. Bubble dynamics in a compressible liquid. part II. second-order theory. *Journal of Fluid Mechanics*, 185:289–321, 1987.

[40] U. Parlitz, R. Mettin, S. Luther, I. Akhatov, M. Voss, and W. Lauterborn. Spatio-temporal dynamics of acoustic cavitation bubble clouds. *Philosophical Transactions of the Royal Society of London A*, 357(1751):pp. 313–334, 1999.

[41] W. Lauterborn and T. Kurz. Physics of bubble oscillations. *Reports on Progress in Physics*, 73:106501, 2010.

[42] E. A. Neppiras. Acoustic cavitation. *Physics Reports*, 61:159–251, 1980.

[43] F. G. Leppington and H. Levine. The sound field of a pulsating sphere in unsteady rectilinear motion. *Proceedings of the Royal Society of London A*, 412:199–221, 1987.

[44] H. N. Oguz and A. Prosperetti. A generalization of the impulse and virial theorems with an application to bubble oscillations. *Journal of Fluid Mechanics*, 218:143–162, 1990.

[45] D. Fuster and T. Colonius. Modelling bubble clusters in compressible liquids. *Journal of Fluid Mechanics*, 688:352–389, 2011.

[46] Q. X. Wang and J. R. Blake. Non-spherical bubble dynamics in a compressible liquid. part I. travelling acoustic wave. *Journal of Fluid Mechanics*, 659:1–34, 2010.

[47] Q. X. Wang and J. R. Blake. Non-spherical bubble dynamics in a compressible liquid. part II. acoustic standing wave. *Journal of Fluid Mechanics*, 679:559–581, 2011.

[48] B. D. Storey and A. J. Szeri. Water vapour, sonoluminescence and sonochemistry. *Proceedings of the Royal Society of London A*, 456:1685–1709, 2000.

[49] C. Herring, United States Office of Scientific Research, and Development. *Theory of the pulsations of the gas bubble produced by an underwater explosion*. OSRD report, vol. 236. Columbia Univ., Division of National Defense Research, 1941.

[50] R. E. Caflisch, M. J. Miksis, G. C. Papanicolaou, and L. Ting. Wave propagation in bubbly liquids at finite volume fraction. *Journal of Fluid Mechanics*, 160:1–14, 1985.

[51] M. J. Miksis and L. Ting. Wave propagation in a bubbly liquid with finite-amplitude asymmetric bubble oscillations. *Physics of Fluids*, 29(3):603–618, 1986.

[52] O. Louisnard and J. Gonzalez-Garcia. *Ultrasound Technologies for Food and Bioprocessing*, chapter 2, Acoustic Cavitation. Springer, 2011.

[53] J. S. Dam and M. T. Levinsen. Size of the light-emitting region in a sonoluminescing bubble. *Physical Review Letters*, 92(14):144301, 2004.

[54] A. Prosperetti. Bubble phenomena in sound fields: part one. *Ultrasonics*, 22(2):69 – 77, 1984.

[55] K. W. Commander and A. Prosperetti. Linear pressure waves in bubbly liquids: Comparison between theory and experiment. *Journal of the Acoustical Society of America*, 85:732–746, 1989.

[56] C. Devin Jr. Survey of thermal, radiation, and viscous damping of pulsating air bubbles in water. *Journal of the Acoustical Society of America*, 31:1654–1667, 1959.

[57] H. Medwin. Counting bubbles acoustically: a review. *Ultrasonics*, 15:7–13, 1977.

[58] A. Prosperetti. Thermal effects and damping mechanisms in the forced radial oscillations of gas bubbles in liquids. *Journal of the Acoustical Society of America*, 61:17–27, 1977.

[59] M. A. Ainslie and T. G. Leighton. Review of scattering and extinction cross-sections, damping factors, and resonance frequencies of a spherical gas bubble. *Journal of the Acoustical Society of America*, 130:3184–3208, 2011.

[60] S. Dähnke, K. M. Swamy, and F. J. Keil. Modeling of three-dimensional pressure fields in sonochemical reactors with an inhomogeneous density distribution of cavitation bubbles. comparison of theoretical and experimental results. *Ultrasonics Sonochemistry*, 6:31–41, 1999.

[61] K. Ando, T. Colonius, and C. E. Brennen. Improvement of acoustic theory of ultrasonic waves in dilute bubbly liquids. *Journal of the Acoustical Society of America*, 126(3):EL69–EL74, 2009.

[62] O. Louisnard. Nonlinear attenuation of sound waves by inertial cavitation bubbles. *Physics Procedia*, 3:735–742, 2010.

[63] O. Louisnard. A simple model of ultrasound propagation in a cavitating liquid. part I: Theory, nonlinear attenuation and traveling wave generation. *Ultrasonics Sonochemistry*, 19:56–65, 2012.

[64] O. Louisnard. A simple model of ultrasound propagation in a cavitating liquid. part II: Primary bjerknes force and bubble structures. *Ultrasonics Sonochemistry*, 19:66–76, 2012.

[65] D. D. Joseph and J. Wang. The dissipation approximation and viscous potential flow. *Journal of Fluid Mechanics*, 505:365–377, 2004.

[66] R. B. Chapman and M. S. Plesset. Thermal effects in the free oscillation of gas bubbles. *Journal of Basic Engineering*, 93:373–376, 1971.

[67] A. A. Doinikov and P. A. Dayton. Spatio-temporal dynamics of an encapsulated gas bubble in an ultrasound field. *Journal of the Acoustical Society of America*, 120:661–669, 2006.

[68] J. G. Kirkwood and H. A. Bethe. The pressure wave produced by an underwater explosion I. Technical report, USA office of science and research and developement report No. 558, May 1942.

[69] T. G. Leighton. *The Acoustic Bubble*. Academic press, London, 1994.

[70] T. J. Matula, P. R. Hilmo, B. D. Storey, and A. J. Szeri. Radial response of individual bubbles subjected to shock wave lithotripsy pulses in vitro. *Physics of Fluids*, 14(3):913–921, Mrach 2002.

[71] R. Toegel, B. Gompf, R. Pecha, and D. Lohse. Does water vapor prevent upscaling sonoluminescence? *Physical Review Letters*, 85(15):3165–3168, 2000.

[72] P. R. Gogate, A. M. Wilhelm, and A. B. Pandit. Some aspects of the design of sonochemical reactors. *Ultrasonics Sonochemistry*, 10:325–330, 2003.

[73] P. J. Harris, H. AlAwadi, and W. K. Soh. An investigation into the effects of heat transfer on the motion of a spherical bubble. *ANZIAM*, 45:361–371, 2004.

[74] M. D. Mattson and K. Mahesh. A one-way coupled, Euler-Lagrangian simulation of bubble coalescence in a turbulent pipe flow. *International Journal of Multiphase Flow*, 40:68–82, 2012.

[75] O. Dahlem, J. Reisse, and V. Halloin. The radially vibrating horn: A scaling-up possibility for sonochemical reactions. *Chemical Engineering Science*, 54:2829–2838, 1999.

[76] A. Kumar, T. Kumaresan, A. B. Pandit, and J. B. Joshi. Characterization of flow phenomena induced by ultrasonic horn. *Chemical Engineering Science*, 61:7410–7420, 2006.

[77] S. Boluriaan and P. J. Morris. Acoustic streaming: from rayleigh to today. *International Journal of aeroacoustics*, 2(3-4):255–292, 2003.

[78] N. P. Vichare, P. R. Gogate, V. Y. Dindore, and A. B. Pandit. Mixing time analysis of a sonochemical reactor. *Ultrasonics Sonochemistry*, 8(1):23–33, 2001.

[79] P. R. Gogate, V. S. Sutkar, and A. B. Pandit. Sonochemical reactors: Important design and scale up considerations with a special emphasis on heterogeneous systems. *Chemical Engineering Journal*, 166(1):1066–1082, 2011.

[80] A. Kumar, P. R. Gogate, and A. B. Pandit. Mapping of acoustic streaming in sonochemical reactors. *Industrial and Engineering Chemistry Research*, 46(1):4368–4373, 2007.

[81] P. Koch. *Partikelmodellierung der Strukturbildung akustischer Kavitationblasen in Wechselwirkung mit dem Schalldruckfeld*. PhD thesis, Georg-August-Universität zu Göttingen, 2006.

[82] R. Mettin, P. Koch, and W. Lauterborn. Modeling acoustic cavitation with bubble redistribution. In *International symposium on Cavitation*, wageningen, The Netherlands, september 2006.

[83] M. Abdel-Maksoud, D. Hänel, and U. Lantermanna. Modeling and computation of cavitation in vortical flow. *International Journal of Heat and Fluid Flow*, 31:1065–1074, 2010.

[84] A. Vallier. Coupling of VOF with LPT in OpenFOAM. ”http://www.tfd.chalmers.se/ hani/kurser/”, September 2011.

[85] Lord Rayleigh. On the circulation of air observed in kundt’s tubes, and on some allied acoustical problems. *Philosophical Transactions of the Royal Society London A*, 175:1–21, 1883.

[86] H. Schlichting. Berechnung ebener periodischer grenzschichtströmungen (calculation of plane periodic boundary layer streaming). *Physikalische Zeitschrift*, 33(8):327–335, 1932.

[87] C. Eckert. Vortices and streams caused by sound waves. *Physical Review*, 73(1):68–76, 1948.

[88] W. L. Nyborg. Acoustic streaming near a boundary. *Journal of the Acoustical Society of America*, 30(4):329–339, 1958.

[89] Sir. James Lighthill. Acoustic streaming. *Journal of Sound and Vibration*, 61(3):391–418, 1978.

[90] K. Matsuda, T. Kamakura1, and M. Maezawa. Local control of eckart streaming near focus of concave ultrasound source with two coaxially arranged transducers. *Japanese Journal of Applied Physics*, 45(5B):4448–4452, 2006.

[91] E. Shams, J. Finn, and S. V. Apte. A numerical scheme for euler-lagrange simulation of bubbly flows in complex systems. *International Journal for Numerical Methods in Fluids*, 67:1865–1898, 2010.

[92] J. Magnaudet and D. Legendre. The viscous drag force on a spherical bubble with a time-dependent radius. *Physics of Fluids*, 10:550–554, 1998.

[93] D. Krefting. *Untersuchung von Einzel- und Mehrblasensystemen in akustischen Resonatoren (Investigation of single and multi bubble systems in acoustic resonators)*. PhD thesis, Georg-August-Universität zu Göttingen, 2003.

[94] R. E. Apfel. Acoustic cavitation inception. *Ultrasonics*, 22:167–173, 1984.

[95] L. A. Crum. Nucleation and stabilization of microbubbles in liquids. *Applied Scientific Research*, 38(3):101–115, 1982.

[96] R. Mettin. *Oscillations, Waves and Interactions*, chapter : From a single bubble to bubble structures in acoustic cavitation, pages 171–198. Universitätsverlag Göttingen, 2007.

[97] I. Akhatov, U. Parlitz, and W. Lauterborn. Pattern formation in acoustic cavitation. *Journal of the Acoustical Society of America*, 96(6):3627–3635, 1994.

[98] B. Selma, R. Bannari, and P. Proulx. Simulation of bubbly flows: Comparison between direct quadrature method of moments (DQMOM) and method of classes (CM). *Chemical Engineering Science*, 65(6):1925 – 1941, 2010.

[99] V. Raman, A. Abbas, and S. C. Joshi. Mapping local cavitation events in high intensity ultrasound fields. In *proceeding of the COMSOL Users Conference*, Bangalore, India (2006), 2006.

[100] J. Klima, A. F. Ferrer, J. G. Garcia, J. Ludvik, V. Saez, and J. Iniesta. Optimization of 20 khz sonoreactor on the basis of numerical simulation of local ultrasonic intensity and

qualitative comparison with experimental results. *Ultrasonics Sonochemistry*, 14:19–28, 2007.

[101] K. Yasui, T. Kozuka, T. Tuziuti, A. Towata, Y. Iida, J. King, and P. Macey. FEM calculation of an acoustic field in a sonochemical reactor. *Ultrasonics Sonochemistry*, 14:605–614, 2007.

[102] O. Louisnard, J. G. Garcia, I. Tudela, J. Klima, V. Saez, and Y. V. Hernandez. FEM simulation of a sono-reactor accounting for vibrations of the boundaries. *Ultrasonics Sonochemistry*, pages 250–259, 2009.

[103] B. Pohl, R. Jamshidi, G. Brenner, and U. A. Peuker. Experimental study of continuous ultrasonic reactors for mixing and precipitation of nanoparticles. *Chemical Engineering Science*, 69(1):365–372, February 2012.

[104] G. Servant, J.L. Laborde, A. Hita, J. P. Caltagirone, and A. Gerard. Spatio-temporal dynamics of cavitation bubble clouds in a low frequency reactor: comparison between theoretical and experimenatl results. *Ultrasonics Sonochemistry*, 8:163–174, 2001.

[105] A. Moussatov, Ch. Granger, and B. Dubus. Cone-like bubble formation in ultrasonic cavitation field. *Ultrasonics Sonochemistry*, 10:191–195, 2003.

[106] F. Burdin, N.A. Tsochatzidis, P. Guiraud, A.M. Wilhelm, and H. Delmas. Characterisation of the acoustic cavitation cloud by two laser techniques. *Ultrasonics Sonochemistry*, 6(1-2):43 – 51, 1999.

[107] Ullmann. *Ullmann's Encyclopedia of Industrial Chemistry*. Wiley-VCH, 2007.

[108] G. Servant, J. P. Caltagirone, A. Gèrard, J. L. Laborde, and A. Hita. Numerical simulation of cavitation bubble dynamics induced by ultrasound waves in a high frequency reactor. *Ultrasonics Sonochemistry*, 7(4):217–227, 2000.

[109] G. Servant, J. P. Caltagirone, A. Gèrard, J. L. Laborde, and A. Hita. On the interaction between ultrasound waves and bubble clouds in mono- and dual-frequency sonoreactors. *Ultrasonics Sonochemistry*, 10(4):347–355, 2003.

[110] V. A. Akulichev. Experimental investigation of an elementary cavitation zone. *Soviet Physics. Acoustics*, 14:284–289, 1969.

[111] L. D. Rozenberg. *High-intensity ultrasonic fields*, chapter : The cavitation zone. Plenum Press, New York, NY, 1971.

[112] A. A. Doinikov and S. T. Zavtrak. On the mutual interaction of two gas bubbles in a sound field. *Physics of Fluids*, 7(8):1923 – 1930, 1995.

[113] A. A. Doinikov. Mathematical model for collective bubble dynamics in strong ultrasound fields. *Journal of the Acoustical Society of America*, 116(2):821–827, 2004.

[114] Q. X. Wang. Interaction of two circular cylinders in inviscid fluid. *Physics of Fluids*, 16(12):4412–4425, 2004.

[115] N. A. Pelekasis, A. Gaki, A. A. Doinikov, and J. A. Tsamopoulos. Secondary bjerknes forces between two bubbles and the phenomenon of acoustic streamers. *Journal of Fluid Mechanics*, 500:317–347, 2004.

C. Declaration

Hereby, I certify that this work is done independently and without assistance and without the use of other sources than indicated by me. All subjects from external sources, including formulas, ideas and theories are refereed properly. The work is not published in the same or similar form elsewhere.

Clausthal-Zellerfeld, February 13, 2014

_____

Rashid Jamshidi

D. Curriculum Vitae

Name:	Rashid Jamshidi
Birth date & place:	05. September 1982, Rasht, Iran
Nationality:	Iranian
1995 - 1999	High school Mathematics & Physics diploma, Kooshyar school, Rasht, Iran
1999 - 2003	Bachelor of Mechanical Engineering in thermo-fluids, Sharif university of technology, Tehran, Iran
2003 - 2006	Master of Mechanical Engineering in energy conversion, Sharif university of technology, Tehran, Iran
2006 - 2008	Supervisor engineer, Army university of medical sciences (for compulsory military service), Tehran, Iran
2008 - 2010	Researcher, Research Institute of Petroleum Industry,Tehran, Iran
2010 - 2013	PhD student, institute of applied mechanics, Clausthal university of technology, Germany